RESTRICTED REPORT 189R

CSIRO
AUSTRALIA

Division of
EXPLORATION GEOSCIENCE

Institute of Minerals, Energy and Construction

ROCK MAGNETISM AND PALAEOMAGNETISM OF THE GREENSTONE BELT IN THE MT KEITH-AGNEW AREA

AMIRA PROJECT 78P96C - Rock Magnetism and Magnetic Petrology Applied to Geological Interpretation of Magnetic Surveys

P.W. SCHMIDT, D.A. CLARK and D. FRENCH

AMIRA

Australian Mineral Industries Research Association Limited

CSIRO
AUSTRALIA

Division of Exploration Geoscience
Underwood Avenue, Floreat Park, WA. Postal Address: CSIRO Private Bag, Wembley WA 6014
Telephone: (09) 387 4233. Telex: AA92178. Fax: (09) 387 6046

Chief: Dr. B.J.J. Embleton

POLICY ON RESTRICTED REPORTS

Restricted Reports issued by this Division deal with projects where CSIRO has been granted privileged access to research material. Initially, circulation of Restricted Reports is strictly controlled, and we treat them as confidential documents at this stage. They should not be quoted publicly, but may be referred to as a "personal communication" from the author(s) if my approval is sought and given beforehand.

The results embodied in a Restricted Report may eventually form part of a more widely circulated CSIRO publication. Agreements with sponsors or companies generally specify that drafts will be first submitted for their approval, to ensure that proprietary information of a confidential nature is not inadvertently included.

After a certain period of time, the confidentiality of particular Restricted Reports will no longer be an important issue. It may then be appropriate for CSIRO to announce the titles of such reports, and to allow inspection and copying by other persons. This procedure would disseminate information about CSIRO research more widely to Industry. However, it will not be applicable to all Restricted Reports. Proprietary interests of various kinds may require an extended period of confidentiality. Premature release of Restricted Reports arising from continuing collaborative projects (especially AMIRA projects) may also be undesirable, and a separate policy exists in such cases.

You are invited to express an opinion about the security status of the enclosed Restricted Report. Unless I hear to the contrary, I will assume that in eighteen months time I have your permission to place this Restricted Report on open file, when it will be generally available to interested persons for reading, making notes, or photocopying, as desired.

B.J.J. Embleton

B J J EMBLETON
Chief of Division

North Ryde
Location: Delhi Road, North Ryde
Postal Address: PO Box 136, North Ryde NSW 2113
Telephone (02) 887 8666
Telex AA25817
Fax (02) 887 8909

Lindfield
Location: Bradfield Road, Lindfield
Postal Address: PO Box 218, Lindfield NSW 2070
Telephone: (02) 467 6733
Telex: AA26296
Fax: (02) 467 1902

TABLE OF CONTENTS

LIST OF TABLES

LIST OF FIGURES

Fig.4 Presentation of stepwise demagnetisation of remanence using orthogonal projections (Zijderveld plots).

Fig.5 Characteristic AF demagnetisation curves of SD, PSD and MD grains of magnetite.

Fig.6 Characteristic normalised k-T curves of paramagnetic, superparamagnetic, SD magnetite, MD magnetite and titanomagnetite grains.

Fig.7 k-T curves for a monzonite containing magnetite and a basalt containing titanomagnetite with 60 mole% ulvospinel

Fig.8 k-T curve of an ilmenite separate from a beach sand.

Fig.9 Diagnostic k-T curves of some iron ores.

Fig.10. Composition of ilmenites in a ternary plot of the end members ilmenite, pyrophanite and haematite (mole %). Legend is olivine orthocumulate crosses; olivine mesocumulate diamonds; talc-carbonate rock squares; chlorite-carbonate rock triangles; gabbro stars.

Fig.11. A. Backscattered electron image of altered chromite showing zoning from a dark aluminous chromite core to light grey magnetite on the rim. Diameter of grain is 200 μm.
B. X-ray map for aluminium of the above grain showing the decrease in aluminium towards the rim.

Fig.12. Composition of spinels in the "oxidised" spinel prism. Legend is olivine adcumulate triangles; olivine mesocumulate diamonds; talc-carbonate rock squares; chlorite-carbonate rock triangles; gabbro stars.

Fig.13 k-T curves for DDH samples

Fig.14 k-T curves for surface samples

Fig.15 AF demagnetisation of SIRM of DDH samples

Fig.16 AF demagnetisation of SIRM of surface samples

Fig.17 Thermal demagnetisation of 3-component IRM of DDH samples: z-axis = hard component (> 1000 Oe); x-axis = intermediate coercivity component (200-1000 Oe); y-axis = soft component (< 200 Oe)

Fig.18 Thermal demagnetisation of 3-component IRM of surface samples: z-axis = hard component (> 1000 Oe); x-axis = intermediate coercivity component (200-1000 Oe); y-axis = soft component (< 200 Oe)

Fig.19 Histograms for susceptibility ,NRM and Q

Fig.20 Magnetic fabric axes

SUMMARY

Magnetic properties of 64 oriented hand samples, from outcrop, and 87 diamond drill hole (DDH) samples have been determined. Eight of the DDH samples were from geotechnical holes and were therefore oriented.

The DDH rock-types are considered as two groups:

i) serpentinised and in some cases talc-carbonate altered ultramafic rocks (komatiites), that are at least moderately or, more usually, strongly magnetic,

ii) basalts, gabbros and metasediments that are weakly magnetic.

The outcrop samples are considered as a separate group because of surface effects (lightning and weathering). Although some of the serpentinised rocks are strongly remanently magnetised, the stability of the magnetisation is low and the remanence appears to represent palaeomagnetic noise due to drilling (drill hole samples) or lightning strikes (most surface samples) rather than bulk *in situ* properties.

Serpentinisation of the komatiites has produced abundant multidomain magnetite and Cr-magnetite that is magnetised predominantly by induction, with the effective susceptibility enhanced by viscous remanence approximately aligned with the present field direction. The observed magnetic anomalies over the ultramafic units are consistent with the measured magnetic properties.

The magnetic mineralogy of the unweathered serpentinised ultramafics is dominated by well-crystallised, magnetically soft magnetite grains, usually containing some chromium, and magnetite-rich rims on primary chromian spinels. Both types of magnetic carriers result from serpentinisation. Weathering produces pervasive alteration of magnetite to maghaemite and haematite, accompanied by a reduction in susceptibility. However, ultramafics exposed at the surface are generally moderately magnetic. Native metals have not been seen in any of the examined samples and there is no evidence that they contribute to the magnetic properties of the ultramafics. Ilmenites in the mafic rocks all have paramagnetic compositions and do not contribute substantially to the magnetisation.

Subsequent alteration of the serpentinites through carbonatisation/talcification tends to destroy the magnetite, reducing their magnetisation. The reduction in susceptibility is minor in the initial stages of carbonate alteration, but extreme carbonate alteration is expected to completely demagnetise the serpentinites.

The high magnesium basalts and gabbros associated with the komatiites are only weakly magnetised and Q values are generally much less than unity. Metasediments and tholeiitic basalts are also weakly magnetic. Because gabbroic and basaltic rocks are generally moderately magnetic when formed, the low susceptibilities of these rocks is probably due to metamorphism, ranging from mid-greenschist grade at Mt Keith to lower amphibolite grade at Mount White. Petrographic evidence suggests that the primary magnetic oxides have been replaced by sphene.

The magnetic fabrics are complex and probably result from the partial overprinting of an original fabric, rendering interpretation in terms of geological structure difficult. A weak ancient remanence present in some of the gabbros and basalts is interpreted as a record of a geomagnetic reversal during slow post-metamorphic cooling about 2650 million years ago. This metamorphic event is associated with gold mineralisation throughout the Yilgarn.

1.0 INTRODUCTION

The geology of the Agnew-Wiluna greenstone belt has been briefly described by Hill and Gole in Exploration Research News 1, published by the Division in January 1989. This article makes special reference to komatiite volcanology and associated mineralisation. Mt Keith forms part of the Wiluna-Norseman greenstone belt of the Eastern Goldfields, WA (Fig.1), comprising a sequence of volcanic and sedimentary assemblages. Mafic and ultramafic volcanics occur towards the base of the sequence, and are generally poorly exposed.

The ultramafics host the vast majority of the gold, silver, nickel and copper of the Eastern Goldfields. A very large (260 million tonnes), though low grade (0.6 percent), disseminated nickel deposit occurs at Mt Keith. Pronounced magnetic anomalies are associated with the greenstone belts in general, and the ultramafic units in particular.

The mafic and ultramafic igneous rocks within the study area fall into four groups. One group consists of discrete lenses, pods, sheets and dykes of serpentine-rich rocks derived from komatiites. Another group is the high magnesium basalts, a third group consists of tholeiitic basalts and the fourth group forms large layered intrusive series (Williams, 1975). Hill and Gole (1989) describe two different styles of komatiite volcanology, corresponding to the former Volcanic Peridotite and Intrusive Dunite Associations. These latter bodies are now thought to be extrusive. This is supported by the occurrence of spinifex texture (formed by quenching or supercooling from high temperature), vesicles, flow-top breccias and chilled margins, and intercalated thin sedimentary units (Fig.2).

Since the ultramafic protoliths were composed mainly of forsteritic olivine (high in magnesium and low in iron), magnesian pyroxene and paramagnetic chromite, they were not highly magnetic. One of the aims of the present work is to define the processes that have produced strongly magnetic units from weakly magnetic parent rocks.

Sixty four oriented hand samples were collected from outcrops at Mt Keith, Six Mile Well, Serp Hill and Mt White. These samples were complemented by 87 diamond drill hole (DDH) samples from Mt Keith, courtesy of ACM. Eight of the DDH samples were from geotechnical holes and were therefore oriented. From this collection twenty six were selected for petrographic examination. Based on preliminary petrographic examination and the magnetic property measurements, thirteen samples were chosen for detailed electron microprobe analysis of the magnetic minerals.

2. REGIONAL GEOLOGY

The area sampled is part of the Agnew-Wiluna Greenstone Belt which forms the northern third of the Norseman-Wiluna Greenstone Belt, lying between Mt Keith and Agnew (Figure 1). Poor exposure and extensive faulting render regional correlation difficult but Naldrett and Turner's (1977) stratigraphic interpretation of the Yakabindie area appears to be valid over much of the study area. They have subdivided the stratigraphy into an Upper and Lower Greenstone Unit, the latter being exposed in the south and pinching out northwards.

The Lower Greenstone includes a basal section consisting of layered gabbros, komatiites, and tholeiitic and komatiitic basalts which are overlain by the Lawlers Conglomerate, an upward coarsening sequence of siltstone, sandstone, pebbly sandstone and conglomerate. The lowermost portion of the Upper Greenstone Unit consists of interbedded acid volcanics, pyroclatics, shales and cherts wich are overlain by an upper sub-unit of pillow basalts and felsic volcanogenic sediments which in turn are overlain by komatiitic flows, tholeiitic and komatiitic basalts and layered gabbroic and ultrmafic sills. The youngest unit is the Jones Creek Conglomerate which ovelies both the greenstones and adjacent granite. Radiometric dating of granite pebbles in the conglomerate and and the underlying granite yield ages of 2.695+-0.015 b.y (Roddick et al., 1976). These are in good agreement with a Rb-Sr age of 2.718+-.05 b.y. obtained from the Kathleen Valley Gabbro of the Lower greenstone Unit (Cooper et al., 1978).

This sequence has been subjected to varying degrees of metamorphism ranging from prehnite-pumpellyite facies in the north near Wiluna to mid-amphibolite in south of Six Mile Well and lower amphibolite in the Mt White area. In the low grade areas metamorphism has involved static recrystallisation so that original igneous textures are preserved whereas in high grade zones dynamic metamorphism has occured resulting in the obliteration of original textures. The regional metamorphic event has been dated at 2.665±0.025 b.y. (Turek, 1966). Nickel mineralization is associated with the ultramafic komatiite flows and is frequently hosted by olivine adcumulates. Most deposits are small (less than 3.0*106 ,tonnes grading 3.0% nickel and 0.3% copper) although large low grade deposits such as that at Mt Keith (260.0 *106 tonnes with an average grade of 0.6% nickel and 0.015% copper) are also present.

3. PETROLOGICAL TECHNIQUES

Polished thin sections were prepared for petrographic and electron microprobe analysis, which provides the advantage that both the opaque and translucent phases can be examined in the same sample and their relationships determined. The electron microprobe analyses were carried out on a CAMECA CAMEBAX automated scanning electron microprobe equipped with four wavelength-dispersive X-ray spectrometers, covering the elemental range boron to uranium and a KEVEX-7000 energy dispersive X-ray spectrometer which is capable of analysing from sodium to uranium. The wavelength spectrometers were used for quantitative analysis, the energy-dispersive system being used for qualitative identification of the phases prior to quantitative analysis.

Two analytical programs were used for the determination of sulphide and oxide phases. For analysis of sulphides an accelerating voltage of 20kV was used and 15kV for oxide analysis with a regulated beam current of 20nA being used in both cases. Each element was counted for 20 seconds or a precision of 0.5%, the count being terminated when either of these two conditions was fulfilled. All analyses were corrected for atomic number effects, X-ray absorption and fluorescence using an iterative ZAF procedure. Corrections for interfering elements due to X-ray line overlap were made offline.

4. ROCK MAGNETIC PRINCIPLES AND TECHNIQUES

Ferromagnetism, Paramagnetism and Diamagnetism

Diamagnetic minerals (e.g. calcite and quartz) have very weak, negative susceptibilities and can be regarded as nonmagnetic for geophysical purposes. Paramagnetic minerals (e.g. olivines, pyroxenes and pure ilmenite) have weak positive susceptibilities and do not carry remanence. They are, therefore, normally unimportant for magnetic interpretation. Magnetically ordered phases that possess spontaneous magnetisations can be ferromagnetic *sensu stricto* (e.g. iron) or ferrimagnetic (e.g. magnetite). For simplicity, all these strongly magnetic minerals will be referred to hereafter as ferromagnetic. Ferromagnetic minerals lose their spontaneous magnetisation at a characteristic temperature, the Curie point, which is a function only of composition and which can therefore be used to detect particular ferromagnetic phases. Below its Curie temperature a ferromagnetic mineral has high susceptibility and can carry remanence. Above the Curie temperature the mineral becomes paramagnetic, with low susceptibility and no remanence. Paramagnetic minerals have greater susceptibility at low temperatures, reflecting a ~ 1/T dependence, and may become magnetically ordered, i.e. ferromagnetic or antiferromagnetic, below a transition temperature (the Curie point or the Néel point, respectively) which is composition dependent and can be used to determine the

presence of particular paramagnetic minerals.

Domain Structure

The bulk magnetic properties of rocks reflect the modal proportions, compositions and microstructure of the magnetic mineral grains, which are usually present in only minor amounts. Microstructure includes, *inter alia*, grain size and shape, degree of crystallinity and textural relationships and strongly influences the magnetic domain state of the grains. The most important control on domain structure is the effective grain size, which is equivalent to the actual grain size in a homogeneous grain, but is related to lamella size in grains with exsolution lamellae and the size of the ferromagnetic zone in a zoned grain.

Sufficiently small grains are uniformly magnetised, i.e. they have single domain (SD) structure. Ultrafine SD grains (< 0.03 μm for equant magnetite) are sufficiently perturbed by thermal fluctuations that the orientation of the spontaneous magnetisation flips rapidly between two or more easy directions. Such grains cannot retain a stable remanence and their magnetisations tend to relax rapidly towards any applied field, leading to a very high susceptibility. This behaviour is called superparamagnetism, and the grains are termed superparamagnetic (SPM).

The relaxation time for superparamagnetism increases exponentially with grain volume. Thus slightly larger grains have very long relaxation times, even on a geological time scale, and can retain remanent magnetisation indefinitely. These stable SD grains, typically in the micron size range, are important carriers of remanent magnetisation in many rocks. Acicular grain shape, or elongated lamellar shape, favours SD behaviour and extends the maximum size for SD behaviour.

With increasing size it becomes energetically favourable for the grain to subdivide into a number of magnetic domains with differently oriented magnetisations. These multidomain (MD) grains have susceptibilities, controlled by self-demagnetisation, which in the case of strongly magnetic minerals, such as magnetite, are comparable to the susceptibilities of SD grains with similar composition. The remanence of MD grains is more easily demagnetised ("softer") than that carried by SD grains and is of lower specific intensity. The case of magnetite will be considered in some detail, but other magnetic minerals exhibit qualitatively similar behaviour. Magnetite grains larger than ~ 20 μm exhibit true MD behaviour. The coercivity, which is a measure of the ease of demagnetisation, and the remanent intensity decrease steadily with increasing grain size until they level out for grain sizes greater than ~ 100 μm. The measure of coercivity used in this study is the median destructive field (MDF) during alternating field demagnetisation (see below). Grains smaller than ~20 μm have properties intermediate between

those of SD and true MD grains and are called pseudosingle domain (PSD). Small PSD grains, a few microns in size, are relatively hard and carry relatively intense remanence. For this reason, small PSD grains are the most important remanece carriers in many rocks, in spite of the fact that they constitute a minor proportion of the magnetic mineral assemblage and even though relatively large MD grains may dominate the susceptibility of the rocks.

The behaviour of some important magnetic properties with increasing grain size (above the SPM threshold size) can be summarised as: remanence, coercivity and Koenigsberger ratio (remanent/induced magnetisation) decrease; susceptibility increases slightly. Typical values of susceptibility, remanent intensity and Koenigsberger ratio of various domain states for a number of magnetic minerals are summarised in Fig.3 (from Clark, 1983). The theoretical maximum sizes for superparamagnetic and single domain behaviour for equant grains of a number of magnetic minerals are summarised below:

Mineral	**SPM threshold size** (μm)	**Critical SD size** (μm)
Iron	< 0.008	0.023
Magnetite	0.03	0.06
Maghaemite	0.02	0.06
Titanomagnetite (60% usp; 40% mt)	0.08	0.40
Haematite	0.03	15.0
Monoclinic pyrrhotite	0.018	1.6

It has become apparent in recent years that magnetic grains frequently occupy metastable domain states of anomalously low domain multiplicity. The above values for the critical SD size assume equilibrium, i.e. that the grain is in the absolute energy minimum state. In fact, grains an order of magnitude larger than the theoretical size can remain in a metastable SD state, because formation of a domain wall requires an energy barrier to be overcome. Thus the effective upper limit for SD behaviour has been extended to ~ 1 μm for magnetite and by a similar factor for other minerals. The threshold sizes are also larger for elongated grains than for equant grains. The domain structure transition sizes for titanomagnetites and other spinel phases with lower spontaneous magnetisations are larger than for magnetite. Thus the single domain/two domain transition, the upper limit of the PSD size range etc. occur at larger grain sizes for spinels with decreasing magnetite

contents. Taking metastable behaviour into account, the approximate size ranges and coercivities for SPM, (stable) SD, PSD and MD behaviour for magnetite are listed below:

Domain structure	Size (μm)	Coercivity (Oe)
SPM	< 0.05	0
(acicular) SD	0.05-1	> 600
PSD	~1-20	100-600
MD	> 20	< 100

Intrinsic Magnetic Properties of Minerals

The intrinsic magnetic properties spontaneous magnetisation at room temperature (J_s) and Curie temperature (T_C), which are dependent only on composition, are given below for a number of minerals, including some end-member spinel phases:

Mineral name	Chemical formula	Magnetic properties
Iron	Fe	T_C = 770°C, J_s = 1710 G
Awaruite	Ni_3Fe	T_C = 620°C, J_s = 950 G
Magnetite	Fe_3O_4	T_C = 580°C, J_s = 480 G
Ulvospinel	Fe_2TiO_4	T_C = -153°C, J_s = 0
Titanomagnetite (100x mole% usp)	$Fe_{3-x}Ti_xO_4$	$0 \leq x < 0.8$ ferro; $x \geq 0.8$ paramag.
Maghaemite	cFe_2O_3	$T_C >> 300°C^*$, J_s = 440 G
Haematite	αFe_2O_3	T_C = 670°C, J_s = 2 G
Titanohaematite (100x mole% ilm)	$Fe_{2-x}Ti_xO_3$	$0 \leq x < 0.5$ antiferro; $0.5 \leq x \leq 0.8$ ferro; $0.8 < x < 1$ paramagnetic
Ilmenite	$FeTiO_3$	T_C = -205°C, J_s = 0
Monoclinic (4C) pyrrhotite	Fe_7S_8	T_C = 320°C, J_s = 90 G
Magnesioferrite	$MgFe_2O_4$	$T_C \lesssim 420°C$, $J_s \lesssim 220$ G
Chromite	$FeCr_2O_4$	T_C = -185°C, J_s = 0

(continued)

Mineral name	Chemical formula	Magnetic properties
Ferrichromite/ Cr-magnetite	$Fe_{3-x}Cr_xO_4$ e.g. Fe_2CrO_4	ferromagnetic for $0 \leq x \leq 1.2$, $T_C = 200^\circ C$, $J_S = 250$ G
Hercynite	$FeAl_2O_4$	$T_C = -265^\circ C$, $J_S = 0$
Magnesian ulvospinel	Mg_2TiO_4	diamagnetic
Picrochromite	$MgCr_2O_4$	$T_C = -258^\circ C$, $J_S = 0$
Spinel	$MgAl_2O_4$	diamagnetic
Jacobsite/ Mn-magnetite	$Fe_{3-x}Mn_xO_4$ e.g. Fe_2MnO_4	ferromagnetic for $0 \leq x \leq 2.5$ $T_C = 300^\circ C$, $J_S = 398$G
Trevorite	$NiFe_2O_4$	$T_C = 595^\circ C$, $J_S = 330$ G
Coulsonite	FeV_2O_4	$T_C = -164^\circ C$, $J_S = 0$

The Curie point of maghaemite cannot be observed directly because maghaemite inverts to haematite at temperatures above ~300°C, depending on impurities. The Curie temperature of magnetite-bearing spinel minerals varies systematically with magnetite content. To a first approximation, the Curie point of a particular spinel composition can be estimated by linear interpolation between T_C of the constituent end members. Diamagnetic minerals can be assigned a nominal T_C of absolute zero (-273°C) for this purpose. For the titanomagnetite series, a more accurate expression relating Curie temperature to mole fraction of ulvospinel (x) is:

$Fe_{3-x}Ti_xO_4$: $T_C\ (^\circ C) = 578 - 580x - 150x^2$.

The effect on T_C of substitution of Cr, Al and V into magnetite is broadly similar to that of Ti substitution. Substitution of Ni increases the Curie point slightly, as does cation deficiency. Thus cation-deficient magnetites ("kenomagnetite"), representing compositions intermediate between stoichiometric magnetite and maghaemite, can have T_C above 600°C. Magnesioferrite is the only important spinel end member, other than magnetite, that is ferromagnetic at room temperature. The magnetic properties of magnesioferrite depend strongly on the cation distribution, which reflects thermal history. The Curie point of $MgFe_2O_4$ is given by:

$MgFe_2O_4$: $T_C\ (^\circ C) = 417 - 490f$,

where f is the fraction of Mg^{2+} ions on tetrahedral sites. Because of the elevated T_C and high spontaneous magnetisation, magnesioferrite-rich spinels and Mg-magnetites are strongly magnetic and can be important contributors to the magnetic properties of rocks in which they occur.

The magnetic phase diagram of the titanohaematite series is complex and the magnetic properties of the compositions that are ferromagnetic at room temperature are influenced by thermal history. $FeTiO_3$-Fe_2O_3 solid solutions have been thoroughly studied. The Curie temperature decreases approximately linearly with increasing ilmenite content. Compositions with less than 20 mole% haematite are paramagnetic at room temperature.

Pure haematite has a diagnostic magnetic transition (the Morin transition) at -20°C. Below this temperature atomic magnetic moments are aligned with the crystallographic c-axis and haematite is antiferromagnetic. Above the transition the moments lie in the basal plane but are slightly canted out of antiparallelism, giving rise to weak ferromagnetism and an increased susceptibility. The Morin transition can also be exploited for diagnosis of well-crystallised haematite by the effect of low temperature demagnetisation on remanence (see below).

Palaeomagnetic Cleaning Techniques

The natural remanent magnetisation (NRM) of a rock may consist of components, carried by different subpopulations of magnetic minerals, acquired at different times. During initial cooling of an igneous rock, magnetic mineral grains make the transition from paramagnetism to ferromagnetism as they cool through their Curie points. A spontaneous magnetisation appears that is initially in equilibrium with the applied field, but becomes "frozen in" or blocked at a somewhat lower temperature, called the blocking temperature, when the relaxation time of the grain's magnetic moment increases prodigiously. Below the blocking temperature the magnetisation is a stable remanence that is known as thermoremanent magnetisation (TRM). If grain growth of magnetic minerals or creation of new magnetic phases occurs below the Curie temperature, there is a huge increase in relaxation time as the grains become larger than the SPM threshold size. This produces a stable chemical remanent magnetisation (CRM). If CRM is acquired at elevated temperatures, the remanence has both thermal and chemical character and is known as thermochemical remanence.

Other components of remanence may be acquired at later times due to metamorphic overprinting, weathering etc. Each separate component of remanence is acquired parallel to the ambient field at the time of its acquisition. Rock samples may also acquire palaeomagnetic noise components due to exposure to magnetic fields, for instance during mining operations or during or after collection. All these components contribute to the measured NRM of a rock sample. Because different remanence components are carried by subpopulations of grains with different characteristics, they can usually be distinguished by their different responses to various demagnetisation techniques.

Alternating field (AF) demagnetisation is similar to degaussing of permanent magnetisation of ships or tape recorder heads. The sample is subjected to an alternating magnetic field that is gradually reduced to zero, thereby randomising the moments of all grains with coercivity less than the initial AF amplitude. This procedure is repeated at successively higher fields, demagnetising successively harder fractions of the magnetic mineral assemblage and isolating the most stable component of remanence. AF demagnetisation is particularly effective at removing isothermal remanent magnetisation (IRM) acquired by exposure to strong magnetic fields, such as those produced by mining equipment or lightning strikes etc.

Thermal demagnetisation involves heating the sample and recooling to room temperature, in zero magnetic field. This randomises the magnetic moments of all grains with blocking temperatures less than the heating temperature. This procedure is repeated at successively higher temperatures, thereby demagnetising successively higher blocking temperature fractions. Thermal demagnetisation is particularly effective at unravelling the thermal history of the rock, for instance by resolving primary TRM from a later metamorphic overprint.

Palaeomagnetic cleaning techniques have three main applications, which can be termed palaeomagnetic, petrophysical and rock magnetic respectively:

(i) Resolution of remanence components acquired at different times, allowing estimation of palaeofield directions and palaeopole positions at the time of formation, at the time of metamorphism etc.,

(ii) Removal of palaeomagnetic noise components, which are not representative of the bulk *in situ* properties, allowing characteristic NRMs of the rock to be determined,

(iii) Identification of magnetic minerals by their demagnetisation characteristics. Information on compositions, domain states and grain sizes of the magnetic minerals can be obtained.

The most useful method of depicting demagnetisation of multicomponent remanence is that of orthogonal projections. These are generally termed Zijderveld plots. The basic idea of these plots is illustrated in Fig.4. The end-points of the remanence vectors after successive demagnetisation steps describe a trajectory in 3D space. Over a treatment interval where a single remanence component is removed this trajectory defines a linear segment. Where two or more remanence components are being removed simultaneously, due to their having overlapped stability spectra, the trajectory is curved. After removal of all less stable components, the trajectory of the most stable component is a straight line heading towards the origin, indicating decreasing intensity without change in direction. The stability spectrum corresponding to thermal

demagnetisation is the blocking temperature spectrum and for AF demagnetisation it is the coercivity spectrum.

The differences in AF demagnetisation behaviour of acicular SD, small PSD and large MD magnetite is shown in Fig.5. The remanence that is being demagnetised is an artificially imparted saturation IRM (SIRM), produced by placing the samples in a very strong field. The plot shows the remanent intensity, normalised to the initial value before AF treatment, versus AF field. The corresponding coercivity spectra can be obtained from the demagnetisation curves by differentiation, as the coercivity spectrum is the magnitude of the slope of the demagnetisation curve. Thus the coercivity spectrum of the large MD grains peaks at low fields (less than 5 mT), the spectrum for the small PSD grains peaks at ~ 15 mT and that of the SD grains peaks above 40 mT. The Lowrie-Fuller test exploits the differences between AF demagnetisation behaviour of small and large grains. For SD and PSD grains weak field remanence, such as TRM, is more resistant to demagnetisation than strong field remanence, particularly SIRM. For true MD grains the relative stability of weak and strong field remanences is reversed.

Demagnetisation behaviour can be used to detect the presence of other magnetic minerals. For example, haematite is very hard (MDF > 1000 Oe) and does not thermally demagnetise until close to 670°C. Goethite has even greater coercivity than haematite, but breaks down to haematite at ~120°C, and is therefore very easily thermally demagnetised.

Thermomagnetic Analysis of Magnetic Mineralogy

The variation of magnetic properties of magnetic minerals with temperature depends on composition and, in some cases, on domain state and microstructure. This variation can therefore be used for analysis of magnetic minerals. The variation of susceptibility with temperature is particularly useful, because of the rapid change in susceptibility close to T_C, which enables well-defined Curie points to be determined, and because of the sensitivity of susceptibility to domain state and microstructure.

The characteristic susceptibility (k) versus temperature (T) behaviour of different magnetic minerals is shown in Fig.6. The k-T curve for paramagnetic minerals is hyperbolic, reflecting the 1/T dependence of paramagnetic susceptibility. The k-T curve of magnetite with MD structure, including PSD grains as well as true MD, grains is very diagnostic. There is a prominent peak at -155°C, which corresponds to the isotropic point of magnetite. Below this temperature the easy magnetisation directions are along the <100> cubic axes, whereas above it the easy directions lie along <111> body diagonals of the cubic unit cell. At the isotropic point the magnetisation rotates freely to align with an applied field, giving rise to an increase in susceptibility. The susceptibility of MD grains is

limited by self-demagnetisation and the observed susceptibility remains almost constant until just below the Curie temperature, when it plummets to paramagnetic values. The isotropic point is very sensitive to composition and substitution of cations other than iron, or departures from stoichiometry, tend to lower the isotropic point. Titanomagnetites containing more than ~10 mole% ulvospinel have isotropic points below liquid nitrogen temperature. Thus the presence of a well-defined peak at ~-155°C is diagnostic of the presence of nearly pure PSD and/or MD magnetite.

The titanomagnetite for which the k-T curve is shown has a Curie point of ~ 200°C and contains ~60 mole% ulvospinel. The k-T curve is irreversible on cooling from high temperature (not shown), due to exsolution of more magnetite-rich and magnetite-poor titanomagnetites than the original composition. Thus two Curie points, one above 500°C and the other shifted somewhat lower than the original T_C, would be seen in the cooling curve.

The k-T curve for SD magnetite does not exhibit a peak at the isotropic point because the properties of SD grains are controlled largely by shape anisotropy, rather than by magnetocrystalline anisotropy. The susceptibility is almost constant at low temperatures, but increases as the Curie temperature is approached. This increase in k reflects unblocking of fine grains below T_C.

The susceptibility of grains increases sharply at the unblocking temperature because the relaxation time suddenly decreases, allowing the magnetic moments of the grains to align freely with the applied field. Above the unblocking temperature the superparamagnetic susceptibility of grains of specified volume is proportional to J_S^2/T and is much higher than the room temperature susceptibility, until the Curie temperature is approached (at which point $J_S \rightarrow 0$, so $k \rightarrow 0$). Thus the presence of significant unblocking of remanence well below the Curie temperature indicates that this portion of the remanence is carried by very fine (submicron) single domain grains.

Even smaller grains unblock at much lower temperatures and exhibit superparamagnetism at room temperature. The k-T curve shown for SPM grains is idealised for an assemblage of identical grains. In rocks there is always a distribution of grain sizes and the superposition of unblocking peaks over a wide range of temperatures leads to a steady increase in susceptibility from below room temperature up to the maximum unblocking temperature of the ultrafine SPM + SD assemblage. This behaviour is commonly seen in soil samples, particularly lateritic soils.

As the Curie temperature of a magnetic mineral is approached, there is a rapid decrease in spontaneous magnetis-ation and an

even more rapid decrease in magnetocrystalline anisotropy. As a consequence the remanence of even the most stable grains unblocks, but without an increase in k. In fact, the susceptibility plummets until it attains paramagnetic values at T_C.

Typical k-T curves of a monzonite containing only PSD/MD magnetite and a basalt containing only MD titaniferous magnetite are shown in Fig.7. The thermomagnetic curve of paramagnetic ilmenite separated from a beach sand deposit is depicted in Fig.8. The irreversibility of the curves for the basalt and the ilmenite extract indicates chemical change has occurred. This illustrates the sensitivity of k-T curves to changes, such as oxidation, exsolution and rehomogenisation, in magnetic minerals during heating.

Thermal demagnetisation of remanence provides another analytical technique. MD grains exhibit a spectrum of unblocking temperatures right up to T_C, whereas the unblocking temperature spectrum of SD grains cuts off below the Curie point. However, given that the grain size range of a particular mineral extends at least to the upper end of the SD range, the maximum unblocking temperature lies just below T_C. Thus Curie points can also be estimated from thermal demagnetisation data. Prominent inflexions in the demagnetisation curve, corresponding to a sharp peak in the blocking temperature spectrum, indicate the approximate Curie temperature of a particular phase. Comparison of the blocking temperature spectra with k-T curves enable phases originally present in samples to be distinguished from phases created during heating. Low temperature demagnetisation also allows magnetic transitions characteristic of magnetite and haematite to be detected. Judicious application of a variety of rock magnetic techniques, including thermomagnetic analysis, allows the relative contributions to susceptibility and remanence of different compositions and grain size ranges to be estimated.

A variant of the traditional thermal demagnetisation of saturation remanence has recently been proposed by Lowrie (1990). This method involves saturating a specimen along one axis (the z-axis for this study), remagnetising in a field of lower strength along the x-axis, and finally applying a weaker field along the y-axis. The specimen then carries three orthogonal components, representing the highest coercivity fraction, an intermediate coercivity fraction and a low coercivity fraction respectively. Thermal demagnetisation of this remanence enables the unblocking temperature spectrum of each of these subsets of the magnetic grains to be determined simultaneously. This technique is particularly useful for detecting the presence of minerals of differing magnetic hardness (e.g. goethite, which is harder than haematite, but demagnetises below 200°C; haematite, which is harder than magnetite and demagnetises predominantly between 600°C and 670°C; magnetite, which demagnetises predominantly between 500°C and 580°C; and pyrrhotite, which may have comparable

coercivity to magnetite (depending on grain size), but which demagnetises predominantly between 280°C and 320°C).

Thermomagnetic curves for a number of iron ore samples with different mineralogies are presented in Fig.9. The detection of MD magnetite, SD magnetite, haematite and maghaemite by thermomagnetic analysis is well illustrated by this collection of k-T curves.

5. PETROGRAPHY

Much of the following description is based upon drill-core material from the Mt Keith area, supplemented by outcrop samples from Serp Hill, Six Mile Well and Mt White (Table 1 and Figure 1). Descriptions are given in terms of the protolith where possible and in those instances where this cannot be determined by the metamorphic mineral assemblage. The protolith has been exposed to varying degrees of metamorphism form middle-upper greenschist grade at Mt Keith to lower amphibolite grade at Mt White. The Six Mile Well and Serp Hill areas are complex, lying at the junction of low, medium and high grade areas (from mid-greenschist to upper amphibolite facies), although the absence of hornblende and metamorphic amphibole suggests that high grade rocks are not represented in the present collection. Low grade prehnite-pumpellyite or lower greenschist facies rocks are also not represented.

5.1 Komatiites

These are the most abundant rock type of the samples selected for petrographic examination and display a wide range of textures. Although komatiites often display a wide range of unusual textures these may be grouped into two basic varieties as illustrated in the type example from Munro Township in the Abitibi greenstone belt, Ontario as described by Arndt et al., 1977). The upper "A Zone" (Fig.2) consists of skeletal olivine which becomes progessively larger downwards passing into large (30cm-1m) bladed crystals in a sub-parallel arrangement ("spinifex texture"). The lower "B Zone" consists of massive peridotite which in the Mt Keith area display cumulate textures. These cumulate textures may be further subdivided on the basis of the proportion of interrcumulus material present (Irvine, 1982). Thus an orthocumulate has greater than 25% of intercumulus material, a mesocumulate 7-25% and an adcumulate less than 7% of intercumulus material.

5.1.1 Spinifex Peridotite

These are present in samples from the Mt Keith drill core and display classic spinifex textures, consisting of long bladed crystals of olivine set in an originally glassy matrix. Subhedral to anhedral scattered chromite grains

400 to 500 μm across are also present. Olivine has been pseudomorphed by talc and the glassy groundmass by talc, chlorite and carbonate with fine grained (less then 10 μm) magnetite being associated with chlorite. Tremolite-actinolite may also replace the groundmass in association with chlorite-carbonate veining and serpentine-chlorite replacement of spinifex olivine grains. Talc-carbonate alteration is a retrograde metamorphic effect superimposed upon a prograde serpentine + chlorite + tremolite - actinolite assemblage.

5.1.2 Olivine Cumulates

These are the most abundant of the rock types sampled and show a range in primary textures and alteration assemblages. Olivine adcumulates consist entirely of olivine with minor occurrence of chrome spinel and are restricted to the Mt Keith section. Primary olivine is replaced by serpentine with the formation of finely granular magnetite concentrated along fracture planes and intergranular boundaries. At triple junctions magnetite tends to form coarser granular aggregates. It is also present as a fine dusting throughout some pseudomorphed olivine grains and occasionally delineates the margins of coarse mesh serpentine. Chromite is rare, occurring as lobate grains which may have a faintly translucent core enclosed by an opaque margin. Sparse grains appear to be of an intercumulus origin.

Olivine mesocumulates are similar, although the polyhedral morphology of olivines grains may be discerned and chromate tends to be more abundant, occurring as lobate grains. Olivine is pseudomorphed by serpentine, many grains having a core of massive pale green antigorite enclosed by a rim of fibrous radiating serpentine. Dusty magnetite is concentrated along original grain boundaries and fracture zones. Carbonate (?siderite) may also be present, forming a trellis of interlocking veins. One sample from MKD77 is unusual in containing large (1mm) subhedral fractured grains of chrome-spinel enclosed in stichite which is also invasive along fractures. Samples from Six Mile Well are weathered to a varying extent as shown by the presence of iron-stained ferromagnesian minerals and the alteration of fine grained magnetite to maghaemite and haematite. Intercumulus phases are replaced by tremolite-actinolite and less commonly, serpentine-chlorite. The proportion of interculumlus material is higher, verging towards orthocumulates unlike those from Mt Keith which are closer to adcumulates. Subhedral to euhedral scattered chrome spinel grains are present, occuring both as an intercumulus phase and as inclusions in altered olivine.

Olivine orthocumulates have been positively identified only in outcrop samples from Serp Hill. These consist of loosely packed olivine polyhedra pseudomorphed by serpentine.

Scattered subhedral to euhedral chrome-spinel grains up to 200 μm across are also present. Finely granular magnetite is concentrated along grain boundaries and less commonly forms irregular trails. Actinolite replaces intercumulus material which may have been clinopyroxene. The effects of weathering are pervasive, amphibole being iron-stained and granular magnetite displaying incipent alteration to maghaemite and haematite. Pyroxene may have been a cumulus phase in an othocumulate sample from Mt Keith which contains massive actinolite apparently pseudomorphing clinopyroxene. Fibrous actinolite is also common and defines a weak foliation. This sample is also unusual in that opaque phases are rare and appear to have been magnetite now replaced by sphene.

5.2.3 Talc-carbonate rocks

These are represented by drill core samples from Mt Keith, particularly those from MKD61 and on the evidence presented below are of retrograde origin. They occur within a sequence of olivine adcumulates and mesocumulates but the extensive alteration and strong shearing have largely destroyed the primary igneous textures. Coarse lenticular carbonate is abundant and may occur in association with brucite. Alternating lenticles of talc and carbonate define a strong foliation and fine grained magnetite may be abundant, forming trails elongated parallel to foliation. Minor fibrous tremolite and chlorite are present in less altered samples. Rarely talc and carbonate define an unsuual trellis textute which appears to be mimicing an original serpentine trellis texure observed in less altered adcumulates. Chrome spinel occurs as scattered lobate and subhedral grains up to 1mm across. One sample is unusual in consisting of abundant carbonate in association with ?tremolite and containing scattered euhedral translucent chrome spinel grains with a narrow, discontinuous rim of magnetite. One sample from within the sequence of talc-carbonate rocks in MKD61 is comprised of chlorite and scattered "lakes" of dusty carbonate. Sparse ilmenite occurs as granular aggregates up to 4mm across or as subhedral corroded grains. Rare monazite, xenotime and zircon are also present. Although the sample occurs within the ultramafic sequence it is clearly different from the enclosing lithologies and its parentage remains uncertain.

5.2 Gabbros

These are represented in the Mt Keith drill core and in outcrop samples from the Mt White areas. Those from Mt Keith consist of coarse (to 1mm) subhedral clinopyroxene replaced by actinolite with incipient development of fibrous actinolite as an epitaxial overgrowth. Zoned plagioclase is frequently saussuritized and partialy replaced by chlorite. Opaque phases are rare (less than 1%) and magnetite is invariably

replaced by sphene, although ilmenite appears to be unaltered. Siderite may also be present, occurring in granular aggregates up to 1mm across and fibrous tremolite-actinolite may also be well developed in some samples. Clinopyroxene appears to have been both a cumulus and intercumulus phase in association with plagioclase.

Gabbros from the Mt White area also appear to be of cumulate origin, being texturally similar to those from Mt Keith although showing a variation from equant to elonagte morphologies and also a greater development of ophitic textures, some specimens consisting of coarse ophitic clinopyroxene replaced by tremolite- actinolite. Plagioclase occurs as an anhedral intercumulus phase and also as stumpy crystals up to 0.5mm across some of which form radiating groups. Sparse subhedral ilmenite to 100 μm is also present which displays a marginal alteration. Original magnetite of a similar morphology is replaced by sphene. In some specimens fibrous amphibole is extensiveley developed and defines a foliation. The petrological affinities of the gabbros are uncertain.

5.3 Basalts

These are represented by one sample from the Mt Keith area and an outcrop sample from Mt White. That from Mt Keith consists of granoblastic and fibrous pale green actinolite, the fibrous form defining a weak foliation. Colourless fibrous ?tremolite is also present to which the actinolite is often interstitial, the association possibly pseudomorhping a fine pyroxene quench texture. Opaques are rare and are replaced by sphene. The apparent quench clinopyroxene would suggest that the sample is of a komatiitic basalt. The parentage of the sample from Mt White is uncertain as it consists of dense fine-grained pale green actinolite forming a felted aggregate cut by coarser quartz+actinolite veins. Scattered fine-grained opaques are replaced by sphene. There is no evidence of primary igneous textures and it is possible that the sample may be of a devitrified glassy flow top.

5.4 Metamorphism

Samples from Mt Keith have been subjected to greenschist facies metamorphism as indicated by the occurrence of tremolite+actinolite in the komatiites and mafic volcanics and the rare occurrence of epidote in the mafic volcanics. The greater development of tremolite+actinolite in the samples from the Serp Hill, Six Mile Well and Mt White areas indicates an increase in grade transitional to lower amphibolite facies. The widespread occurence of talc +carbonate±brucite in the Mt Keith komatiites is attributed to retrograde metamorphism as it appears to be restricted to zones of high strain as indicated by the development of a

foliation and passes laterally into less deformed serpentinised ultramafics with a decrease in talc+carbonate contents.

6.0 MAGNETIC MINERALOGY

6.1 Ilmenite

Ilmenite is the sole visible oxide phase in the layered gabbro from Mt White and is dominant in the chlorite-carbonate rock from Mt Keith in which it occurs in association with minor rutile. Sporadic ilmenite is also present in the olivine mesocumulates from Six Mile Well and the olivine orthocumulates from Serp Hill. Magnetite was originally present in the layered gabbro from Mt White but has been replaced by sphene during regional metamorphism. Ilmenite in the Mt Keith chlorite-carbonate sample occurs as anhedral to subhedral tabular to elongate grains varying in size from 100 μm to 2mm. Many have an irregular outline suggestive of corrosion although evidence is lacking as to if this is a primary feature or a consequence of metamorphism. Rutile occurs sporadically as exsolution lamellae in some grains. Chemically they are essentially pure ilmenite, only minor amounts (approximately 1.0 wt % MnO) of manganese being present. Ferric iron contents are negligible the maximum recorded being 1.0 wt % Fe2O3. The Mt White layered gabbro contains finer grained ilmenite, the size range being from 30 μm to 200 μm and all are anhedral having an irregular outline and an unusual spongy appearence. Chemically they are similar to those described above apart from having a slightly higher MnO content.

Ilmenite is rare in the Six Mile Well mesocumulates and is present as anhedral, sub-equant to tabular grains varying in size from 10 to 80 μm. They may be distinguished chemically from those occurring in the mafic units by their higher manganese contents (from 2.4 to 9.4 wt % MnO) although ferric iron contents are similar. Those occurring in sample 112084 are unusual in that they contain significant cobalt (from 0.4 to 0.8 wt % CoO). The two samples examined of the Serp Hill orthocumulates show distinct differences in ilmenite morphology. It is rare in sample 112083, occuring as 20 to 30 μm subhedral tabular to equant grains. In contrast, ilmenite is more abundant in sample 112087 (although still sparse) and occurs as 50 to 100 μm subhedral to anhedral grains. It is also present as smaller grains in association with maghaemite. Chemically they are similar to those present in the Six Mile Well mesocumulates, manganese contents varying from 8.2 to 17.6 wt % MnO with the highest

values being recorded from sample 112087. Two groups may be distinguished in sample 112087 on the basis of magnesium contents, one containing less than 1.0 wt % MgO and the other from 2.7 to 5.6 wt % MgO.

Sparse ilmenite is present in sample 112073, a talc-carbonate rock from Mt Keith. The typical occurrence is as 10 to 30 μm subhedral tabular to elongate grains. Chemically they are similar to the mafic units and have the lowest manganese contents (less than 1.0 wt % MnO). Ferric iron contents are higher but are still low, the maximum being 5.0 wt % Fe2O3.

Ilmenite compositions in the system ilmenite-haematite-pyrophanite are plotted in Fig.10 and the analsyses are given in Table2.

6.2 Spinels

Although the spinels display a wide chemical variability they are discussed as a group rather than separately as the chemical groups exhibit a complex textural association. As described above primary magnetite may have been present in the mafic units but has now been replaced by sphene as a consequence of regional metamorphism. Chrome spinel was the primary spinel phase in the komatiites but has suffered pervasive alteration to magnetite which has also formed due to the breakdown of ferromagnesian silicate phases during metamorphism.

Chromite is sparsely distributed throughout the olivine mesocumulates as subhedral to anhedral rounded equant grains ranging from 10 to 300 μm, although most fall within the range 10 to 100 μm. Many grains have an extermely irregular outline due to replacement by chromian magnetite. It is doubtful if any of the analysed grains reflect primary compositions the closest being aluminous ferrochromite. Titanium and manganese are the only other significant components, both averaging 1.0 wt % TiO2 and MnO respectively, although manganese contents in sample 112084 tend to be slightly lower. Zoning is common and is reflected by a decrease in chromium, aluminium and magnesium from core to rim with a concomitant increase in both ferrous and ferric iron. There is a distinct break between these compositions and those of the chromian magnetites which occur as rims on chromite and as discrete anhedral equant grains varying from less than 1 μm to 20 μm. Chrome contents vary from 20 wt % Cr2O3 to 1.6 wt % Cr2O3 although most most analyses fall below 10 wt % Cr2O3. Contents of other elements are insignificant, titanium and manganese having dropped considerably as have magnesium and aluminium. When recast in term of the spinel end-members magnetite is shown to be the dominant phase with the occurrence of variable but minor ferrochromite. As reflected in the k/T plots the spinels have been oxidised, probably due to weathering so much of the original magnetite

has been made over to maghaemite and, in extreme cases haematite.

Spinels present in the olivine orthocumulates from Serp Hill have also been affected by weathering as described above with the formation of maghaemite and rare haematite. Chrome spinel in sample 112083 occurs as 300 μm to 400 μm equant, rounded and embayed crystals which is in contrast to that present in sample 112087 in which the grain size varies from 50 μm to 150 μm and the grains are anhedral and frequently fractured. Compositionally they are aluminous ferrochromites similar to those in the mesocumulates, although titanium and manganese contents are more variable. Zinc contents are also higher and average 1.3 wt % ZnO in sample 112087. Zoning patterns are also similar to those observed in the mesocumulates, although there is a suggestion that manganese contents may increase towards the rim in sample 112087, rather than remaining constant.

Chromian magnetite is present in both samples as rims on chrome spinel (Fig.11) and as discrete grains which display distinct morphological differences between the two samples. In sample 112083 it occurs as 10 to 100 μm anhedral equant to tabular grains with the rare occurrence of subhedral grains whereas in sample 112087 it varies in size from 10 to 300 μm, is frequernlty elongate and extensively fractured and in some cases, appears to form granular aggregates pseudomorphing primary chrome spinel. Chrome contents show a similar range to that described for the mesocumulates although the average for sample 112083 is 12.8 wt% Cr_2O_3 and 76.3 wt % Cr_2O_3 for sample 112087 reflecting the greater abundance of low values (less than 2.0 wt % Cr_2O_3) in the latter sample. Manganese and titanium decrease with increasing iron and zinc contents are uniformly low in contrast to the high values seen in the chrome spinels.

Magnetite is present in sample 112083 occurring as 5 μm to 10 μm anhedral elongate and subhedral equant grains. It is essentially pure magnetite, apart from the presence of minor silica in some analyses (less than 1.0 wt % SiO_2). Magnetite may also have been present in ssample 112087 but the two grains analysed have been altered to haematite.

Olivine cumulates represented in the Mt Keith drill core samples invariably contain sparsely distributed chrome-spinel displaying a wide morphological variation. Thus in the serpentinised olivine mesocumulate (sample 112082) it occurs as large (400 μm) rounded subequant grains and in the adcumulate (sample 112071) anhedral irregular 50 to 150 μm grains which may form millimetre sized aggregates. In contrast in the talc-carbonate rocks it is present as subhedral tabular to elongate fractured grains 200 μm to 300 μm long. They are also compositionally different from the chrome spinels in the outcrop olivine cumulates in having higher magnesium and alunminium contents and lower

titanium and manganese, although the latter tends to be variable. Sample 112071 is distinctive in having elevated zinc (average of 0.8 wt% ZnO) and chromites in sample 112082 have higher magnesium and aluminium contents. The effects of metamorphism are most evident in the adcumulate (112071) magnesium, aluminium and chromium decreasing towards the rim with a concomitant increase in total and ferric iron. Zinc contents also drop towards the rim and there is a suggestion that nickel, titanium and manganese may increase. This difference is also reflected in the spinel end-member compositions, picotite being dominant in sample 112082 containing subequal amounts of spinel (*sensu stricto*), magnesiochromite and ferrochromite. Compositons of chromite in the adcumulate and talc-carbonate rocks are similar to those in the outcrop olivine cumulates, although spinel (*sensu stricto*) contents are higher and the adcumulate is distinctive in that many analyses contain significant magnesioferrite.

Chromian magnetite is scarce in the talc carbonate and olivine mesocumulate samples but relatively abundant in the adcumulate in which it occurs as 5 μm to 100 μm (most grains falling in the range 5 μm to 20 μm) anhedral equant grains which clump together to form elongate trails. Chrome contents are low in the talc-carbonate and mesocumulates (1.0 to 2.0 wt % Cr_2O_3) but the mesocumulate is distinctive in having elevated nickel contents (1.5 wt% NiO). Chromian spinel in the olivine adcumulate displays a greater variability in chromium contents comparable to that described previously but contains between 1.0 to 2.0 wt % magnesium and elevated nickel contents similar to those of chromian magnetite in the mesocumulate. Magnetite is present in all samples occuring as 5 μm to 50 μm anhedral elongate grains although subhedral equant to tabular grains are also present in the talc-carbonate rock. Compositionally they are almost pure magnetite. Both the mesocumulate and adcumulate contains higher and more variable nickel contents than the talc carbonate rock and magnesium contents are higher in the adcumulate.

Compositions of analysed spinels are plotted in the "oxidised" spinel prism in Fig.12. Analyses of chromites, Cr-magnetites and magnetites are given in Tables 3, 4 and 5 respectively.

7. ROCK MAGNETIC CHARACTERISATION OF MAGNETIC MINERALOGY

The behaviour of susceptibility with temperature is a powerful diagnostic tool for magnetic mineral identification. These measurements are performed using a small furnace and the CSIRO susceptibility bridge. Small crushed samples (~1 cm^3) are cooled initially to liquid nitrogen temperature (-197°C), allowed to warm to room temperature and then heated to 600°C or 700°C, depending on the Curie temperature of the mineral being measured.

The observed k-T curves for the moderately to strongly magnetic ultramafic rocks fall into two distinct groups, corresponding to surface samples and drill core material. Susceptibility versus temperature (k-T) curves for the drill core samples are shown in Fig.13 and for the surface samples are shown in Fig.14. Fresh drill core samples typically show a large peak in susceptibility near the isotropic point of magnetite (-155°C), although sometimes significantly above, nearer -100°C (curve 61-190.05), as shown in Fig.13a. This peak is usually interpreted as indicating coarse grained multidomain magnetite, although the shift to higher temperatures may indicate that the magnetite is slightly impure. The rapid descent of the curve towards the Curie point at ~580°C also demonstrates that nearly pure magnetite dominates the susceptibility. However the slight rounding of the shoulder of the k-T curve, immediately preceding the sharp drop in susceptibility, indicates that a range of compositions with a corresponding range of Curie points between ~500°C and 580°C is present. Given the microprobe analyses, these phases are interpreted as Cr-magnetites containing up to ~10 mole% chromite.

The curves consist of a reversible component and an irreversible component in different ratios. The reversible component is due to multidomain magnetite. The irreversibility arises from the presence of maghaemite that inverts to weakly magnetic haematite on heating. This phase alters between 300°C and 500°C imparting another peculiarity of shape to these curves. The curve for sample 56-172 was cooled from 375°C to 325°C after the susceptibility dropped before beginning heating again. This shows that the maghaemite began to invert at about 300°C.

One curve, for sample 52-1654, that is reversible shows two discrete Curie temperatures. The presence of magnetite is shown by the Curie temperature at about 580°C, while another phase has a Curie temperature of about 520°C. In this case the second phase is stable. In the light of the petrographic examination and microprobe analyses of spinel phases from these rocks, the Curie point of ~520°C probably represents a Cr-magnetite with a relatively narrow compositional range, occurring as thin rims on altered primary chromites. It may be significant that this sample comes from the relict dunite core at Betheno and is less serpentinised than the other ultramafic samples.

AF demagnetisation curves and coercivity spectra for SIRMs imparted to drill core samples are shown in Fig.15. Figure 16 presents the corresponding plots for the surface samples. Thermal demagnetisation data for drill core and surface samples are shown in Figs.17 and 18 respectively. AF demagnetisation of SIRM of specimen 61-190c (Fig.15) shows that the median destructive field is less than 50 Oe and that the remanence is almost completely destroyed by 200 Oe AF. This indicates that the magnetic mineralogy is dominated by soft multidomain grains. Thermal demagnetisation of SIRM for the same specimen

(Fig.17) shows steady unblocking from room temperature, indicating remanence carriers of low stability that are unlikely to retain ancient remanence. A minor peak in the unblocking temperature spectrum from 335°C to 380°C corresponds to the breakdown of the minor magnetic phase over a similar temperature range that occurred during the k-T run. The main unblocking peak occurs at ~580°C, confirming that essentially pure magnetite is the dominant magnetic mineral in this sample.

While nearly pure magnetite is the predominant phase, both before and after cooling, some susceptibilty curves showed a distinctive peak at around 300°C on cooling, e.g. curves 61-142.5 and 61-160.7. The first of these curves was reheated to determine if this feature was an artifact. The peak appears to be repeatable and is probably related to alteration of the initially paramagnetic chromian spinel by exsolution of a phase that contains substantial magnetite in solid solution with (Mg-Al-)Cr-spinel. The carbonate-altered mesocumulate sample 83-245.8 also exhibits this feature. For this sample the magnetic alteration product is relatively abundant, suggesting that the carbonate alteration has preferentially dissolved magnetite rather than chromian spinel grains. This could well reflect grain size, with fine magnetite grains completely dissolved, whilst larger grains are only partially destroyed.

The k-T curves for the ultramafic surface samples (Fig.14) typically show no magnetite isotropic point and are dominated by maghaemite that breaks down dramatically above 300°C. Two coolings and reheatings for curve KA28a shows that the characteristic rise in susceptibility, giving the curves a humpback form, is reversible up to 300°C, but is irreversible at 400°C. This is reminiscent of the irreversible components of curves from some of the drill hole samples. The interpretation that the irreversibility is due to the inversion of maghaemite, is supported by the petrographic detection of maghaemite, the characteristic thermomagnetic signature and the fact that a similar feature is particularly prominent in surface samples, where it tends to dominate the k-T curves. Three core samples from a single hole, representing highly weathered, partially weathered and unweathered serpentinised olivine adcumulate (77-77.6, 77-101 and 77-108.3 respectively) show a striking development of an irreversible susceptibility peak and concomitant decrease in reversible susceptibilty with increased intensity of weathering, corresponding to replacement of magnetite by maghaemite, accompanied by a reduction in bulk susceptibility.

Curves for spinifex textured peridotites (Fig.13) show weak magnetite isotropic points and low Hopkinson peaks, indicating the dominance of multidomain magnetite. On cooling a dramatic Hopkinson peak appears at about 480°C, e.g. curves 55-115.3 and 55-117.0. This phase is a very fine grained alteration product, possibly produced by exsolution of fine magnetite-rich phases from chromian spinel, although the end-member magnetite component remains unaltered.

The remaining curves are from basalts, gabbros, and pyroxene cumulates that are weakly magnetic (Fig.14). The curves predominantly show the inverse relationship of susceptibility and temperature that characterises paramagnetic material, i.e. the ferromagnetic content of these samples is volumetrically minute compared to the ferromagnesian silicates. Traces of magnetite present in the basalt, gabbro and pyroxenite samples are reflected in Curie temperatures of about 580°C.

Thermal demagnetisation of three-component IRMs imparted to drill core and surface samples (Figs.17 and 18 respectively) are very diagnostic of the magnetic minerals present, including minor phases. The magnetisation of the surface samples is dominated by maghaemite, with haematite also commonly present. These are clearly weathering products, which are absent or much less prominent in drill core samples. Some surface samples, e.g. 23b2, exhibit a sharp drop in intensity of the highest coercivity component (z-component) at < 200°C. This indicates the presence of goethite. The relative hardness of the maghaemite is variable, but it most cases it has coercivities predominantly above 1000 Oe, indicating that it is single domain and must therefore be very finely subdivided.

8.0 BULK MAGNETIC PROPERTIES

8.1 Drill Hole Samples

The DDH rock-types are considered as three groups:

(i) The first comprises highly serpentenised ultramafics, variably carbonatised and talcified. As seen above, these rocks are the most magnetic.

(ii) The second group are the ultramafics that are less serpentinised. Some of these samples are fairly magnetic but as a group they are not as highly magnetic as the above group. The pyroxenites are weakly magnetic.

(iii) The third group covers basalts, gabbros and metasediments that are weakly magnetic.

The outcrop samples are considered as a separate group because of surface effects (mainly lightning, although weathering is also important). Tables 6 to 9 list the susceptibilites, natural remanent magnetisations (NRMs), Koenigsberger ratios (Q values) and anisotropies. However, the results are better summarised by the set of histograms (Fig.19).

Susceptibilities (Fig.19a) are trimodally distributed with frequency peaks below 1000 μG/Oe (0.012 SI), between 3000 μG/Oe (0.036 SI) and 4000 μG/Oe (0.048 SI) and a broader peak from 7000 μG/Oe to 0.01 G/Oe (about 0.08 SI to 0.12 SI). The susceptibilities of the majority of samples comprising the low peak are less than 100 μG/Oe (0.00012 SI) indicating their

susceptibilities are dominated by paramagnetic minerals. The samples with the highest susceptibilities (61-234 and 61-249 Table 1, 15709 μG/Oe and 14540 μG/Oe, or almost 0.2 SI) are carbonatised serpentinite dunites, with some preserved adcumulate texture.

Partial carbonatisation of highly magnetic serpentinised ultramafics appears to have only a minor effect on susceptibility, because the magnetite is redistributed rather than being destroyed. Initially the carbonising fluids flush out iron, dissolving the dusty magnetite associated with serpentinisation, but redeposit it as coarser magnetite grains in cracks. Extreme carbonate alteration in similar rocks is known to eventually dissolve magnetite completely, with the iron entering magnesite as a siderite component.

Remanent intensities vary greatly and when plotted on a histogram altogether, they do not reveal much detail. Nine samples with extremely high NRM intensities (from 10 to 95 mG, or from 10 to 95 Am^{-1}) dominate the distribution and have been omitted from the histogram for clarity. Thus, NRMs less than 10 mG (10 Am^{-1}) only are plotted in Fig.19b. Again the serpentinised komatiites contribute to the highly magnetic end of the spectrum, and the basalts, gabbros and metasediments contribute to the weakly magnetic end. The most intensely remanently magnetised sample (82-146 Table 1) is a partly carbonatised yellow-green serpentinised dunite with flushings of dust-sized magnetite in fissures. It is thought these relatively coarse magnetites have acquired their remanence during drilling. Magnetic grains that are this easily reset would almost certainly be viscously magnetised in the Earth's field direction in their natural state. This is discussed further below. Other serpentinised samples described as being carbonatised appear to have anomalously high Q values although not necessarily anomalously high remanent intensities. Sample 25-613 (Table 3), for instance, has a Q of 85.9 and a remanence of 6219 μG (6219 mAm^{-1}). However, this sample is classified as weakly magnetic since its susceptibiliy is only 134 μG/Oe (1680 SI). The carbonatisation appears to be associated with coarse grained magnetite making these rocks very susceptible to acquiring a drilling induced remanence (DIR). Koenigsberger ratios much greater than unity in rocks with magnetically soft multidomain grains indicate DIR overprinting of the *in situ* remanence and are not representative of bulk properties. Some of the measured Koenigsberger ratios are high ($Q > 5$). These Q values are probably spurious and have therefore been omitted from Fig.19c. However, the Q values are predominantly much less than unity, indicating the relative unimportance of remanent magnetisation in these rocks.

Anisotropy of magnetic susceptibility of some of the serpentinised rocks is high, and consistent within sample. The highest anisotropy encountered was 1.73 for sample 61-175 (Table 1), a carbonatised/talcified serpentinised dunite. Fig.20 shows typical anisotropy data for different rock types.

The magnetic foliation is better developed in the serpentinised rocks than is the magnetic lineation. Since most drill core samples were not oriented the directions of the anisotropy axes are not plotted in Fig.20. In general, anisotropy axes are consistent within each sample. However, the anisotropy axes of the oriented core samples are inconsistent between sample, as shown in Fig.20, probably indicating that the magnetic fabrics present are complex, resulting from the partial overprinting of an original fabric. The anisotropies of these rocks as a whole are probably unimportant in magnetic modelling, but may be useful in small scale structural analysis.

Although the remanent magnetisation of the serpentinised komataiites, and to a certain extent other ultramafics/peridotites, is intense, it is of low stability (low coercivity) and is easily reset. DDH samples show clear evidence of drilling induced remanence (DIR), as mentioned above, suggesting that any remanence prior to drilling is probably viscous remanent magnetisation (VRM). Fig.21 is a stereoplot of magnetisation directions in drill core co-ordinates, i.e. the drill core axes are all vertical. The distribution shows a pronounced bias to the vertical irrespective of drill core orientation. In geographic coordinates the directions are scattered, as shown in Fig.22a. Also plotted in Fig.22 are examples of alternating field (Fig.22b) and thermal (Fig.22c) demagnetisation. The median destructive field of the remanence is much less than 100 Oe (10 mT). It is unlikely that any ancient (Archaean) remanence contributes significantly to the magnetic anomalies in the Mt Keith area. These results concur with those from the previous AMIRA project on the southern (Kalgoorlie-Norseman) part of this greenstone belt. It is also notable that the magnetic anomalies over the greenstones are invariably positive.

8.2 Outcrop Samples

The magnetic properties of outcrop samples (Table 4) are similar to their DDH counterparts except for the intensities of NRM of some samples. Very high intensities of outcrop samples, some associated with Q values over 100, are most likely the result of lightning. However, while NRM directions from Mt Keith are scattered (Fig.23a), NRM directions of outcrop samples from Mt White show a grouping in the northwest-up octant (Fig.23b).

Magnetic cleaning of the outcrop samples has yielded a palaeomagnetic overprint signature of geological importance. Samples from stratigraphically equivalent units at Mt Keith and Mt White show similar demagnetisation trends. A gabbro (site 25) from Mt Keith and basalts (sites 44 and 45) and a gabbro (site 49) from Mt White reveal two components of magnetisation during thermal demagnetisation (Fig.23c). Below 500°C a component directed northwest-up is removed leaving a more stable (higher unblocking temperature) component to the

southeast-down. The only significant component found in other samples is of low stability (low unblocking temperature) aligned with the present field and is probably a VRM. Because the structural attitudes of the stratigraphy at Mt Keith and Mt White are different, it is possible to perform a fold test to determine the relative age of the magnetisations and the deformation. Most strata at Mt Keith are dipping steeply westward, while those at Mt White are dipping to the northwest. Not surprisingly, the low temperature component attributed to VRM scatters after restoring the units to their palaeohorizontal (Fig.24a). Figs.24b and 24c show the intermediate (northwest-up) and high (east-down) temperature components before and after restoring the strata to their palaeohorizontal. Both the groupings scatter indicating that these components of magnetisation post-date the deformation.

The characteristics of these overprint components is consistent with metamorphic cooling spanning a geomagnetic reversal, and can be correlated with other magnetic overprints Yilgarn-wide. The normal polarity magnetisation is associated with grains which have lower blocking temperatures than those which are carrying the reversed magnetisation, indicating that the geomagnetic field changed polarity from reversed to normal. A comparison with the Australian apparent polar wander path suggests a late Archaean age (Fig.25). There is also isotopic age evidence that this magnetisation is related to the gold mineralisation throughout the Yilgarn. This seems to have been the last orogenic event that has affected these rocks. Such a widespread remagnetisation event predicts that in greenstone belts throughout the Yilgarn the only ancient remanence is directed northeast-up or southeast-down.

9. CONCLUSIONS

* The serpentinisation of the komatiites has produced abundant multidomain magnetite that is magnetised predominantly by induction, with the effective susceptibility enhanced by viscous remanence approximately aligned with the present field direction. The observed magnetic anomalies over the ultramafic units are consistent with the measured magnetic properties.

* The magnetic mineralogy of the unweathered serpentinised ultramafics is dominated by well-crystallised, magnetically soft magnetite grains, usually containing some chromium, and magnetite-rich rims on primary chromian spinels. Both types of magnetic carriers result from serpentinisation. Weathering produces pervasive alteration of magnetite to maghaemite and haematite, accompanied by a reduction in susceptibility. However, ultramafics exposed at the surface are generally moderately magnetic. Native metals have not been seen in any of the examined samples and there is no evidence that they contribute to the magnetic properties of the ultramafics. Ilmenites in the mafic rocks all have paramagnetic compositions and do not contribute substantially to the magnetisation.

* Subsequent alteration of the serpentinites through carbonatisation/talcification tends to destroy the magnetite, greatly reducing their magnetisation. It is expected that extreme carbonate alteration should completely demagnetise the serpentinites.

* The high magnesium basalts and gabbros associated with the komatiites are only weakly magnetised and Q values are generally much less than unity. Metasediments and tholeiitic basalts are also weakly magnetic. Because gabbroic and basaltic rocks are generally moderately magnetic when formed, the low susceptibilities of these rocks is probably due to metamorphism, ranging from mid-greenschist grade at Mt Keith to lower amphibolite grade at Mount White. Petrographic evidence suggests that the primary magnetic oxides have been replaced by sphene.

* The magnetic fabrics are complex and probably result from the partial overprinting of an original fabric.

* A weak ancient remanence present in these latter rock-types is interpreted as a record of a geomagnetic reversal during slow post-metamorphic cooling about 2650 million years ago. This metamorphic event is associated with gold mineralisation throughout the Yilgarn.

10. ACKNOWLEDGEMENTS

We thank ACM Ltd and, in particular, Noel Sheppy for providing drill core samples, geological information and aeromagnetic data for this study. Rob Hill and Sarah Dowling were of great assistance as guides in the field and as tutors in komatiite volcanology.

11. REFERENCES

Arndt, N.T., Naldrett, A.J, and Pyke, D.R.,1977. Komatiitic and iron-rich tholeiitic lavas of Munro Township, Northeast Ontario. Journ. Petrol., v.18, pp319-369.

Cooper,J.A., Nesbitt, R.W., Platt, J.P., and Mortimer, G.E., 1978. Crustal development in the Agnew Region, Western Australia, as shown by Rb/Sr isotopic and geochemical studies. Precamb. Res., v.7, pp31-59.

Naldrett, A.J., and Turner, A.R, 1977. The geology and petrogenesis of a greenstone belt and related nickel sulfide mineralization at Yakabindie, Western Australia. Precamb. Res., v.5, pp43-103.

Roddick, J.C., Compston, W., and Durney, D.W., 1976. The radiometric age of the Mt Keith granodiorite, a maximum estimate for an Archean greenstone sequence. Precamb. Res., v.3, pp55-78.

Table 1. List of Samples Examined Petrographically.

Sample Number	Field Number	Lithology
Mt Keith		
112068	MKD27 96.5	Basalt
112069	MKD49 103.7	Gabbro
112070	MKD49 145.2	Gabbro
112071	MKD52 576.2	Olivine adcumulate
112072	MKD53 183.2	olivine+pyroxene orthocumulate
112073	MKD55 117.0	Talc+carbonate (olivine cumulate)
112074	MKD56 106.6	Komkatiitic spinifex basalt
112075	MKD56 115.7	Spinifex Peridotite
112076	MKD56 172.0	Talc+carbonate (olivine cumulate)
112077	MKD61 142.5	Talc+carbonate(olivine cumulate)
112078	MKD61 160.7	Talc+carbonate (olivine cumulate)
112079	MKD61 175.9	Talc+carbonate (olivine cumulate)
112080	MKD61 190.1	Talc+carbonate (olivine cumulate)
112081	MKD61 203.0	Chlorite+carbonate
112082	MKD61 234.0	Olivine Mesocumulate
112138	MKD77 179.6	Olivine Mesocumulate
112137	MKD80 86.9	Spinifex Peridotite
Serp Hill		
112083	KA26B	Olivine Orthocumulate
112087	KA30A	Olivine Orthocumulate
Six Mile Well		
112084	KA28A	Olivine mesocumulate
112085	KA28C	Olivine Mesocumulate
112086	KA29B	Olivine Mesocumulate
Mt White		
112088	KA46A	Gabbro
112089	KA46B	Gabbro
112090	KA47A	?Basalt
112091	KA49A	Gabbro

Note: Drill hole depths for the Mt Keith samples are in metres.

Table 2. Representative electron microprobe analyses of ilmenites.

Oxide wt%	Gabbro	Chlorite carbonate rock	Talc carbonate rock	Olivine orthocumulate		Olivine mesocumulate	
	112088	112081	112073	112083	112087	112084	112085
SiO2	0.04	0.06	0.12	0.01	0.06	0.14	0.02
TiO2	51.90	53.09	51.10	51.69	54.23	52.24	52.48
Al2O3	0.02	0.01	0.04	0.04	-	-	0.03
Cr2O3	0.04	-	0.03	0.02	0.07	0.04	0.03
V2O3	0.03	0.01	-	-	0.05	-	-
FeO*	44.86	45.58	46.48	38.96	28.58	39.89	44.48
MnO	1.96	1.52	0.73	8.34	11.58	5.72	2.64
MgO	0.03	0.12	0.16	0.22	4.89	0.21	0.13
CaO	0.14	0.16	0.03	-	0.03	0.03	-
CoO	0.05	0.01	-	0.06	0.10	0.83	0.18
NiO	0.01	-	-	0.05	0.06	0.04	0.03
ZnO	0.03	-	-	0.18	-	0.11	-
Total	99.12	100.56	98.70	99.57	99.64	99.23	100.01
FeO	44.41	45.58	45.04	37.39	28.20	39.89	44.11
Fe2O3	0.50	-	1.60	1.75	0.42	-	0.41
Total	99.17	100.56	98.86	99.74	99.69	99.23	100.05
Ilmenite End Members (mole %)							
FeTiO3	94.78	95.89	96.19	79.54	57.71	86.55	93.45
MgTiO3	0.10	0.44	0.60	0.83	17.82	0.80	0.48
MnTiO3	4.23	3.25	1.58	17.97	24.01	12.57	5.65
CaTiO3	0.39	0.42	0.09	-	0.07	0.09	-
Fe2O3	0.49	-	1.54	1.67	0.39	-	0.39

Table 3. Representative electron microprobe analyses of chromites.

	Olivine orthocumulate		Olivine mesocumulate		Olivine adcumulate	Talc-carbonate rock
Oxide wt%	112083	112084	112085	112082	112071	112073
SiO2	0.10	0.09	0.06	0.06	0.23	0.20
TiO2	0.73	0.70	1.21	0.48	0.59	0.25
Al2O3	9.66	16.19	15.44	20.13	16.17	10.87
Cr2O3	45.28	42.64	40.09	46.52	50.01	55.06
V2O3	0.30	0.27	0.21	0.17	0.14	0.04
FeO*	37.46	32.68	36.27	16.80	21.72	19.61
MnO	0.70	0.77	1.31	0.21	0.48	0.20
MgO	2.56	4.20	2.45	13.46	9.15	12.65
CaO	-	0.01	0.02	0.03	0.01	0.01
CoO	0.10	0.13	0.12	0.09	0.16	-
NiO	0.10	0.22	0.12	0.07	0.04	0.18
ZnO	0.83	0.64	0.89	0.09	1.00	0.16
Total	97.82	98.55	98.19	98.11	99.71	99.22
FeO	28.30	26.88	29.10	14.13	19.79	14.26
Fe2O3	10.17	6.44	7.96	2.96	2.15	5.95
Total	98.84	99.19	98.99	98.40	99.93	99.81
Spinel End Members (mole %)						
Fe3O4	9.67	4.09	3.99	-	-	-
Fe2TiO4	1.99	0.54	3.23	1.14	1.46	0.62
MgCr2O4	-	-	-	23.19	13.77	33.44
FeCr2O4	64.85	58.02	56.00	34.70	51.69	37.66
MgAl2O4	13.81	21.52	12.91	37.33	31.39	20.93
FeAl2O4	6.82	11.26	19.25	-	-	-
MnAl2O4	-	-	-	-	0.15	-
FeV2O4	0.44	0.37	0.30	0.22	0.19	0.05
MgFe2O4	-	-	-	2.60	-	7.20
MnFe2O4	2.14	2.23	3.92	0.55	1.21	0.11
NiFe2O4	0.29	0.59	0.34	0.17	0.10	-
CaFe2O4	-	0.04	0.07	0.10	0.05	-

Table 4. Representative electron microprobe analyses of chromian magnetite.

	Olivine orthocumulate		Olivine mesocumulate			Olivine adcumul.	Talc-carbonate rock
Oxide wt%	112083	112087	112085	112086	112082	112071	112073
SiO2	0.04	0.08	0.04	0.12	0.11	0.12	0.10
TiO2	2.29	0.25	0.10	0.15	0.02	-	0.01
Al2O3	0.11	-	0.04	0.04	-	0.01	-
Cr2O3	14.78	2.83	11.07	10.34	1.38	2.79	1.33
V2O3	0.22	0.10	0.11	0.08	-	0.02	0.16
FeO*	74.92	86.27	80.15	82.24	89.36	85.26	91.96
MnO	0.76	0.26	0.34	0.42	0.04	0.56	0.08
MgO	0.30	1.13	0.07	0.10	0.33	2.29	-
CaO	0.02	0.01	0.02	-	0.02	0.01	0.13
CoO	-	0.01	0.05	0.03	-	0.06	0.03
NiO	0.17	0.63	0.38	0.36	1.79	0.95	0.10
ZnO	0.20	-	0.19	-	0.01	-	0.05
Total	93.81	91.56	92.57	93.88	93.05	92.08	93.96
FeO	31.45	28.17	29.73	30.44	28.84	25.75	31.01
Fe2O3	48.31	64.57	56.04	57.57	67.25	66.14	67.74
Total	98.64	98.03	98.18	99.64	99.79	98.71	100.74
Spinel End Members (mol %)							
Fe3O4	65.57	85.92	79.56	81.47	91.03	78.50	97.14
FeTiO4	6.67	0.72	0.28	0.43	0.06	0.01	0.02
FeV2O4	0.34	0.15	0.18	1.28	-	0.03	0.25
MgCr2O4	-	-	-	-	-	-	-
FeCr2O4	22.63	4.36	17.16	15.77	2.11	4.25	2.02
MgAl2O4	0.25	0.01	0.09	0.08	-	0.02	-
FeAl2O4	-	-	-	-	-	-	-
MgFe2O4	1.46	6.54	0.33	0.50	1.90	13.08	0.03
MnFe2O4	2.48	0.85	1.11	1.37	0.12	1.83	0.26
NiFe2O4	0.53	1.40	1.19	0.25	4.70	2.24	-
CaFe2O4	0.07	0.04	0.08	-	0.09	0.04	0.28

Table 5. Representative electron microprobe analyses of magnetite.

Oxide wt %	Olivine orthocum. 112083	Olivine mesocum. 112082	Olivine adcum. 112071	Talc carbonate rock 112073
SiO2	0.39	0.26	0.15	0.13
TiO2	0.07	0.02	0.02	0.04
Al2O3	-	-	0.01	0.01
Cr2O3	0.04	0.01	-	0.45
V2O3	-	-	-	0.11
FeO*	91.29	90.37	91.89	92.89
MnO	-	0.06	0.20	-
MgO	0.07	0.22	0.66	0.03
CaO	0.04	0.01	0.03	0.05
CoO	0.02	0.05	0.12	-
NiO	0.07	0.82	0.12	0.29
ZnO	0.05	-	0.09	0.06
Total	92.04	91.82	93.30	94.06
FeO	30.94	29.70	29.75	31.10
Fe2O3	67.07	67.43	69.05	68.68
Total	98.76	98.58	100.22	100.94
Spinel End Members (mol %)				
Fe3O4	99.90	97.68	95.55	98.61
Fe2TiO4	-	0.06	0.07	0.11
FeV2O4	-	-	-	0.16
MgCr2O4	-	-	-	-
FeCr2O4	0.06	0.01	-	0.68
MgAl2O4	0.04	-	0.03	0.01
FeAl2O4	-	-	-	-
MnFe2O4	-	0.21	0.61	-
MgFe2O4	-	1.27	3.76	0.15
NiFe2O4	-	0.71	-	0.05
CaFe2O4	-	0.05	-	0.22

Table 6 Mount Keith Strongly Magnetic DDH Samples

Susceptibilities > 4000 μG/Oe (0.05 SI)

DDH	Depth	Rock-type	J(μG)	k(μG/Oe)	Q	AMS
51	568	serp. OAC	2181	8283	0.49	1.08
51	593	serp. OAC	955	7007	0.25	1.03
52	1889	serp. OAC	3421	9736	0.65	1.16
55	83	peridotite	1417	4596	0.57	1.16
56	120	spin. peri.	2039	8265	0.46	1.06
56	129	spin. peri.	770	9804	0.15	1.04
56	172	serp. OAC	1563	4248	0.68	1.47
61	160	serp. OAC	23961	8080	5.49	1.55
61	161	ch. carb.	16603	11785	2.61	1.32
61	175	serp. OAC	14125	12878	2.03	1.73
61	190	serp. OAC	3367	4552	1.37	1.60
61	234	carb. serp.	4050	15709	0.48	1.06
61	249	carb. serp.	11062	14540	1.41	1.03
69	214	serp. OMC	10272	5235	3.63	1.24
76	274	serp. OMC	5926	8358	1.41	*
77	108	serp. OAC	27289	7469	6.77	1.21
77	179	carb. serp.	43598	7691	10.5	1.34
78	188	carb. serp.	17365	6497	4.95	1.08
82	146	carb. serp.	94708	8797	19.9	1.10
82	495	serp. OAC	36338	7188	9.36	1.08
82	503	tot. carb.	5135	4145	2.29	1.28

Depth may be metres or feet depending on age of drill hole
J intensity of natural remanent magnetisation (1μG = 1 mAm^{-1})
k low field magnetic susceptibility (1μG/Oe = 4π SI)
Q Koenigsberger ratio (J/kH), where H = 0.54 Oe (54 μT)
AMS anisotropy of magnetic susceptibilty
* AMS not measured on quarter core samples because of odd shape effects.

Table 7 Mount Keith Moderately Magnetic DDH Samples
Susceptibilities > 200 μG/Oe (0.0025 SI)
< 4000 μG/Oe (0.05 SI)

DDH	Depth	Rock-type	J(μG)	k(μG/Oe)	Q	AMS
52	1166	serp OAC	4135	3749	2.04	*
52	1178	serp OAC	2104	3008	1.30	*
52	1184	serp OAC	3124	3999	1.45	*
52	1201	serp OAC	2906	2717	1.98	*
52	1292	serp OAC	1108	3400	0.60	*
52	1403	serp OAC	83.4	1112	0.14	*
52	1418	serp OAC	295	666	0.82	*
52	1645	dunite	1284	917	2.59	1.17
52	1668	serp OAC	1060	1870	1.05	*
52	1697	serp OAC	997	1290	1.43	*
52	1740	serp OAC	874	2228	0.73	*
55	82	peridotite	173	3487	0.09	1.14
55	117	peridotite	468	1158	0.75	1.11
55	137	carb. talc	1884	1392	2.51	1.12
56	96	peridotite	318	1709	0.34	1.06
56	115	peridotite	256	1446	0.33	1.10
61	123	carb. talc	1696	3093	1.02	*
61	142	carb. talc	1535	2369	1.20	1.29
75	135	carb. serp.	1593	3288	0.90	*
75	288	serp. OMC	4456	3131	2.64	1.12
75	388	carb. serp.	9996	3385	5.47	1.08
75	462	po serp.	15111	3615	7.74	1.24
77	77.6	w.serp.dun	6498	3077	3.91	*
77	101	w.serp.OAC	2212	1245	3.29	1.10
80	86	serp. OC	1416	3928	0.67	1.26
83	245	tot. carb	17000	981	32.1	1.24

Depth may be metres or feet depending on age of drill hole
J intensity of natural remanent magnetisation (1μG = 1 mAm^{-1})
k low field magnetic susceptibility (1μG/Oe = 4π SI)
Q Koenigsberger ratio (J/kH), where H = 0.54 Oe (54 μT)
AMS anisotropy of magnetic susceptibilty
* AMS not measured on quarter core samples because of odd shape effects.

Table 8 Mount Keith Weakly Magnetic DDH Samples
Susceptibilities < 200 μG/Oe (0.0025 SI)

DDH	Depth	Rock-type	J(μG)	k(μG/Oe)	Q	AMS
25	613	t.carb talc	6219	134	85.9	1.44
27	132	hg.Mg bas.	1.34	62.9	0.04	1.06
27	173	pyroxenite	2.80	54.3	0.10	*
27	316	gabbro	0.92	52.2	0.03	1.01
27	470	tuff	0.09	52.9	3.15	1.21
27	530	mass.sulph.	56.2	16.1	6.50	*
27	551	pyroxenite	0.70	39.7	0.03	*
46	394	gabbro	0.04	10.0	0.01	1.02
46	470	gabbro	0.20	26.5	0.01	1.02
47	237	bas. tuff	0.16	7.56	0.04	1.03
49	174	bas. tuff	0.38	31.8	0.02	1.03
49	183	basalt	0.42	30.0	0.03	1.03
49	340	gabbro	13.4	51.5	0.48	1.04
49	476	gabbro	0.39	35.4	0.02	1.02
49	1253	lamproph?	0.10	5.10	0.03	*
49	1263	gabbro	0.03	6.02	0.01	*
50	585	gabbro	0.04	4.90	0.02	1.04
50	604	gabbro	0.15	0.57	0.49	1.29
53	600	gabbro	0.04	46.2	0.00	1.10
53	620	gabbro	27.9	116	0.45	1.07
55	70	w. peri.	0.32	52.9	0.01	1.05
55	115	peridotite	158	326	0.90	1.05
55	168	metased.	3.20	37.1	0.16	1.16
56	106	hg.Mg. bas.	0.05	59.6	0.00	1.03
56	112	hg.Mg. bas.	0.07	42.8	0.00	1.05
56	227	metased.	0.52	48.4	0.02	1.09
61	203	carb. serp.	230	281	1.52	1.12
61	297	schist	0.33	30.4	0.02	1.17
74	222	felsic ig.	0.22	13.4	0.03	1.04
81	67	felsic sed.	0.29	12.5	0.04	1.12
81	89	carb. gab.	0.49	54.1	0.02	1.04

Depth may be metres or feet depending on age of drill hole
J intensity of natural remanent magnetisation ($1\mu G = 1\ mAm^{-1}$)
k low field magnetic susceptibility ($1\mu G/Oe = 4\pi$ SI)
Q Koenigsberger ratio (J/kH), where H = 0.54 Oe (54 μT)
AMS anisotropy of magnetic susceptibilty
* AMS not measured on quarter core samples because of odd shape effects.

Table 9 Mount Keith\Mt White Surface Sites

	Rock-type	J(μG)	k(μG/Oe)	Q	AMS
Strong - Susceptibilities > 4000 μG/Oe (0.05 SI)					
27	serp. OAC	6858	7134	1.78	1.11
30	gabbro	5628	4699	2.22	1.07
Moderate - Susceptibilities > 200 μG/Oe (0.025 SI) < 4000 μG/Oe (0.05 SI)					
26	serp. OAC	123480	2196	104	1.13
28	serp. OC	5816	3692	2.92	1.03
29	u.mafic	31750	3923	15	1.04
32	serp. OC	4558	1323	6.38	1.06
33	serp. OC	6262	3261	3.56	1.09
34	serp. OC	13675	1250	20.3	1.03
35	serp. OC	1432	1594	1.66	1.03
40	u.mafic	328	395	1.54	1.11
41	serp. OC	3042	1480	3.81	1.05
42	serp. OC	353	362	1.81	1.05
Weak - Susceptibilities < 200 μG/Oe (0.0025 SI)					
22	conglom.	174	210	1.53	1.06
23	basalt	0.42	74.2	0.01	1.03
24	basalt	0.35	65.4	0.01	1.04
25	gabbro	376	158	2.70	1.04
31	m.conglom.	1.00	6.89	0.27	1.04
36	basalt	2.05	62.6	0.06	1.02
37	basalt	9.80	64.1	0.28	1.02
38	gabbro	60.0	53.1	2.09	1.02
39	gabbro	1.14	49.0	0.04	1.01
43	gabbro	33.9	55.3	1.14	1.01
Mt White					
44	hg.Mg.bas.	53.0	97.4	1.01	1.02
45	hg.Mg.bas.	6.20	51.0	0.23	1.01
46	gabbro	8.43	67.5	0.23	1.01
47	hg.Mg.bas.	283	66.1	7.92	1.03
48	hg.Mg.bas.	1039	64.1	30.0	1.01
49	gabbro	497	154	5.98	1.02

J intensity of natural remanent magnetisation (1μG = 1 mAm^{-1})
k low field magnetic susceptibility (1μG/Oe = 4π SI)
Q Koenigsberger ratio (J/kH), where H = 0.54 Oe (54 μT)
AMS anisotropy of magnetic susceptibilty

Figure 1. Regional geology of the Wiluna-Agnew greenstone belt.

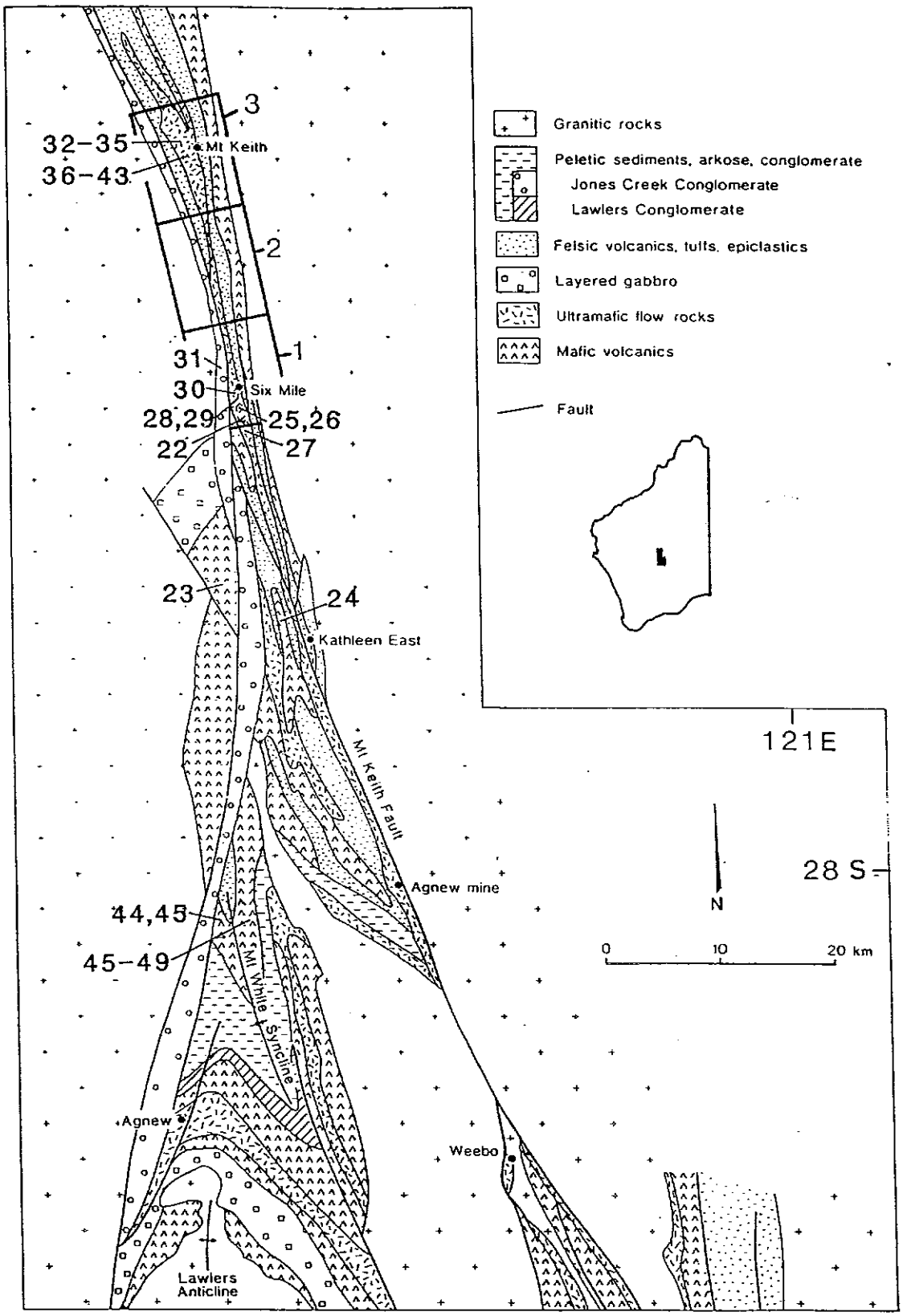
3
32–35
Mt Keith
36–43
2
1
31
30
Six Mile
28,29
25,26
22
27
23
24
Kathleen East
Mt Keith Fault
Agnew mine
44,45
45–49
Mt White Syncline
Agnew
Weebo
Lawlers Anticline
Granitic rocks
Peletic sediments, arkose, conglomerate
Jones Creek Conglomerate
Lawlers Conglomerate
Felsic volcanics, tuffs, epiclastics
Layered gabbro
Ultramafic flow rocks
Mafic volcanics
Fault
121E
28 S
N
0
10
20 km

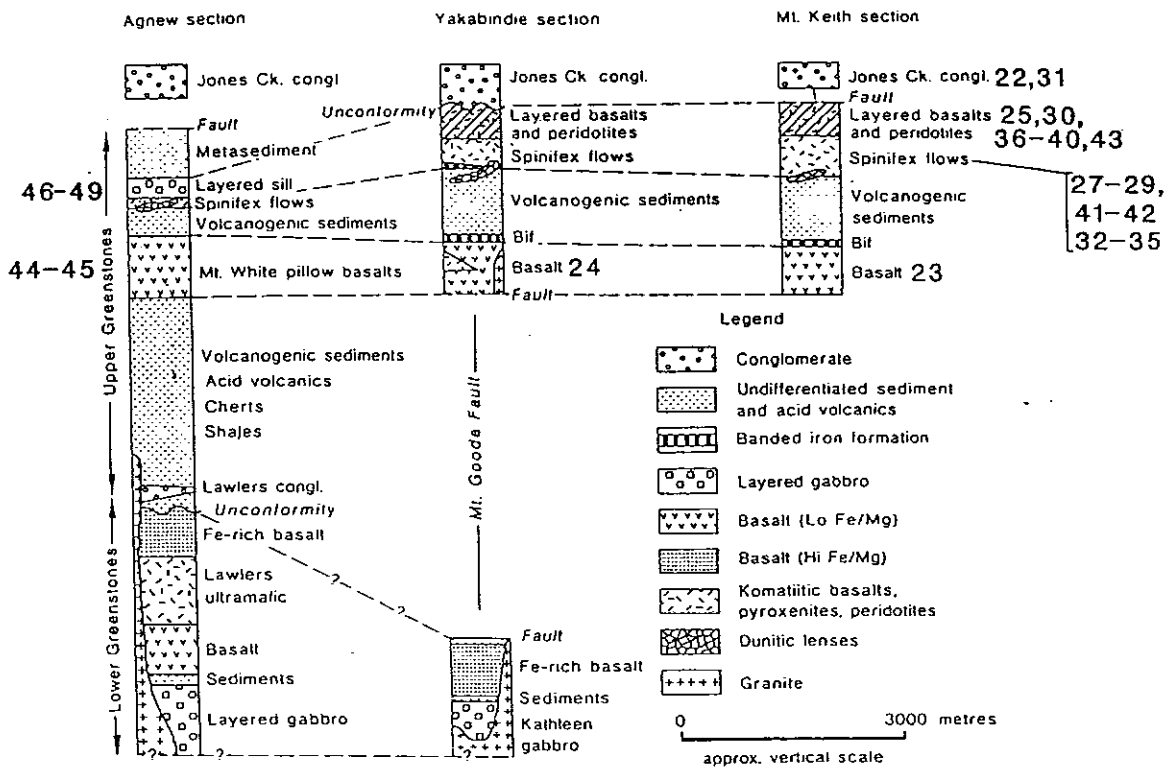
Agnew section
Yakabindie section
Mt. Keith section
Jones Ck. congl
Unconformity
Fault
Metasediment
46-49
Layered sill
Spinifex flows
Volcanogenic sediments
44-45
Mt. White pillow basalts
Upper Greenstones
Volcanogenic sediments
Acid volcanics
Cherts
Shales
Lawlers congl.
Unconformity
Fe-rich basalt
Lawlers ultramafic
Basalt
Sediments
Layered gabbro
Lower Greenstones
Mt. Goode Fault
Jones Ck congl.
Layered basalts and peridotites
Spinifex flows
Volcanogenic sediments
Bif
Basalt 24
Fault
Fault
Fe-rich basalt
Sediments
Kathleen gabbro
Jones Ck. congl. 22,31
Fault
Layered basalts and peridotites 25,30, 36-40,43
Spinifex flows
27-29, 41-42 32-35
Volcanogenic sediments
Bif
Basalt 23
Legend
Conglomerate
Undifferentiated sediment and acid volcanics
Banded iron formation
Layered gabbro
Basalt (Lo Fe/Mg)
Basalt (Hi Fe/Mg)
Komatiitic basalts, pyroxenites, peridotites
Dunitic lenses
Granite
0
3000 metres
approx. vertical scale

Figure 2. Internal structure of a spinifex komatiite flow (after Arndt, 1977).

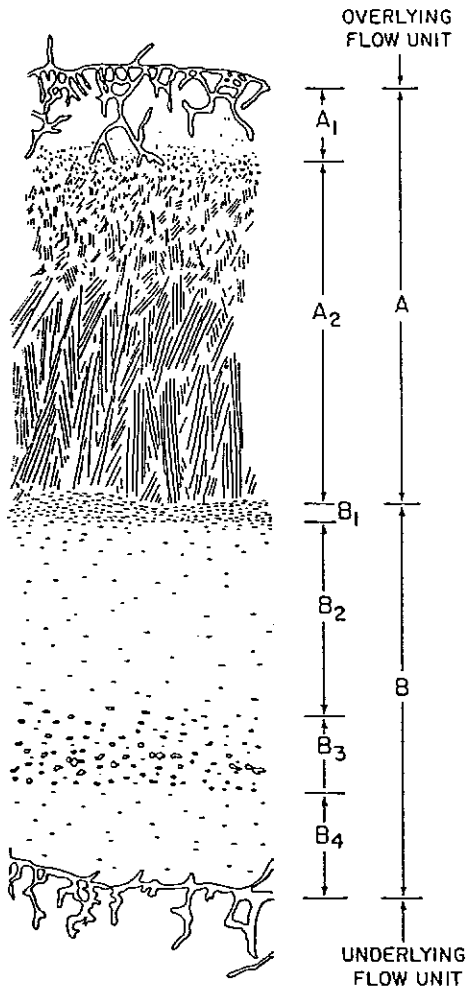

A_1 Chilled and fractured flow top

A_2 Spinifex

B_1 Foliated skeletal olivine

B_2–B_4 Medium- to fine-grained peridotite

B_3 Knobby peridotite

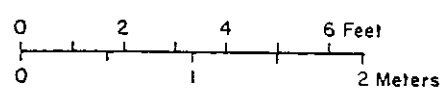

Figure 3. Composition of ilmenites in a ternary plot of the end members ilmenite, pyrophanite and haematite (mole %). Legend is olivine orthocumulate crosses; olivine mesocumulate diamonds; talc-carbonate rock squares; chlorite-carbonate rock triangles; gabbro stars.

CSIRO

DIVISION OF
EXPLORATION
GEOSCIENCE

21-NOV-90

LEGEND

Squares	Talc-carbonate rock
Triangles	Chlorite-carbonate rock
Crosses	Olivine orthocumulate
Diamonds	Olivine mesocumulate
Stars	Gabbro

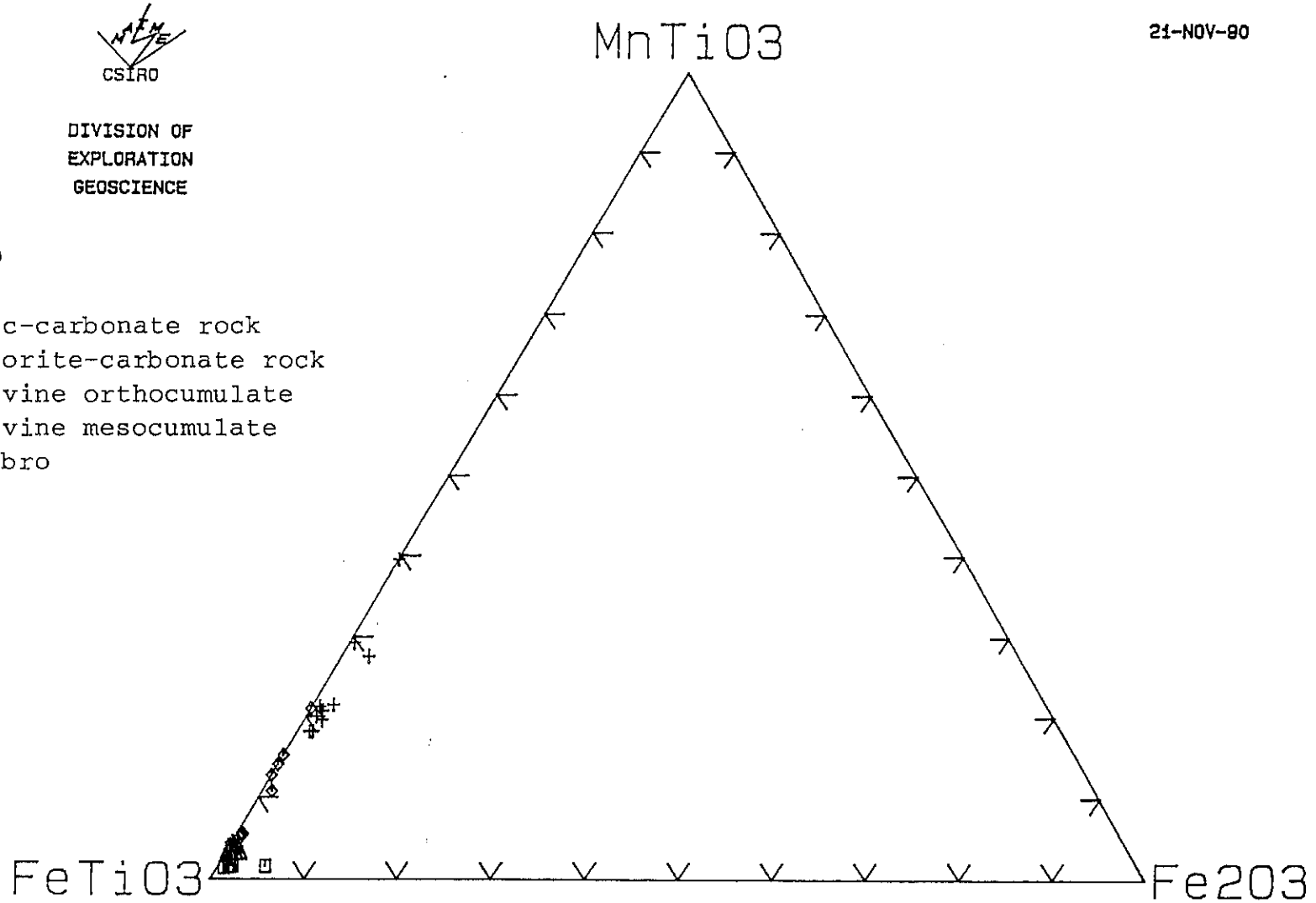

Figure 4. A. Backscattered electron image of altered chromite showing zoning from a dark aluminous chromite core to light grey magnetite on the rim. Diameter of grain is 200 μm.
B. X-ray map for aluminium of the above grain showing the decrease in aluminium towards the rim.

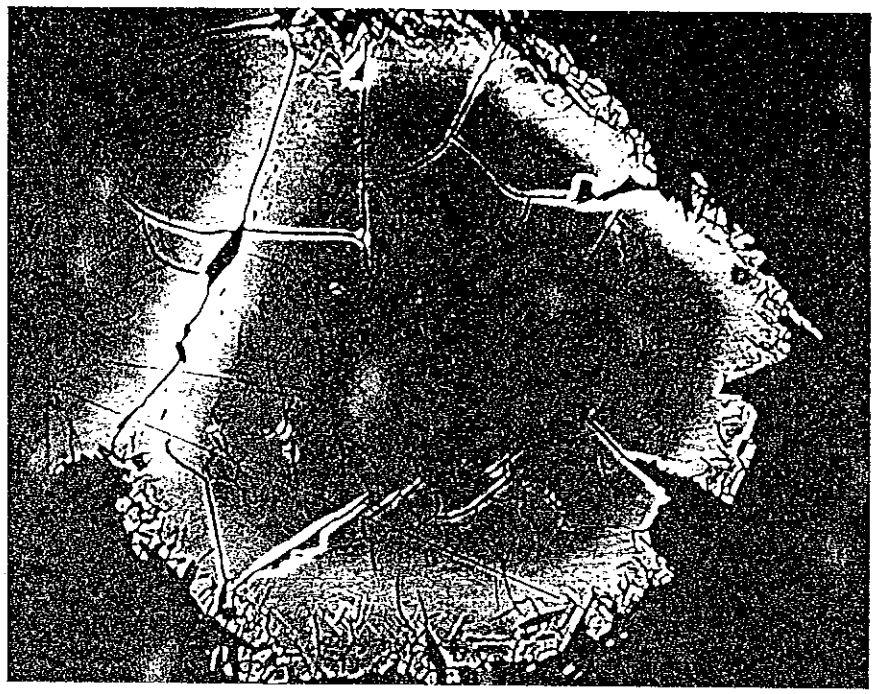

A

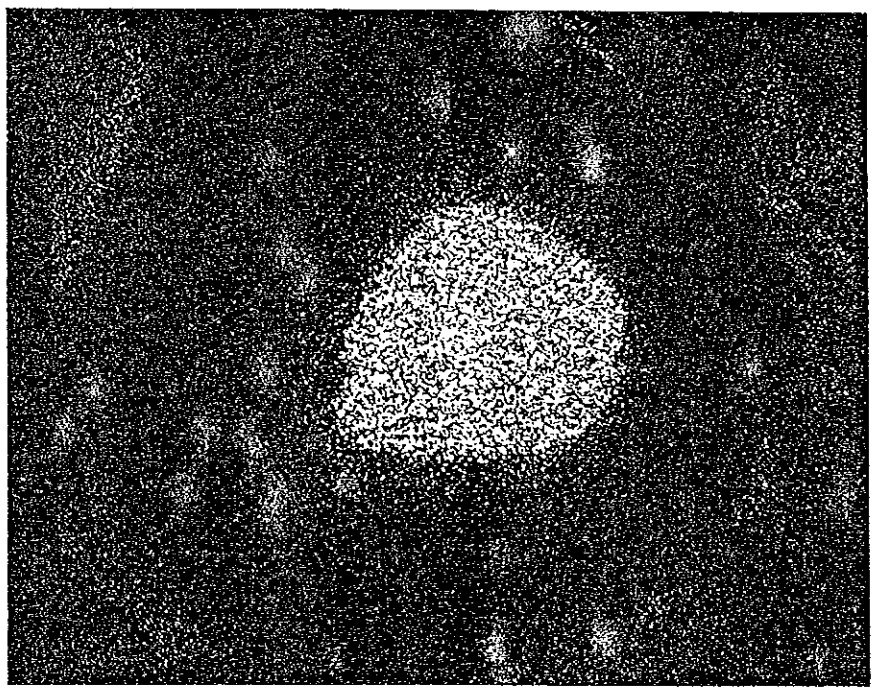

B

Figure 5. Composition of spinels in the "oxidised" spinel prism. Legend is olivine adcumulate triangles; olivine mesocumulate diamonds; talc-carbonate rock squares; chlorite-carbonate rock triangles; gabbro stars.

CSIRO

DIVISION OF
EXPLORATION
GEOSCIENCE

21-NOV-90

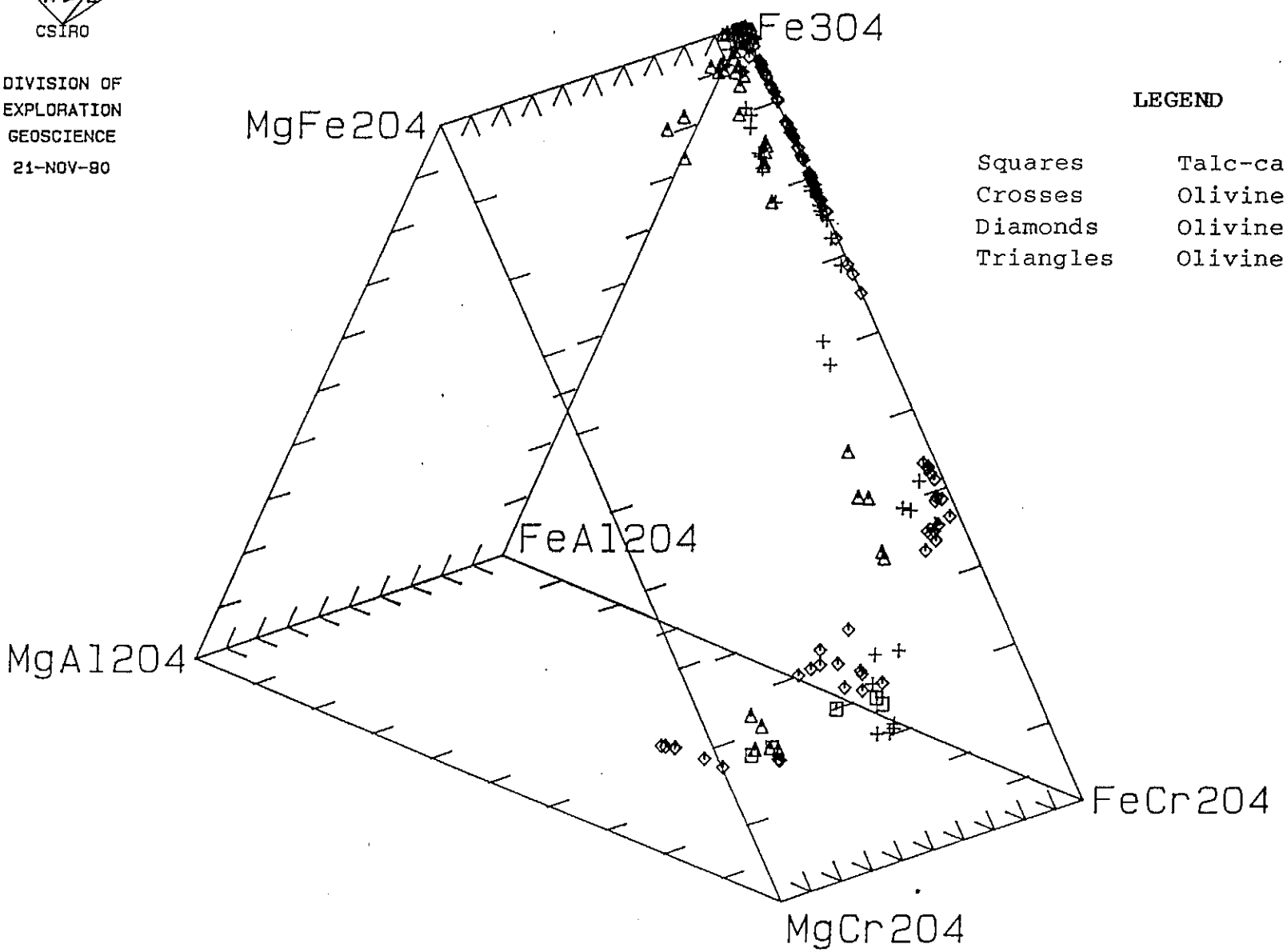

LEGEND

Squares	Talc-carbonate rock
Crosses	Olivine orthocumulate
Diamonds	Olivine mesocumulate
Triangles	Olivine adcumulate

Fig.6. Susceptibility, remanent intensity and Koenigsberger ratio of magnetic minerals as a function of domain state and remanence type. The properties apply to dispersed grains, but kand J are normalised to unit volume.

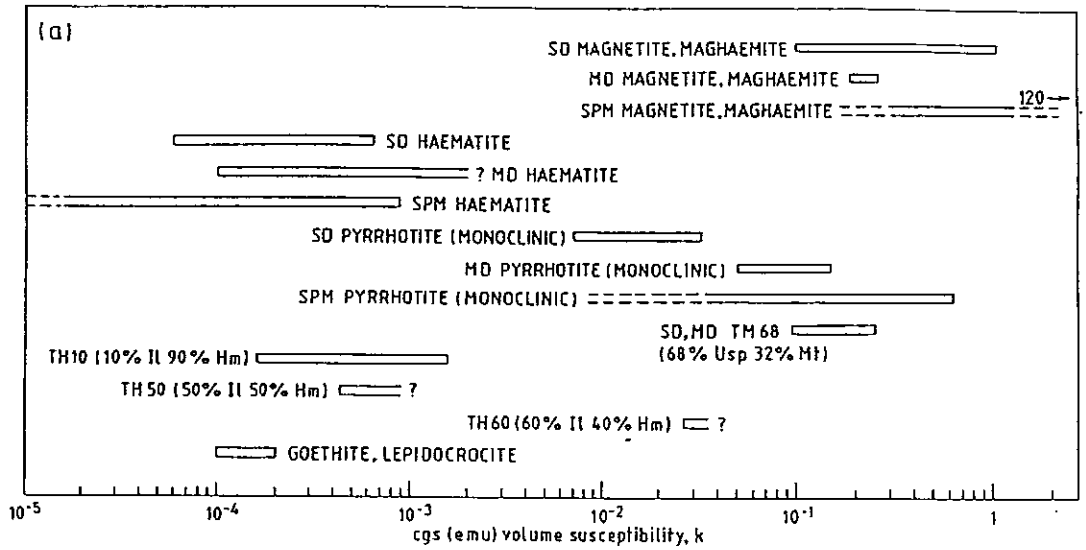
(a)
SD MAGNETITE, MAGHAEMITE
MD MAGNETITE, MAGHAEMITE
SPM MAGNETITE, MAGHAEMITE
120
SD HAEMATITE
? MD HAEMATITE
SPM HAEMATITE
SD PYRRHOTITE (MONOCLINIC)
MD PYRRHOTITE (MONOCLINIC)
SPM PYRRHOTITE (MONOCLINIC)
SD, MD TM 68
(68% Usp 32% Mt)
TH10 (10% Il 90% Hm)
TH 50 (50% Il 50% Hm) ?
TH60 (60% Il 40% Hm) ?
GOETHITE, LEPIDOCROCITE
10-5
10-4
10-3
10-2
10-1
1
cgs (emu) volume susceptibility, k

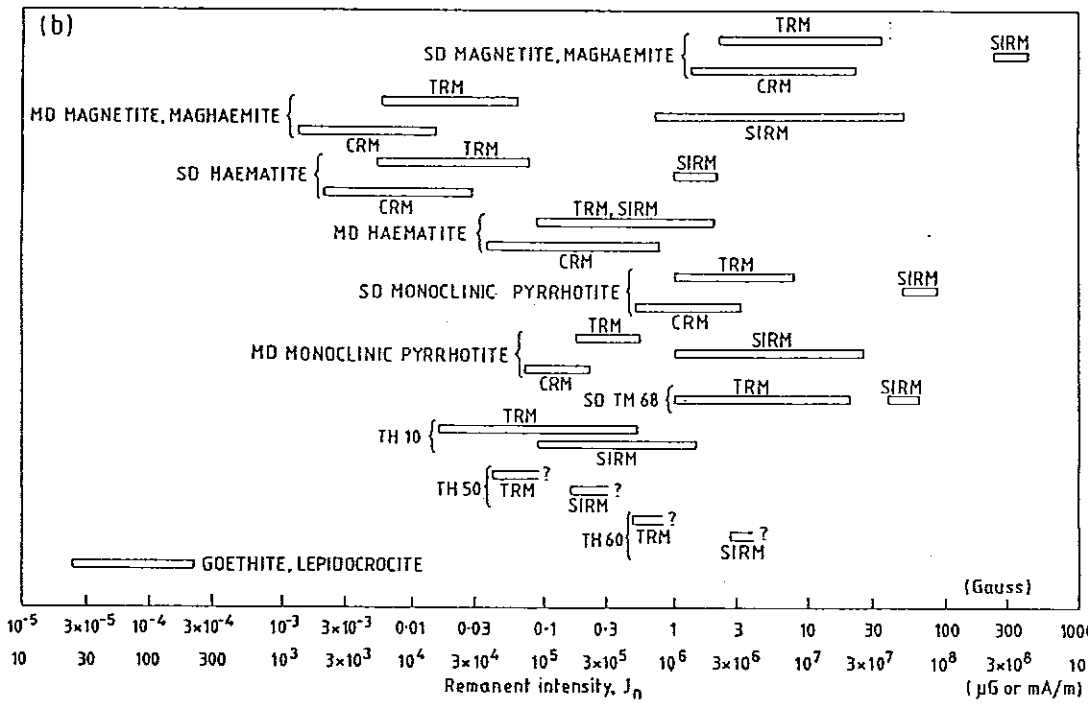
(b)
SD MAGNETITE, MAGHAEMITE
MD MAGNETITE, MAGHAEMITE
SD HAEMATITE
MD HAEMATITE
SD MONOCLINIC PYRRHOTITE
MD MONOCLINIC PYRRHOTITE
SD TM 68
TH 10
TH 50
TH 60
GOETHITE, LEPIDOCROCITE
TRM
CRM
SIRM
TRM, SIRM
(Gauss)
10-5 3×10-5 10-4 3×10-4 10-3 3×10-3 0·01 0·03 0·1 0·3 1 3 10 30 100 300 1000
10 30 100 300 10³ 3×10³ 10⁴ 3×10⁴ 10⁵ 3×10⁵ 10⁶ 3×10⁶ 10⁷ 3×10⁷ 10⁸ 3×10⁸ 10⁹
Remanent intensity, Jn
(μG or mA/m)

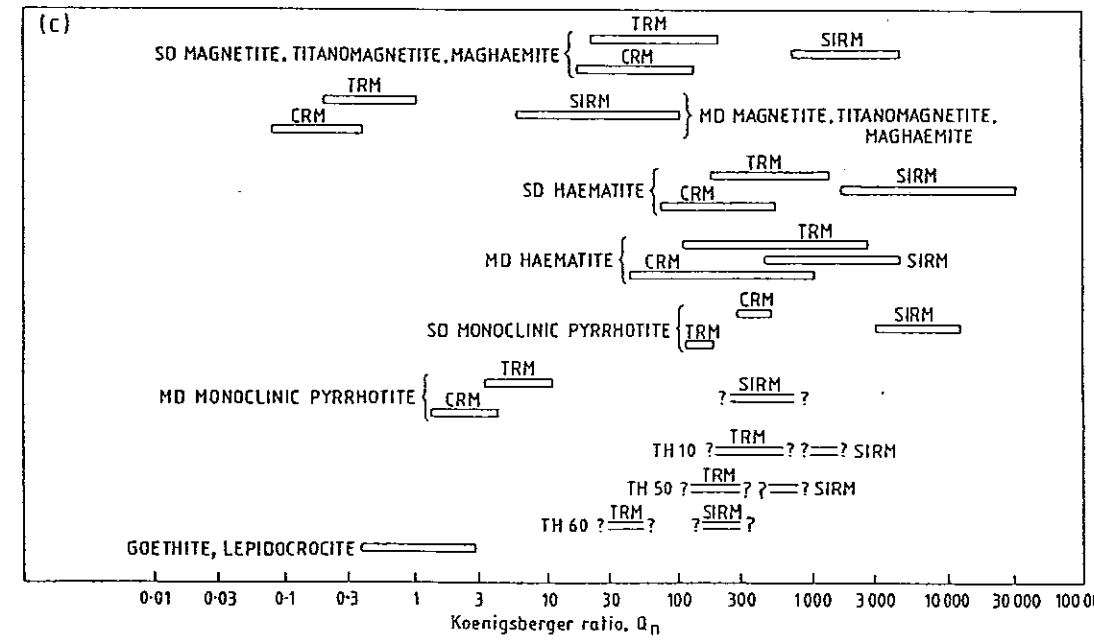
(c)
SD MAGNETITE, TITANOMAGNETITE, MAGHAEMITE
MD MAGNETITE, TITANOMAGNETITE, MAGHAEMITE
SD HAEMATITE
MD HAEMATITE
SD MONOCLINIC PYRRHOTITE
MD MONOCLINIC PYRRHOTITE
TH 10
TH 50
TH 60
GOETHITE, LEPIDOCROCITE
TRM
CRM
SIRM
0·01 0·03 0·1 0·3 1 3 10 30 100 300 1000 3000 10000 30000 100000
Koenigsberger ratio, Qn

Fig.7 Principle of Zijderveld plots of demagnetisation data. The remanence vector is remeasured after successive demagnetisation steps.

(a) Successive remanence vectors, showing initial removal of a low stability component (linear segment), followed by simultaneous removal of two components with overlapped stability spectra (curved trajectory) and, finally, removal of the most stable component (linear segment, heading towards the origin).

(b) By simply plotting the vector end-points the diagram is clarified. However the directions of the low and high stability components are not very clear from this single diagram.

(c) The NRM as the resultant of soft and hard remanence components. When the directions of the components have been determined by fitting straight lines to the soft and hard segments, the intensities of each component can be calculated.

(d) By projecting the vector end-points onto orthogonal planes, the horizontal plane and either the N-S or the E-W vertical plane, the directions of the remanence components can be visualised. Corresponding segments that are linear in both projections indicate linear trajectories in 3-space, i.e. single remanence components. When a segment is curved in at least one projection, more than one component is being removed by the demagnetisation. If the linear segments representing the most stable resolved component are bypassing the origin, this indicates the presence of a harder unresolved component.

ORTHOGONAL PROJECTIONS (ZIJDERVELD PLOTS)

(a) Successive remanence vectors

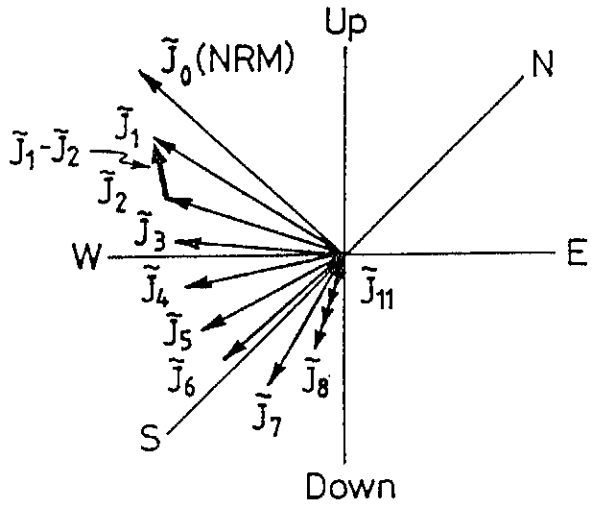

(b) Vector end-points

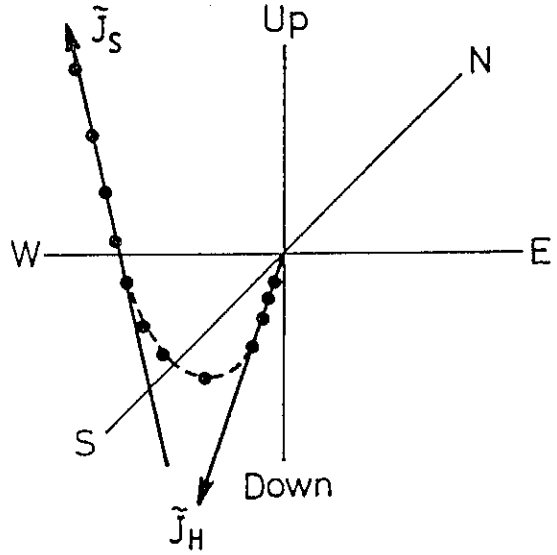

(c) Decomposition of two-component NRM

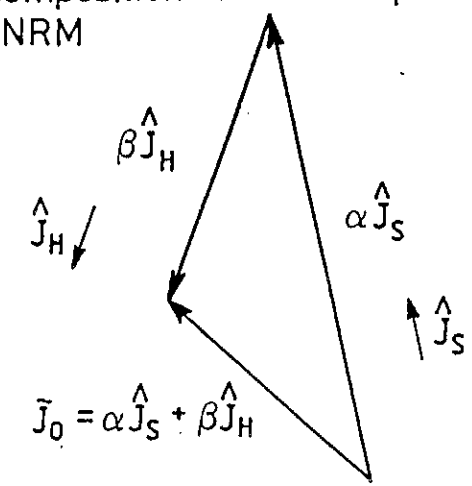

(d) Orthogonal projections

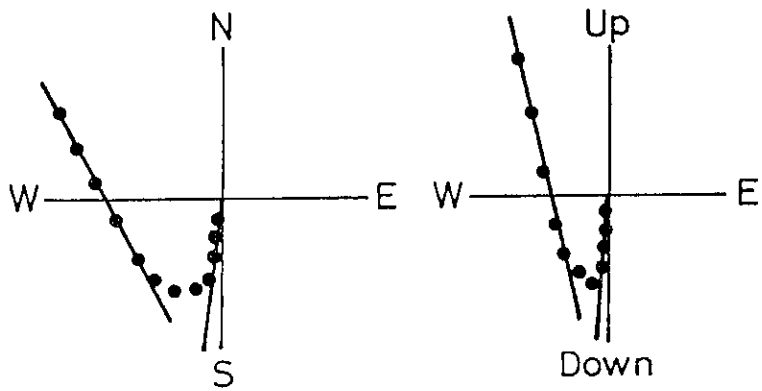

Fig.8 Characteristic AF demagnetisation curves of acicular single domain (SD), small pseudosingle domain (PSD) and large multidomain (MD) grains of magnetite. The corresponding grain sizes are submicron, one to several microns and greater than 100 μm respectively.

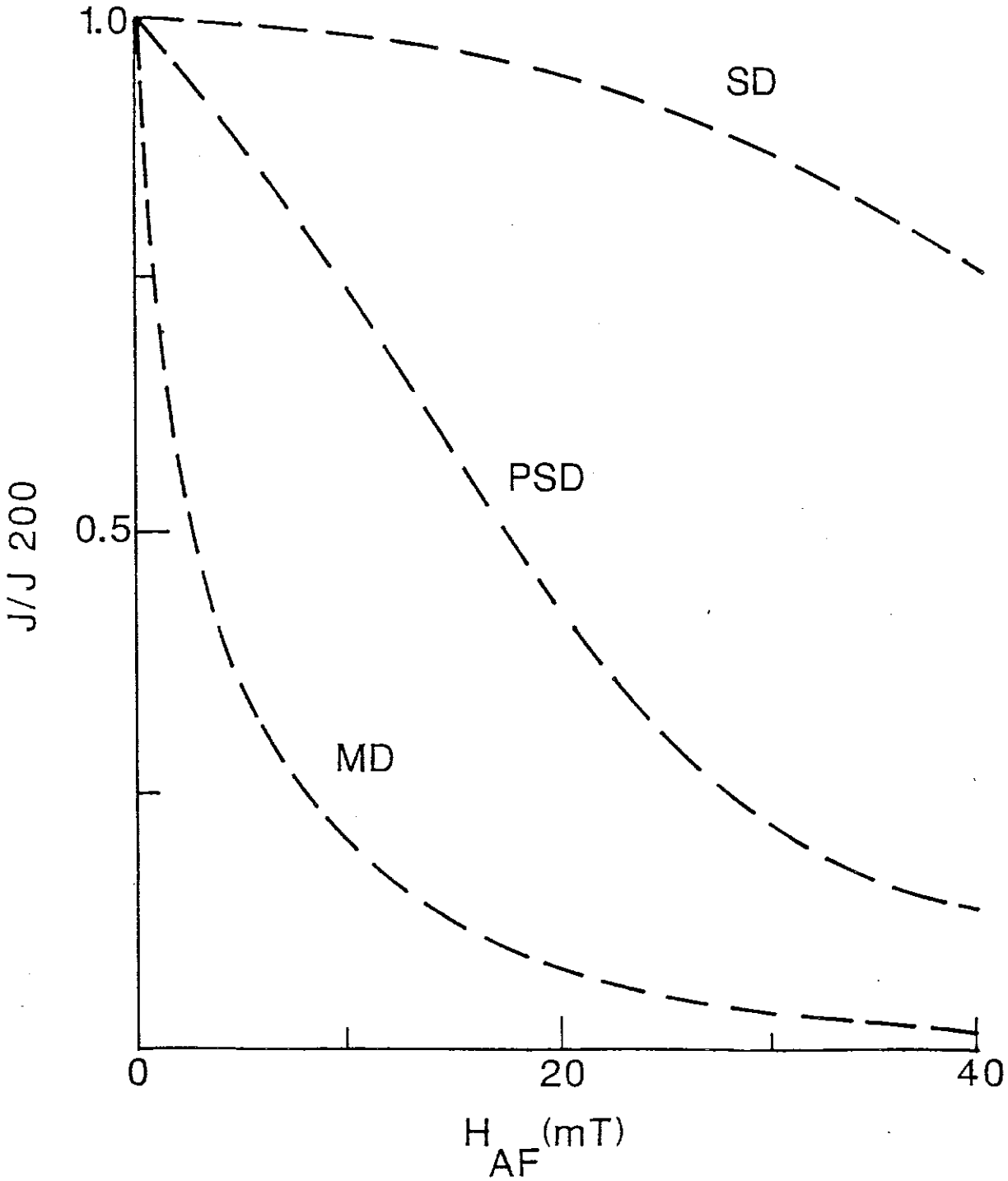
1.0
0.5
J/J 200
SD
PSD
MD
0
20
40
H AF (mT)

Fig.9 Characteristic normalised k-T curves of paramagnetic, superparamagnetic, titanomagnetite, SD magnetite and MD magnetite grains.

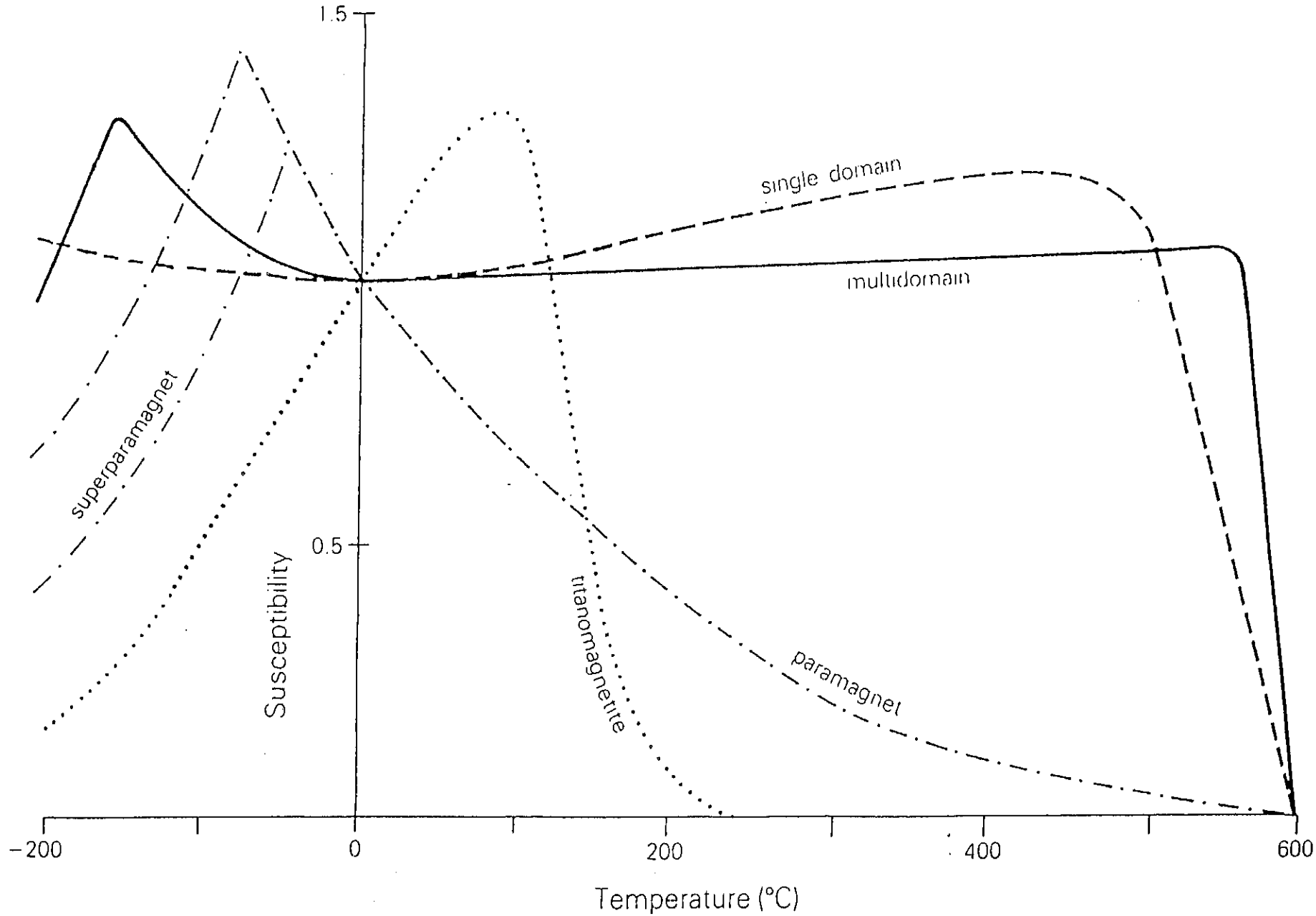
1.5
0.5
single domain
multidomain
superparamagnet
titanomagnetite
paramagnet
Susceptibility
−200
0
200
400
600
Temperature (°C)

Fig.10 Typical k-T curves of a monzonite containing MD magnetite and a basalt containing titanomagnetite (60 mole% t

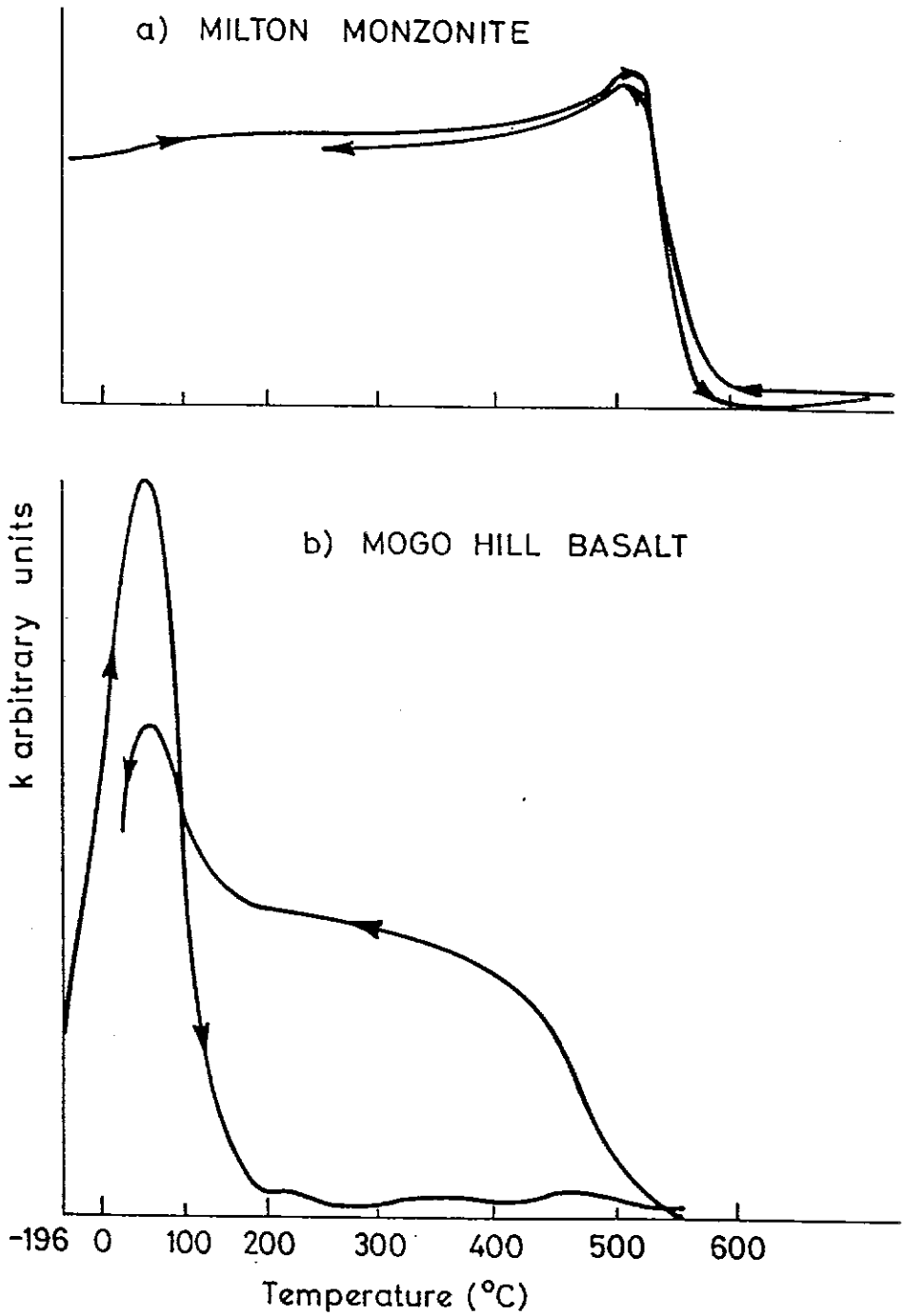
a) MILTON MONZONITE
b) MOGO HILL BASALT
k arbitrary units
-196
0
100
200
300
400
500
600
Temperature (°C)

Fig.11 k-T curve of an ilmenite separate from a beach sand. The irreversibility of the curve on cooling indicates chemical change has occurred during heating. The ilmenite is paramagnetic over the whole temperature range examined and exhibits a 1/T dependence of susceptibility at low temperatures.

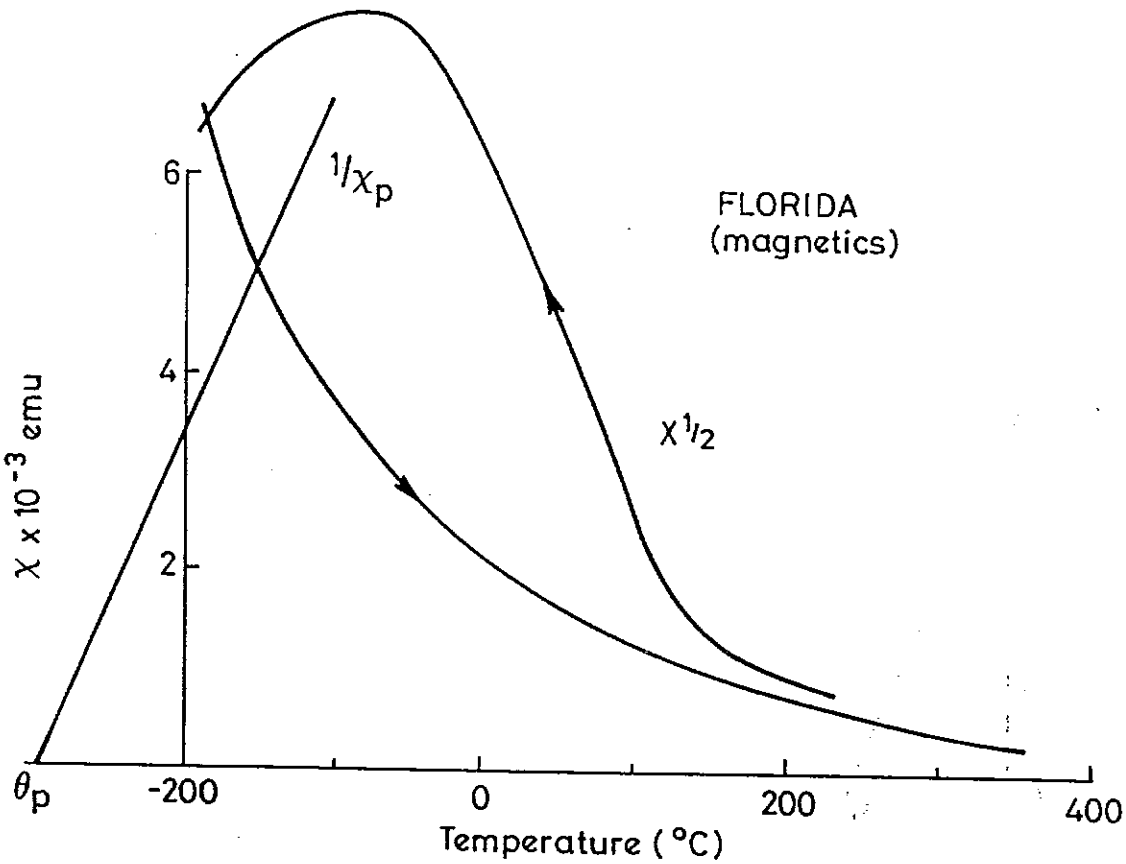
6
4
2
$\chi \times 10^{-3}$ emu
$1/\chi_p$
FLORIDA
(magnetics)
$\chi^{1/2}$
θ_p
-200
0
200
400
Temperature (°C)

Fig.12 Diagnostic k-T curves of some iron ores. Labelled features are: (a) the isotropic point of magnetite (-155°C), characteristic of MD or PSD pure magnetite; (b) the Morin transition (-20°C), indicating well-crystallised pure haematite; (c) the unblocking peak, immediately preceeding the steep descent to the Curie point. The Curie points are 580°C for magnetite and 670°C for haematite. The Curie point for cation-deficient magnetite (kenomagnetite) is variable, but is often ~610°C. The samples are: DDH 42/ 300.5 = BIF containing MD magnetite; TP01B = haematite ore with minor MD magnetite (which dominates the susceptibility); MN01B = haematite ore with minor SD magnetite; Channar = haematite ore with minor MD magnetite; PB01B = pure haematite ore; CANGA = pisolitic laterite containing SPM and SD kenomagnetite.

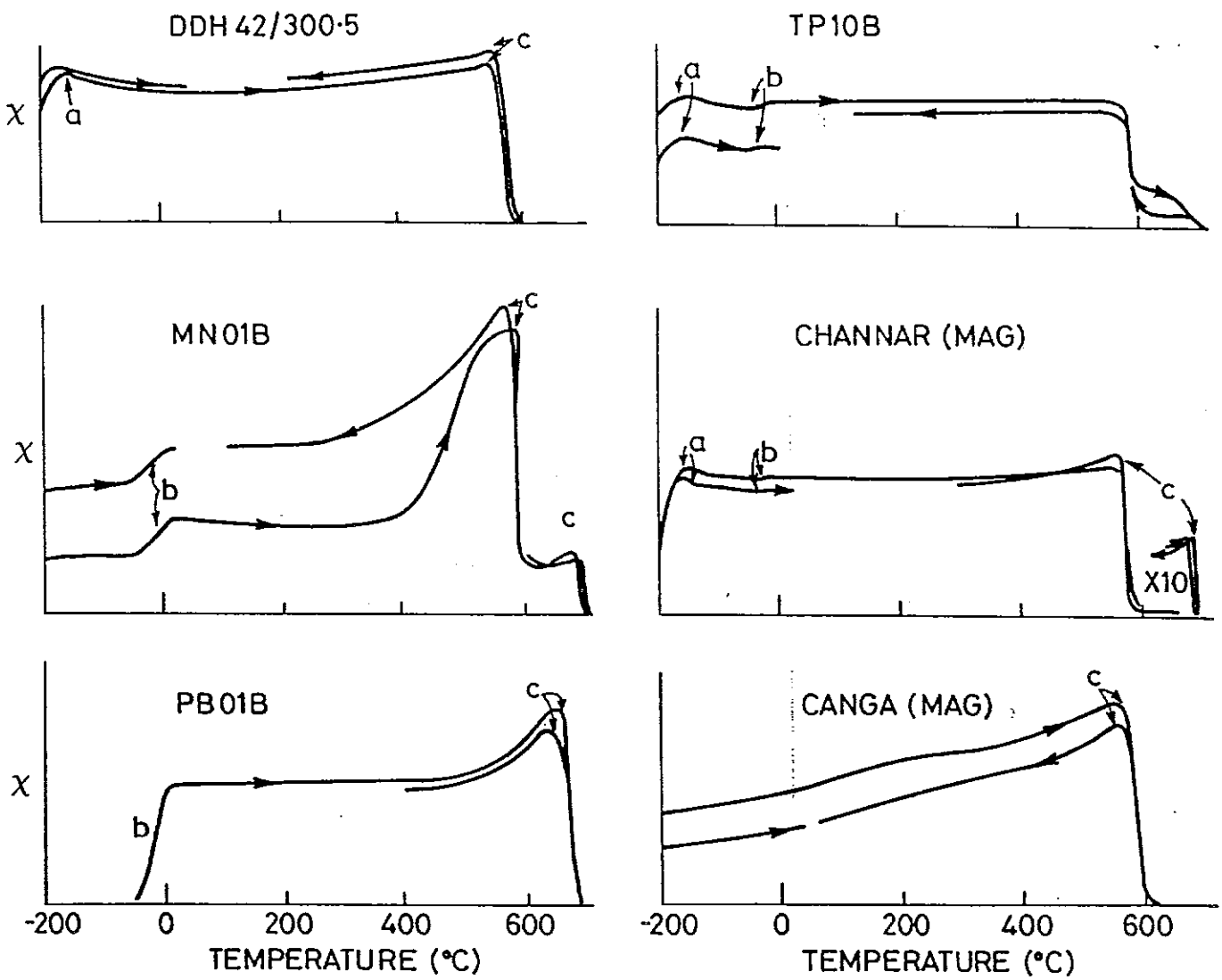
DDH 42/300·5
TP10B
MN01B
CHANNAR (MAG)
PB01B
CANGA (MAG)
χ
a
b
c
X10
-200
0
200
400
600
TEMPERATURE (°C)

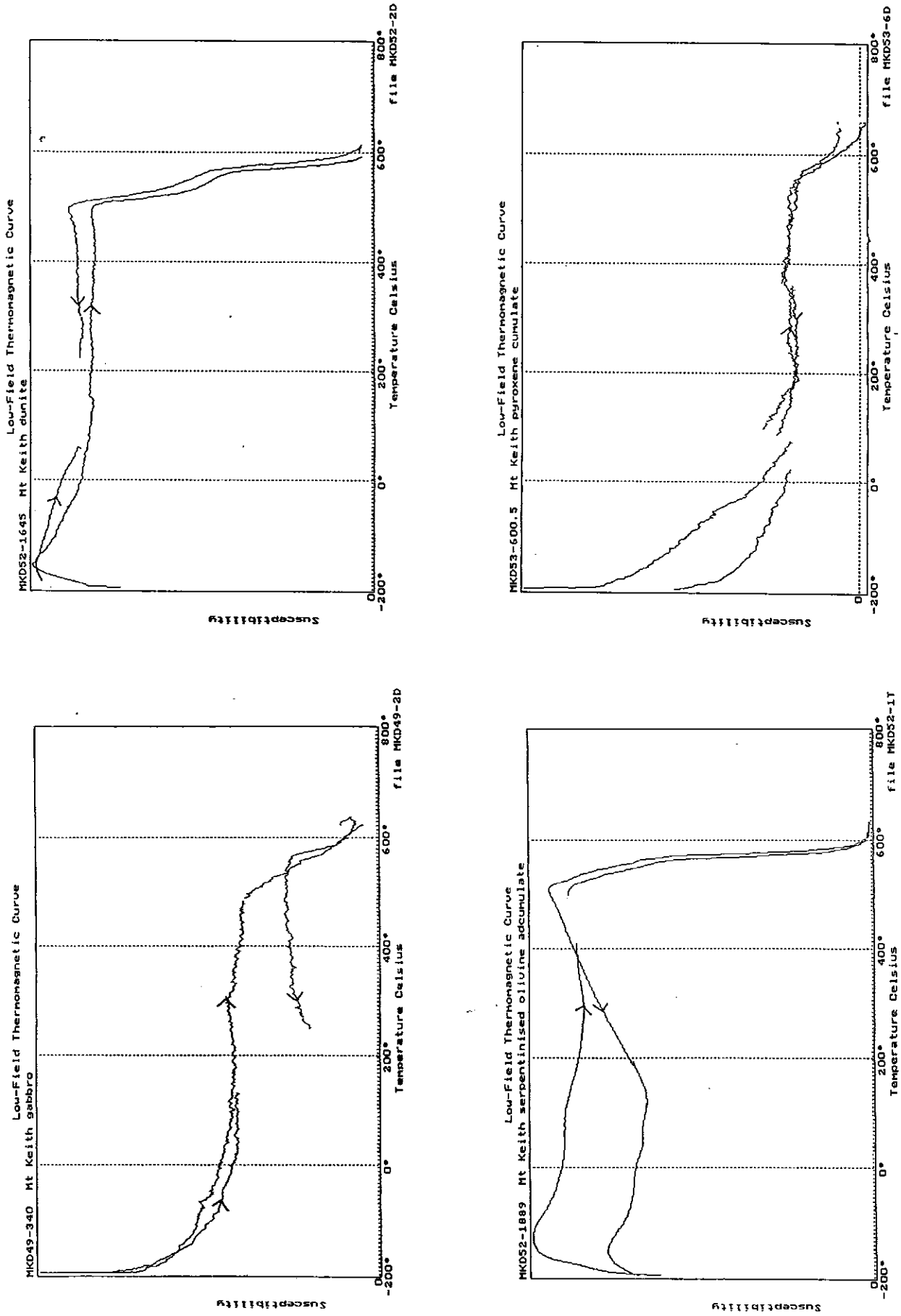

Fig.13 k-T curves for DDH samples

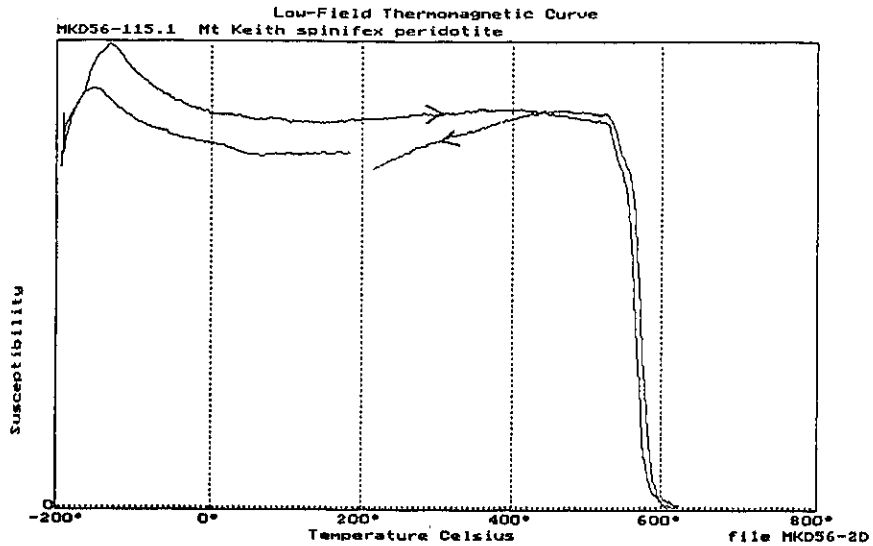
Low-Field Thermonagnetic Curve
MKD56-115.1 Mt Keith spinifex peridotite
Susceptibility
0
-200°
0°
200°
400°
600°
800°
Temperature Celsius
file MKD56-2D

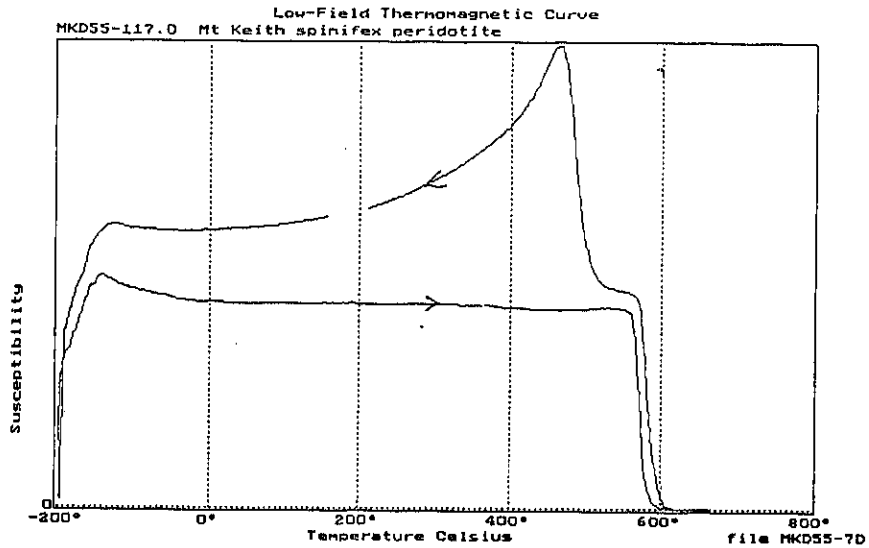
Low-Field Thermonagnetic Curve
MKD55-117.0 Mt Keith spinifex peridotite
Susceptibility
0
-200°
0°
200°
400°
600°
800°
Temperature Celsius
file MKD55-7D

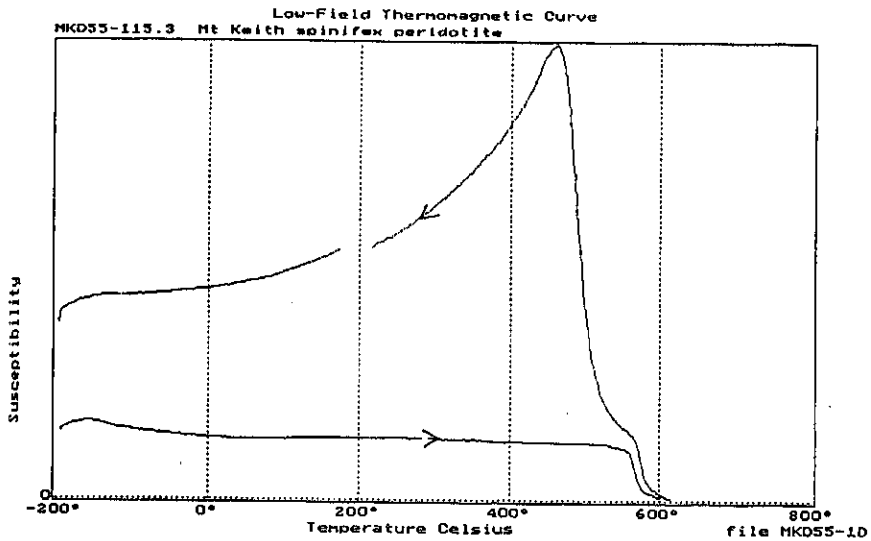
Low-Field Thermonagnetic Curve
MKD55-115.3 Mt Keith spinifex peridotite
Susceptibility
0
-200°
0°
200°
400°
600°
800°
Temperature Celsius
file MKD55-1D

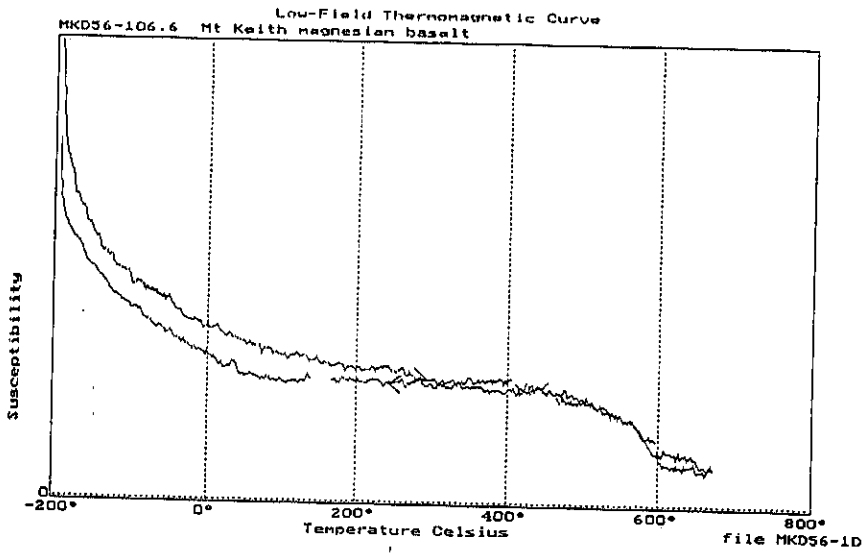
Low-Field Thermonagnetic Curve
MKD56-106.6 Mt Keith magnesian basalt
Susceptibility
0
-200°
0°
200°
400°
600°
800°
Temperature Celsius
file MKD56-1D

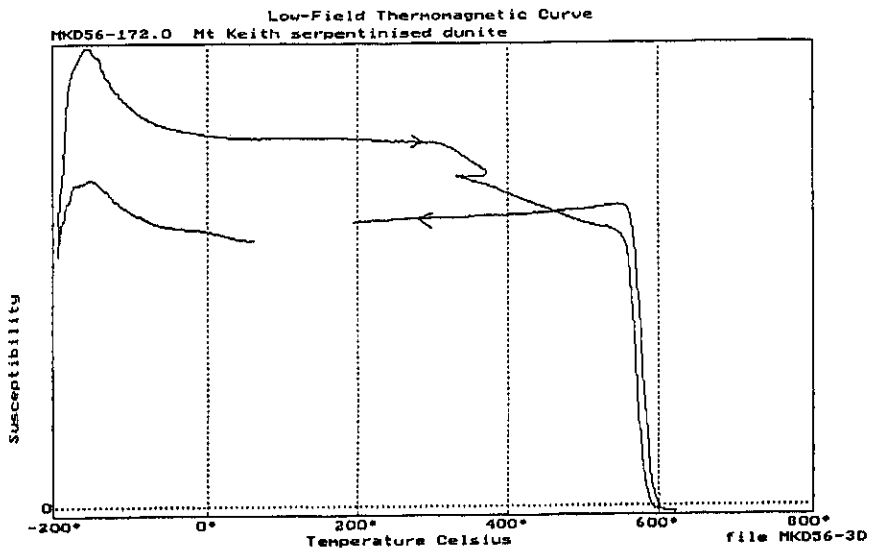
Low-Field Thermomagnetic Curve
MKD56-172.0 Mt Keith serpentinised dunite
Susceptibility
0
-200°
0°
200°
400°
600°
800°
Temperature Celsius
file MKD56-3D

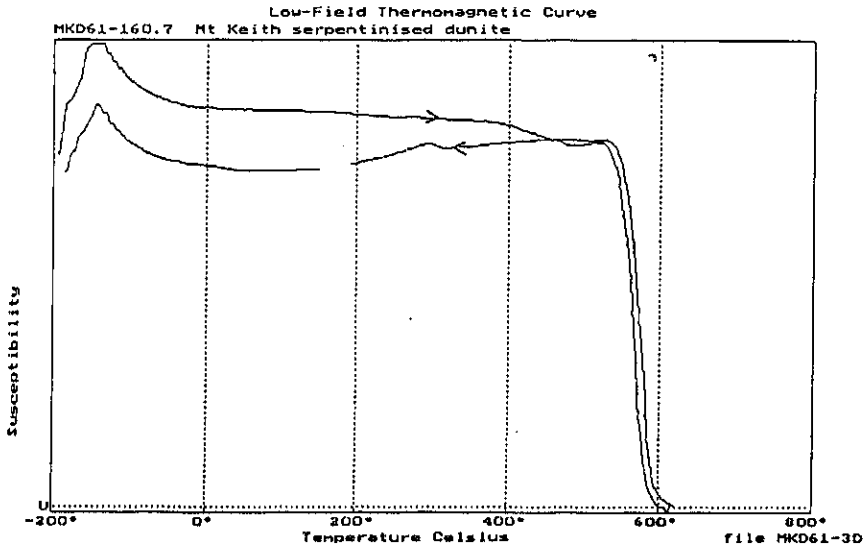
Low-Field Thermomagnetic Curve
MKD61-160.7 Mt Keith serpentinised dunite
Susceptibility
0
-200°
0°
200°
400°
600°
800°
Temperature Celsius
file MKD61-3D

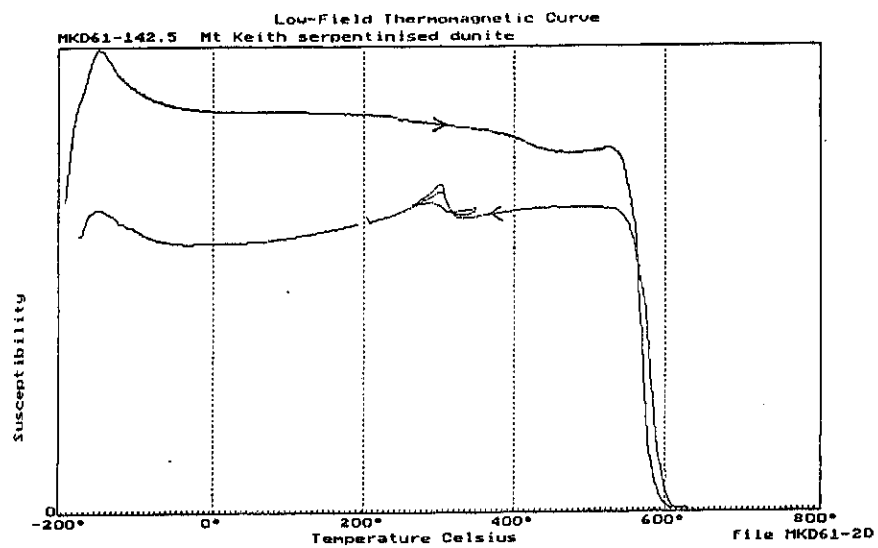
Low-Field Thermomagnetic Curve
MKD61-142.5 Mt Keith serpentinised dunite
Susceptibility
0
-200°
0°
200°
400°
600°
800°
Temperature Celsius
file MKD61-2D

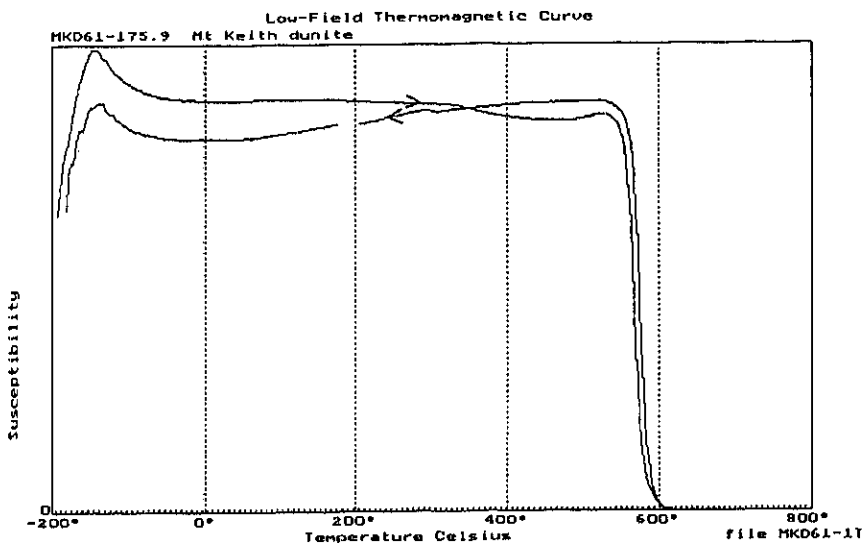
Low-Field Thermomagnetic Curve
MKD61-175.9 Mt Keith dunite
Susceptibility
0
-200°
0°
200°
400°
600°
800°
Temperature Celsius
file MKD61-1T

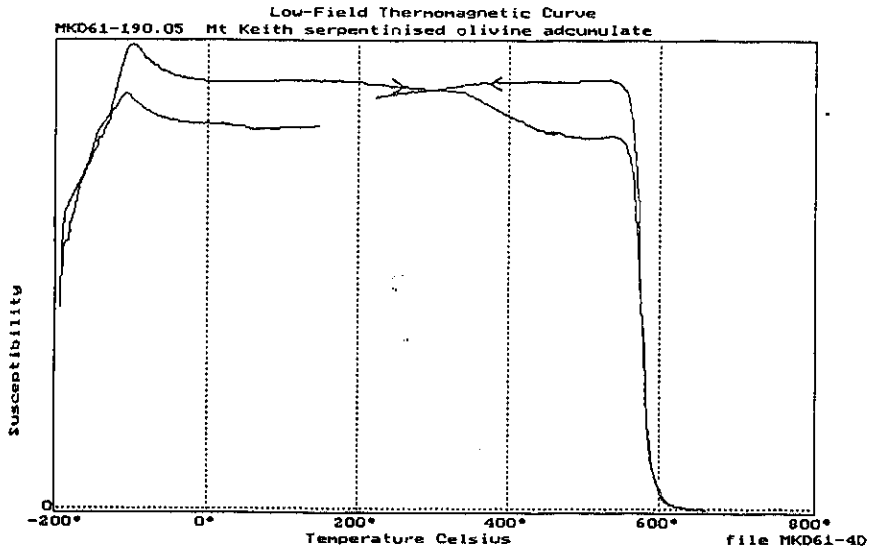
Low-Field Thermomagnetic Curve
MKD61-190.05 Mt Keith serpentinised olivine adcumulate
Susceptibility
0
-200°
0°
200°
400°
600°
800°
Temperature Celsius
file MKD61-4D

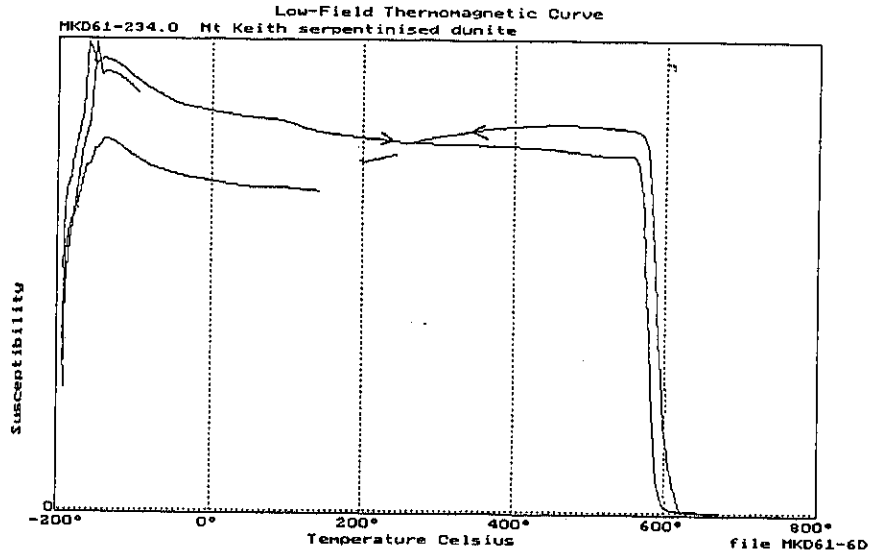
Low-Field Thermomagnetic Curve
MKD61-234.0 Mt Keith serpentinised dunite
Susceptibility
0
-200°
0°
200°
400°
600°
800°
Temperature Celsius
file MKD61-6D

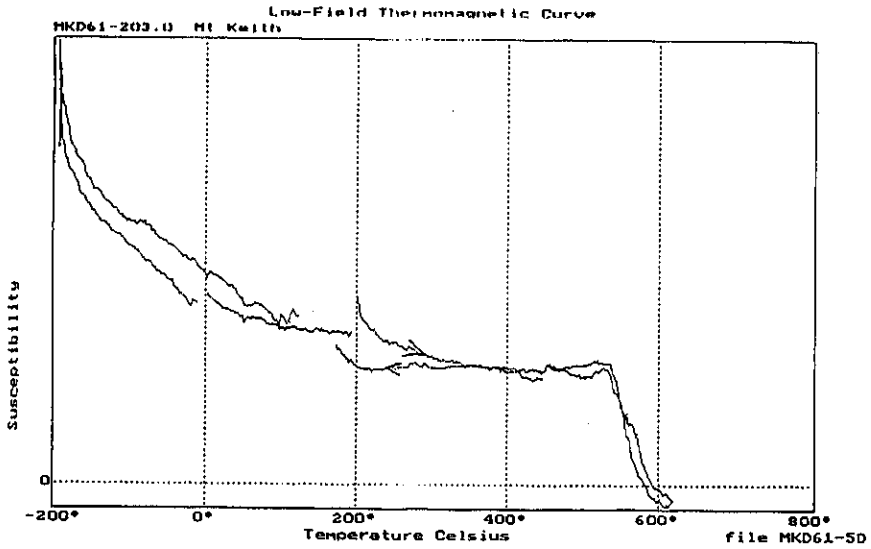
Low-Field Thermomagnetic Curve
MKD61-203.0 Mt Keith
Susceptibility
0
-200°
0°
200°
400°
600°
800°
Temperature Celsius
file MKD61-5D

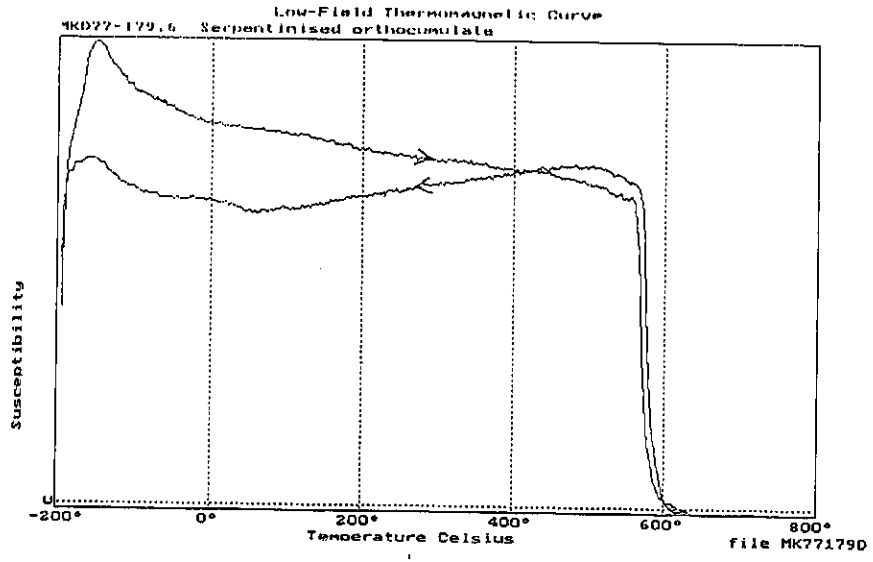
Low-Field Thermomagnetic Curve
MKD77-179.6 Serpentinised orthocumulate
Susceptibility
0
-200°
0°
200°
400°
600°
800°
Temperature Celsius
file MK77179D

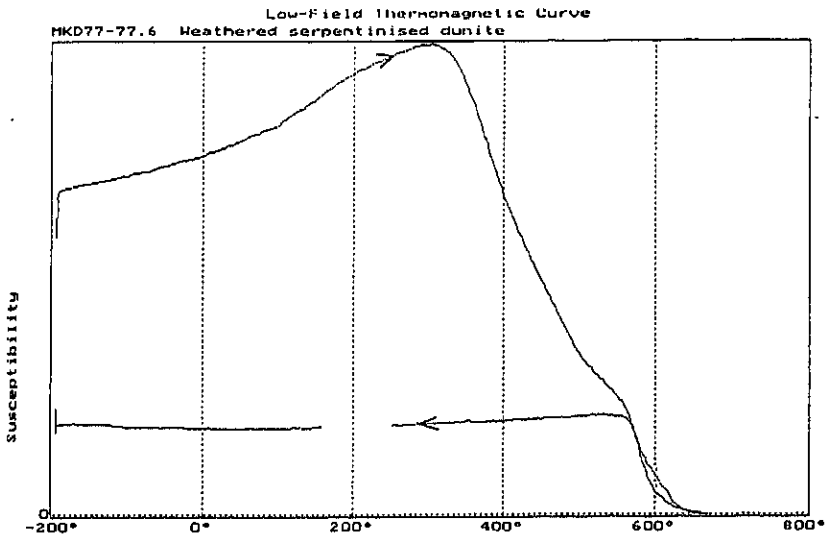
Low-Field Thermomagnetic Curve
MKD77-77.6 Weathered serpentinised dunite
Susceptibility
0
-200°
0°
200°
400°
600°
800°

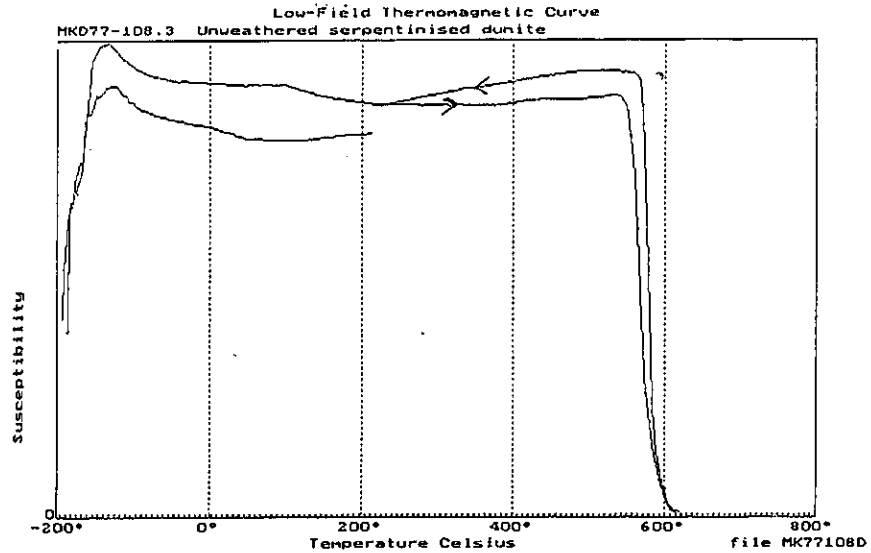
Low-Field Thermomagnetic Curve
MKD77-108.3 Unweathered serpentinised dunite
Susceptibility
0
-200°
0°
200°
400°
600°
800°
Temperature Celsius
file MK77108D

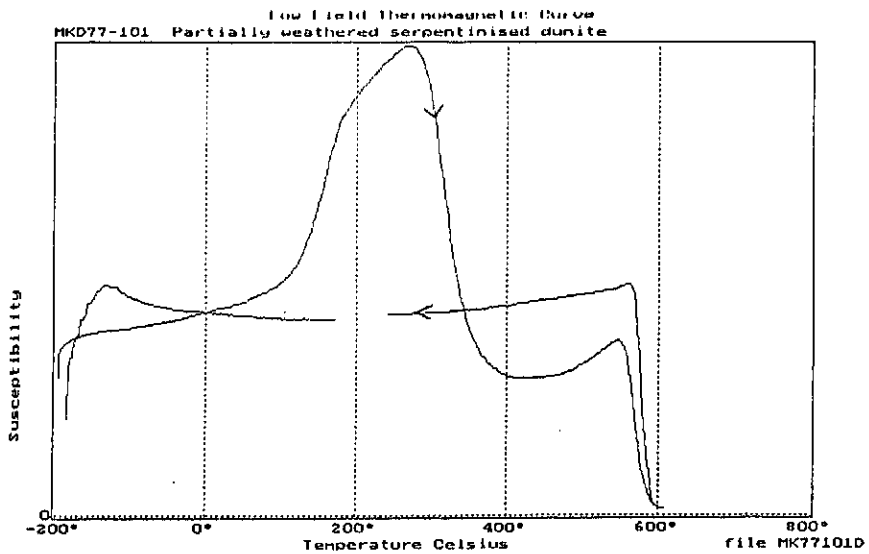
Low-Field Thermomagnetic Curve
MKD77-101 Partially weathered serpentinised dunite
Susceptibility
0
-200°
0°
200°
400°
600°
800°
Temperature Celsius
file MK77101D

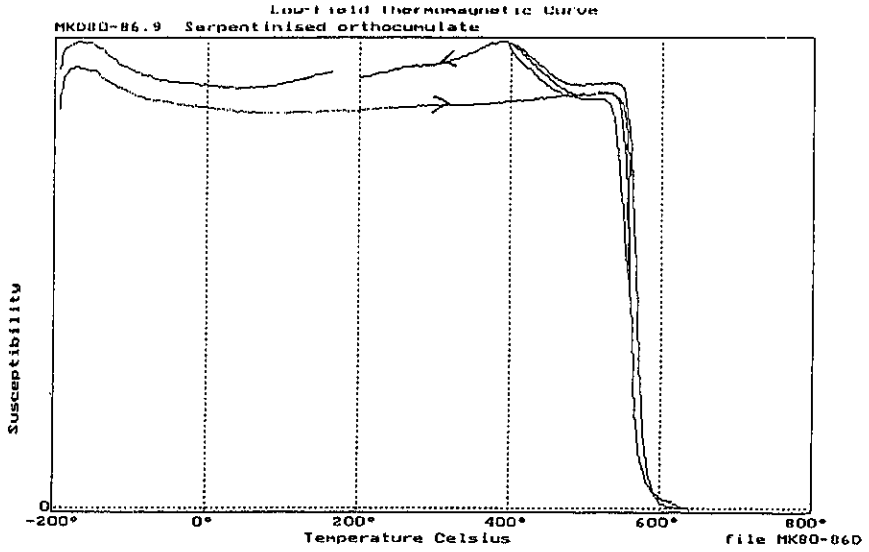
Low-Field Thermomagnetic Curve
MKD80-86.9 Serpentinised orthocumulate
Susceptibility
0
-200°
0°
200°
400°
600°
800°
Temperature Celsius
file MK80-86D

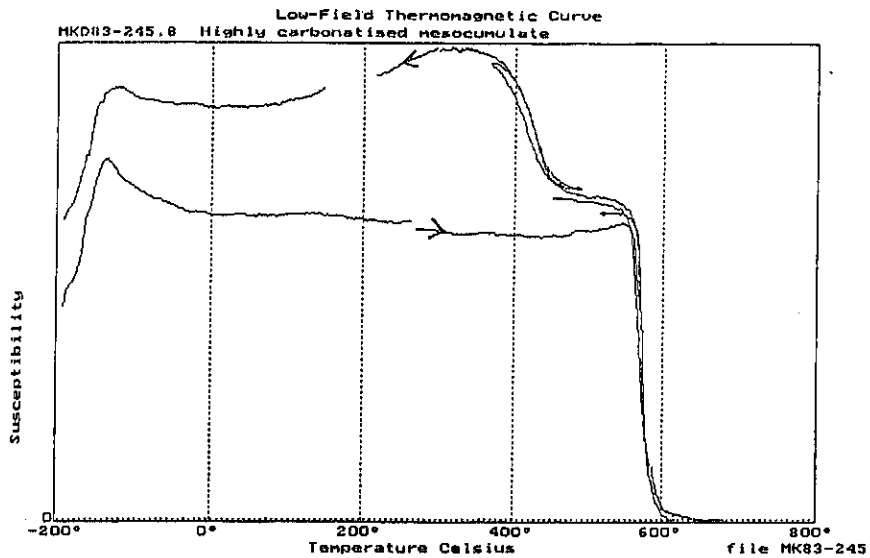
Low-Field Thermomagnetic Curve
MKD83-245.8 Highly carbonatised mesocumulate
Susceptibility
-200°
0°
200°
400°
600°
800°
Temperature Celsius
file MK83-245

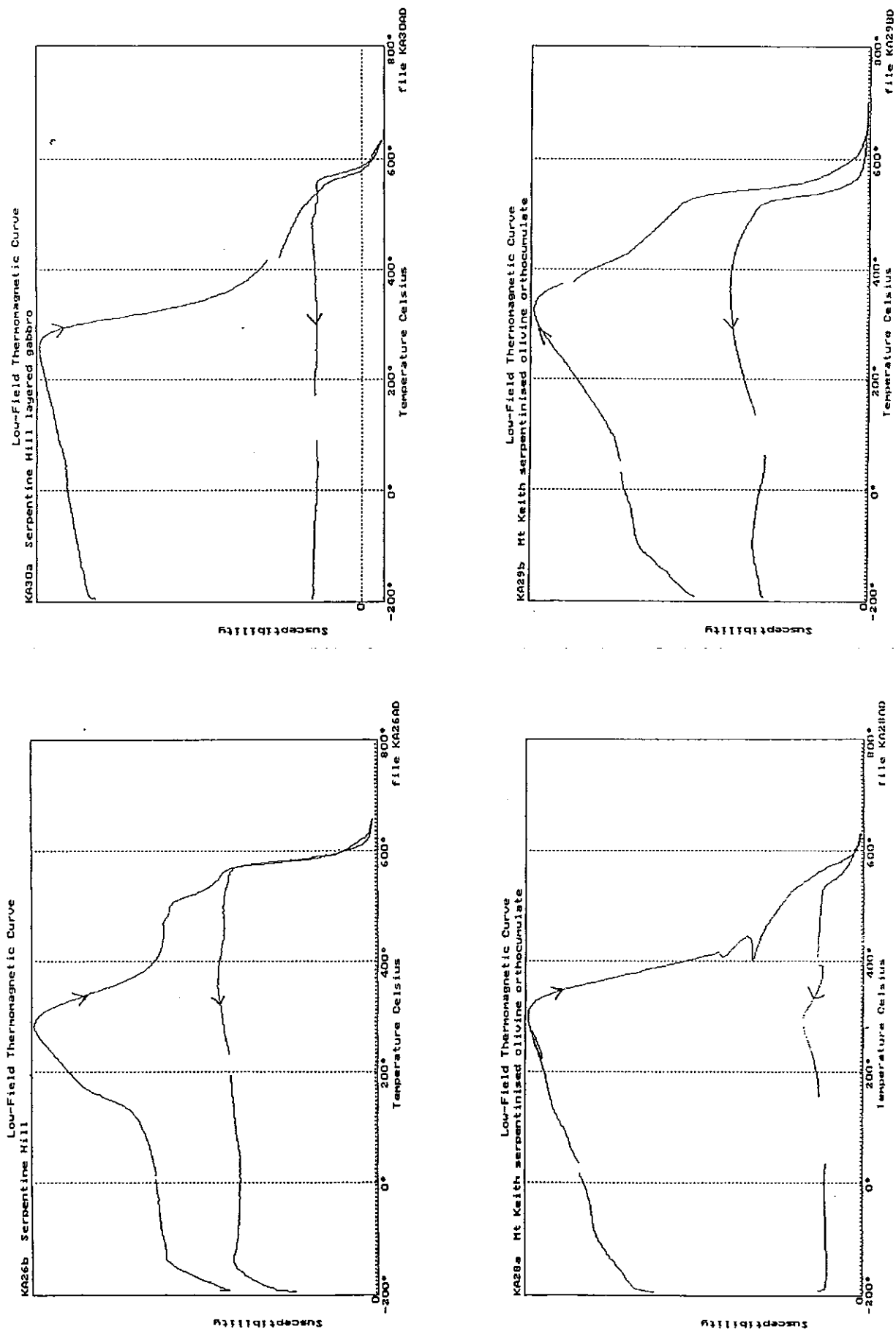

Fig.14 k-T curves for surface samples

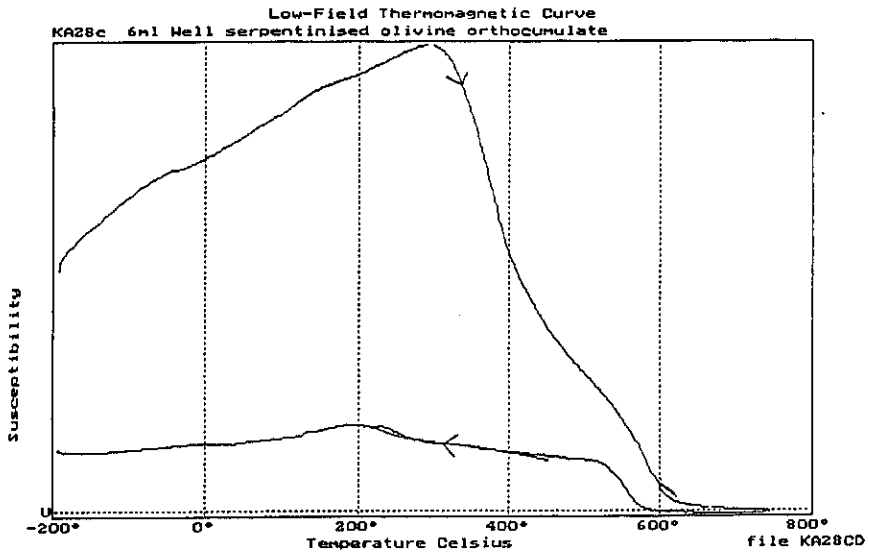
Low-Field Thermomagnetic Curve
KA28c 6m1 Hell serpentinised olivine orthocumulate
Susceptibility
-200°
0°
200°
400°
600°
800°
Temperature Celsius
file KA28CD

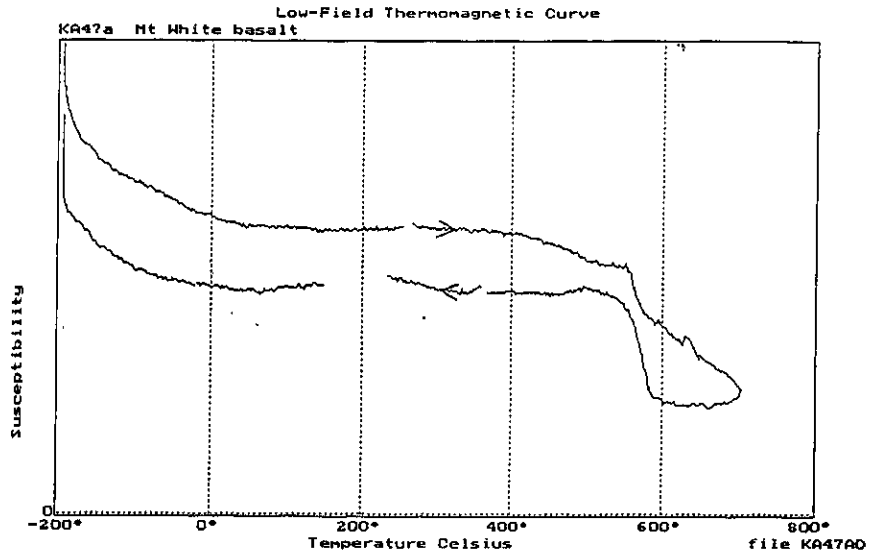
Low-Field Thermomagnetic Curve
KA47a Mt White basalt
Susceptibility
-200°
0°
200°
400°
600°
800°
Temperature Celsius
file KA47AD

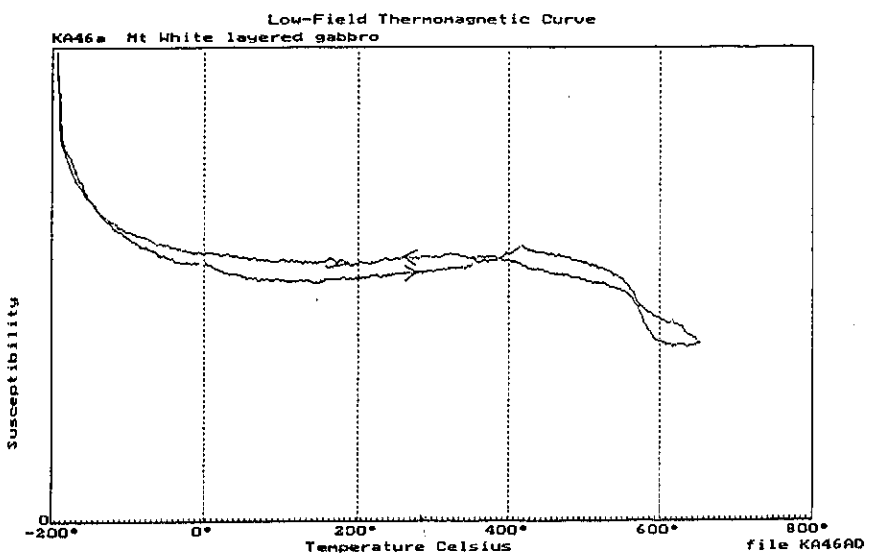
Low-Field Thermomagnetic Curve
KA46a Mt White layered gabbro
Susceptibility
-200°
0°
200°
400°
600°
800°
Temperature Celsius
file KA46AD

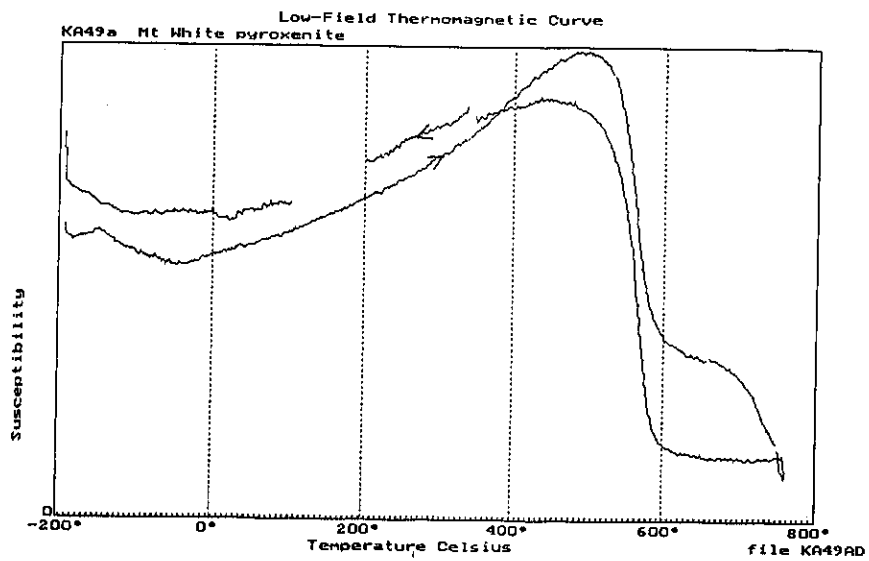
Low-Field Thermomagnetic Curve
KA49a Mt White pyroxenite
Susceptibility
-200°
0°
200°
400°
600°
800°
Temperature Celsius
file KA49AD

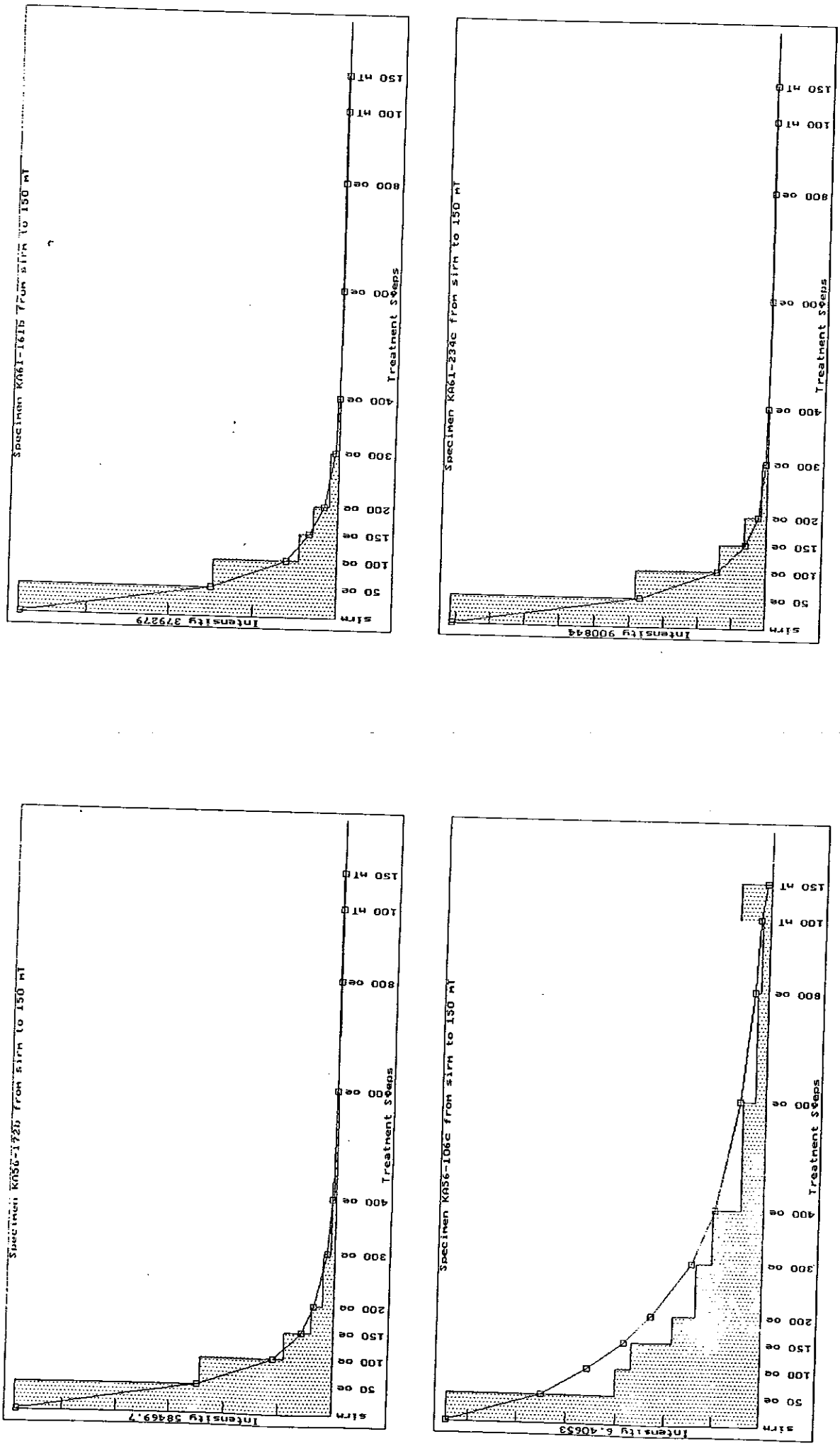

Fig.15 AF demagnetisation of SIRM of DDH samples

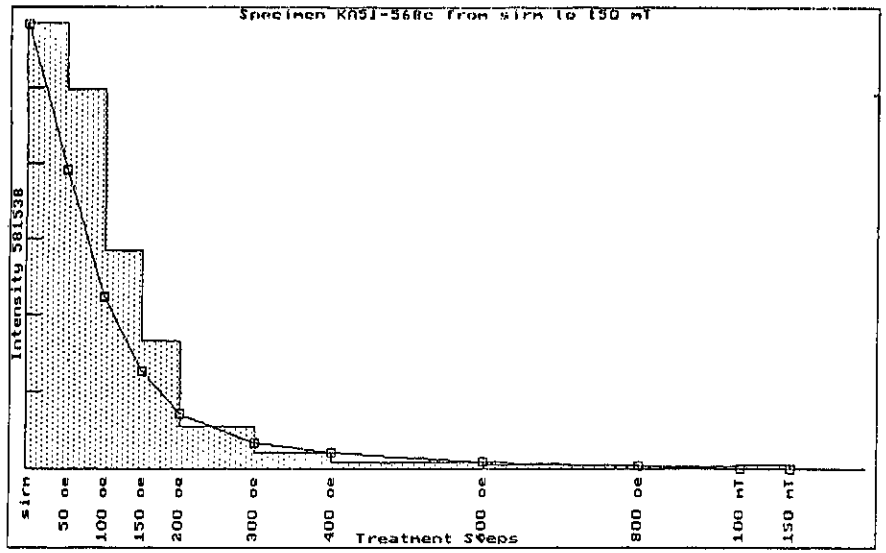
Specimen KA51-568c from sirm to 150 mT
Intensity 581538
sirm
50 oe
100 oe
150 oe
200 oe
300 oe
400 oe
600 oe
800 oe
100 mT
150 mT
Treatment Steps

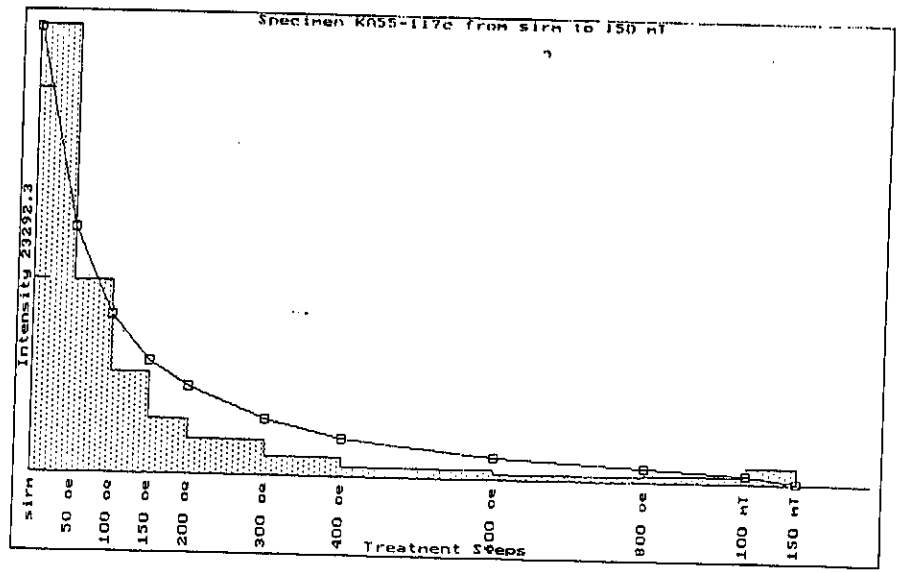
Specimen KA55-117c from sirm to 150 mT
Intensity 29292.3
sirm
50 oe
100 oe
150 oe
200 oe
300 oe
400 oe
600 oe
800 oe
100 mT
150 mT
Treatment Steps

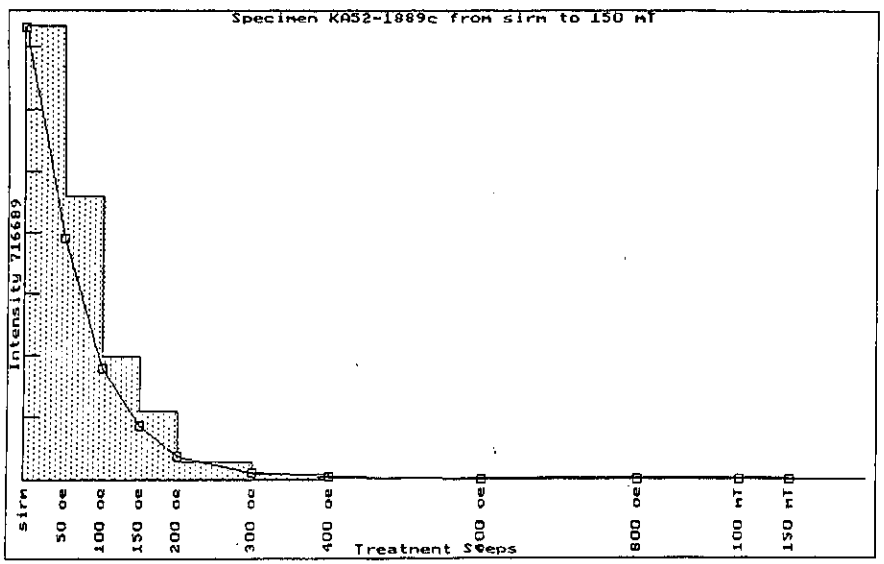
Specimen KA52-1889c from sirm to 150 mT
Intensity 716689
sirm
50 oe
100 oe
150 oe
200 oe
300 oe
400 oe
600 oe
800 oe
100 mT
150 mT
Treatment Steps

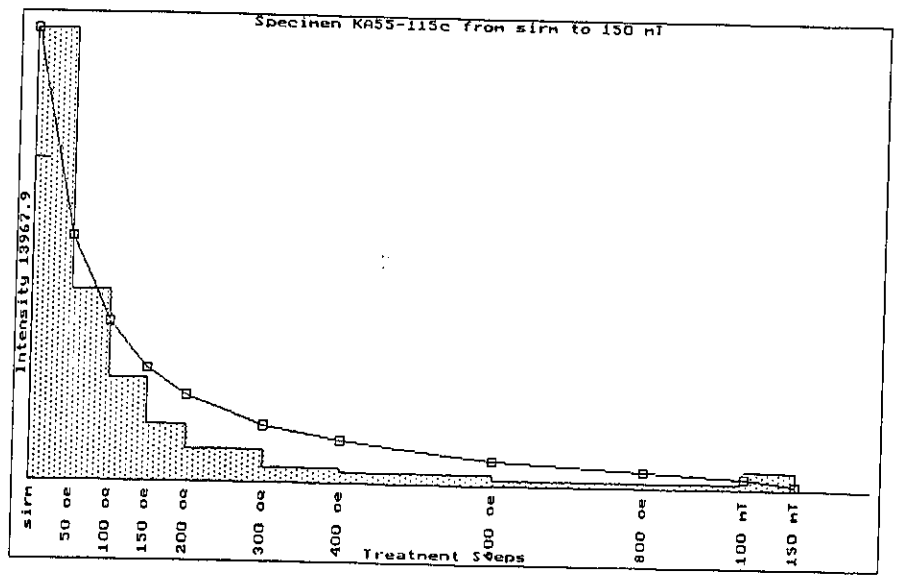
Specimen KA55-115c from sirm to 150 mT
Intensity 13967.9
sirm
50 oe
100 oe
150 oe
200 oe
300 oe
400 oe
600 oe
800 oe
100 mT
150 mT
Treatment Steps

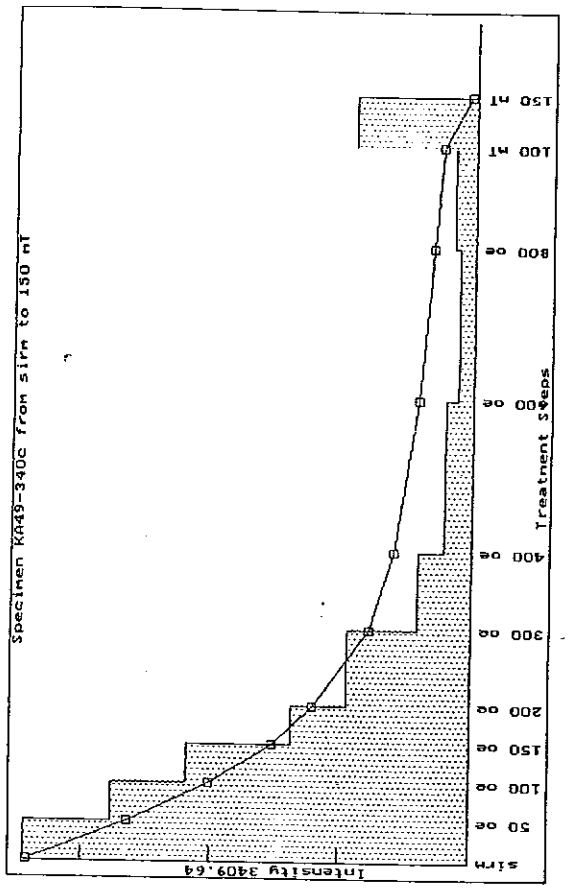
Specimen KA49-340c from sirm to 150 mT
Intensity 3409.64
Treatment Steps
sirm
50 oe
100 oe
150 oe
200 oe
300 oe
400 oe
800 oe
1600 oe
100 mT
150 mT

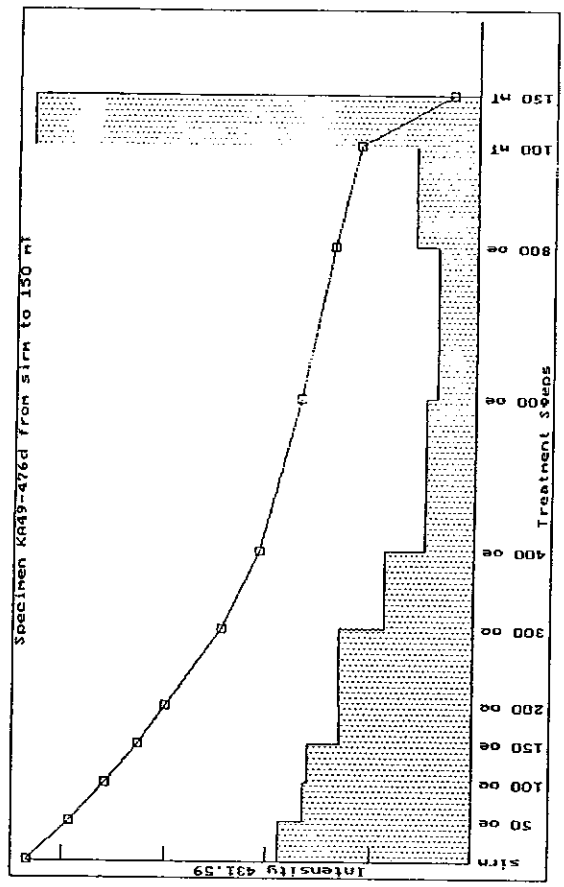
Specimen KA49-476d from sirm to 150 mT
Intensity 431.59
Treatment Steps
sirm
50 oe
100 oe
150 oe
200 oe
300 oe
400 oe
800 oe
1600 oe
100 mT
150 mT

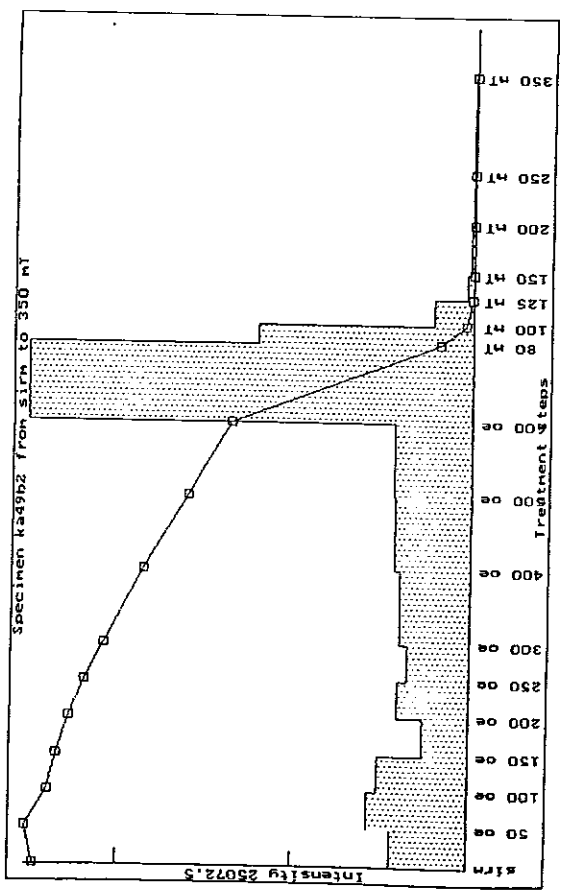
Specimen Ka49b2 from sirm to 350 mT
Intensity 25072.5
Treatment Steps
sirm
50 oe
100 oe
150 oe
200 oe
250 oe
300 oe
400 oe
800 oe
1600 oe
80 mT
100 mT
125 mT
150 mT
200 mT
250 mT
350 mT

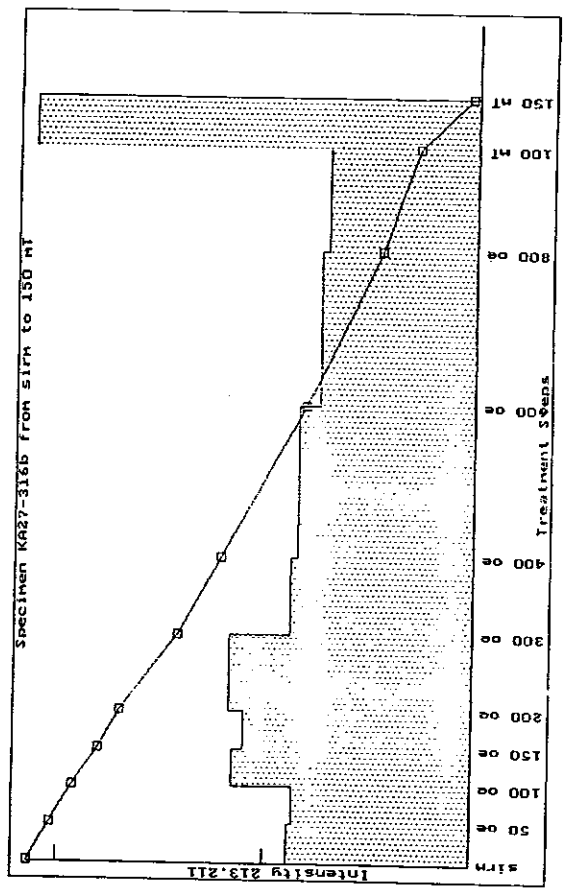
Specimen KA27-316b from sirm to 150 mT
Intensity 213.211
Treatment Steps
sirm
50 oe
100 oe
150 oe
200 oe
300 oe
400 oe
800 oe
1600 oe
100 mT
150 mT

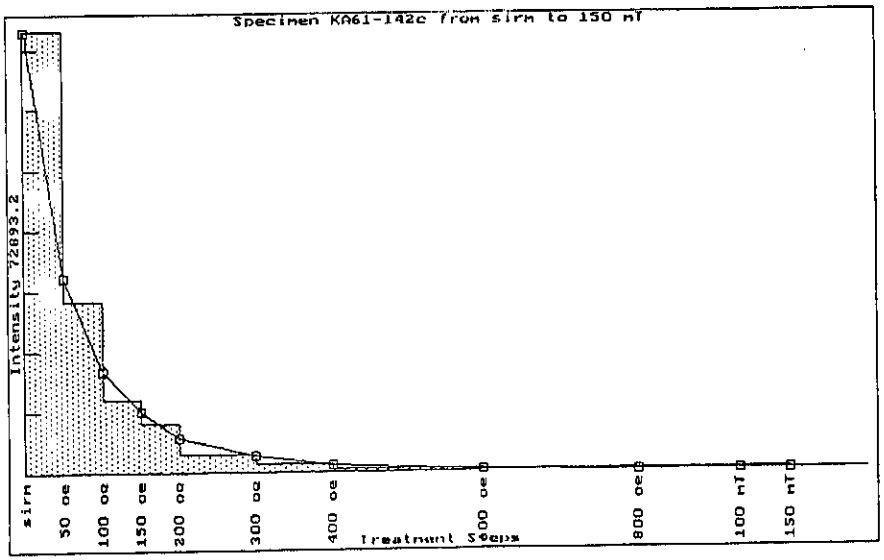
Specimen KA61-142c from sirm to 150 mT
Intensity 72693.2
sirm
50 oe
100 oe
150 oe
200 oe
300 oe
400 oe
500 oe
800 oe
100 mT
150 mT
Treatment Steps

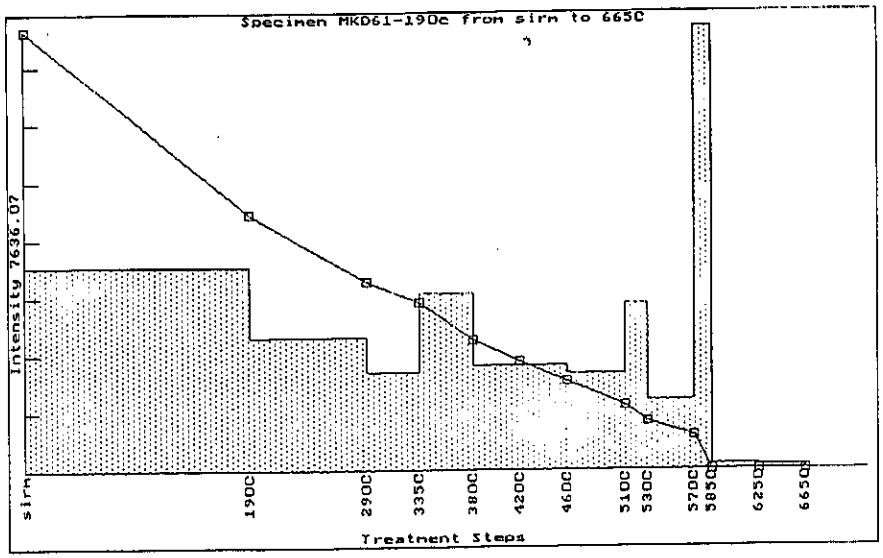
Specimen MKD61-190c from sirm to 665C
Intensity 7636.07
sirm
190C
290C
335C
380C
420C
460C
510C
530C
570C
585C
625C
665C
Treatment Steps

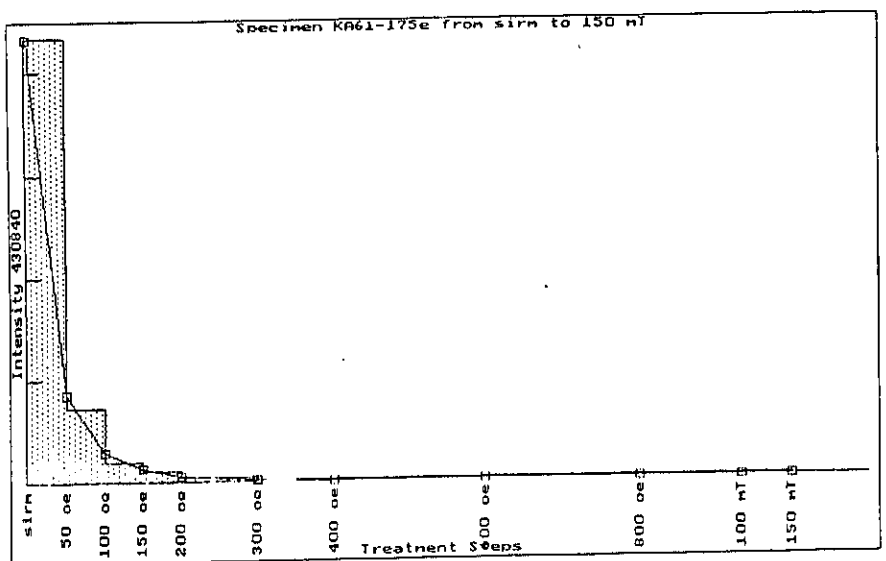
Specimen KA61-175c from sirm to 150 mT
Intensity 430840
sirm
50 oe
100 oe
150 oe
200 oe
300 oe
400 oe
500 oe
800 oe
100 mT
150 mT
Treatment Steps

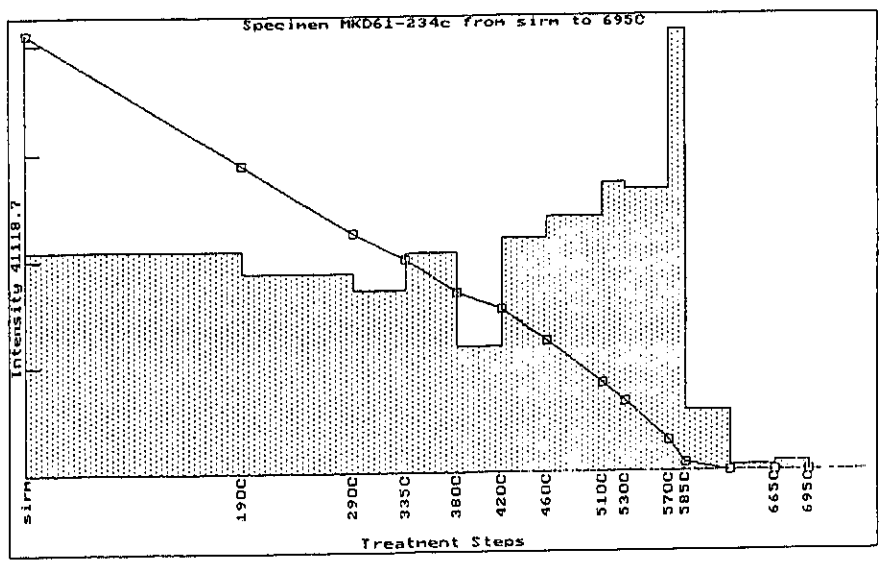
Specimen MKD61-234c from sirm to 695C
Intensity 41118.7
sirm
190C
290C
335C
380C
420C
460C
510C
530C
570C
585C
665C
695C
Treatment Steps

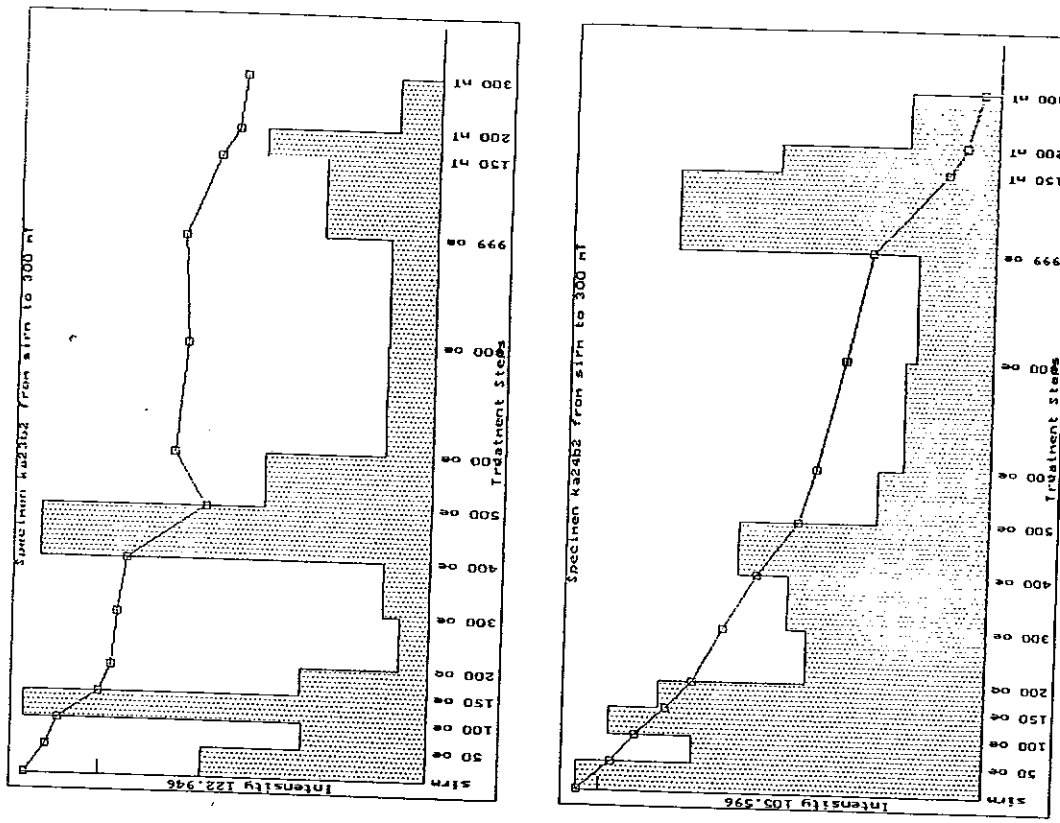

Fig.16 AF demagnetisation of SIRM of surface samples

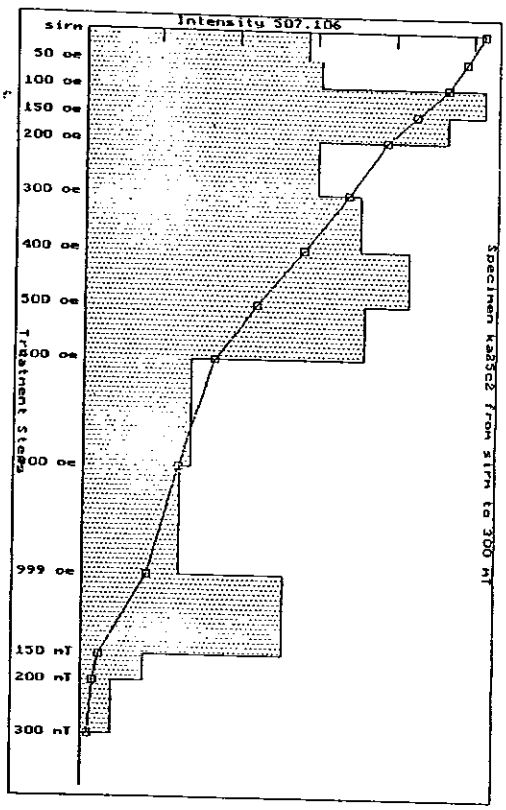
Intensity 307.106
Specimen ka25c2 from sirm to 300 mT
Treatment steps
sirm
50 oe
100 oe
150 oe
200 oe
300 oe
400 oe
500 oe
600 oe
800 oe
999 oe
150 mT
200 mT
300 mT

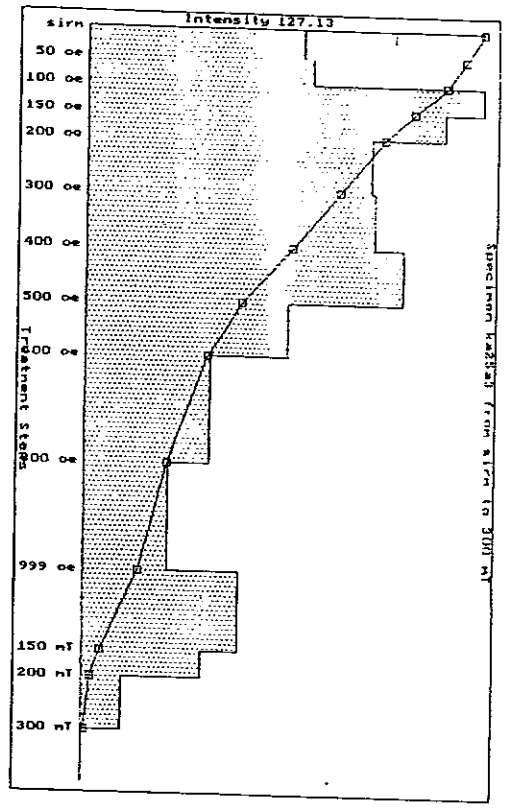
Intensity 127.13
Specimen ka25a1 from sirm to 300 mT
Treatment steps
sirm
50 oe
100 oe
150 oe
200 oe
300 oe
400 oe
500 oe
600 oe
800 oe
999 oe
150 mT
200 mT
300 mT

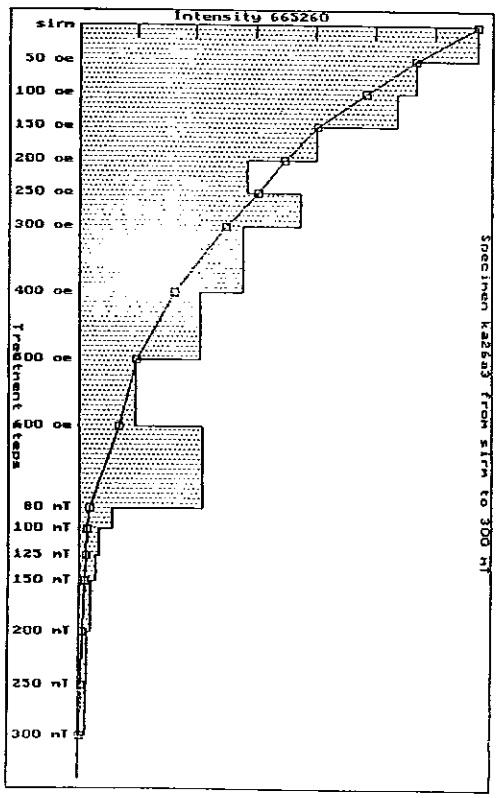
Intensity 665260
Specimen ka25a3 from sirm to 300 mT
Treatment steps
sirm
50 oe
100 oe
130 oe
200 oe
250 oe
300 oe
400 oe
600 oe
800 oe
80 mT
100 mT
125 mT
150 mT
200 mT
250 mT
300 mT

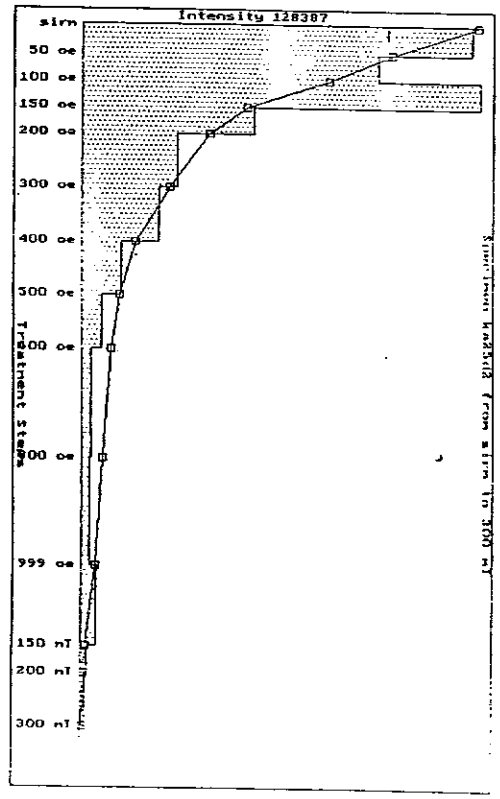
Intensity 128387
Treatment steps
sirm
50 oe
100 oe
150 oe
200 oe
300 oe
400 oe
500 oe
600 oe
800 oe
999 oe
150 mT
200 mT
300 mT

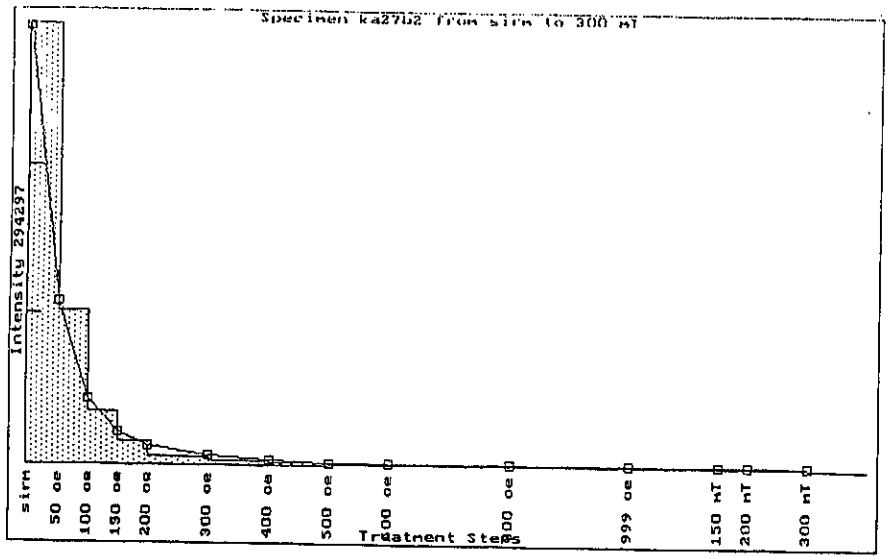
Specimen ka27b2 from sirm to 300 mT
Intensity 294297
sirm
50 oe
100 oe
150 oe
200 oe
300 oe
400 oe
500 oe
600 oe
800 oe
999 oe
150 mT
200 mT
300 mT
Treatment Steps

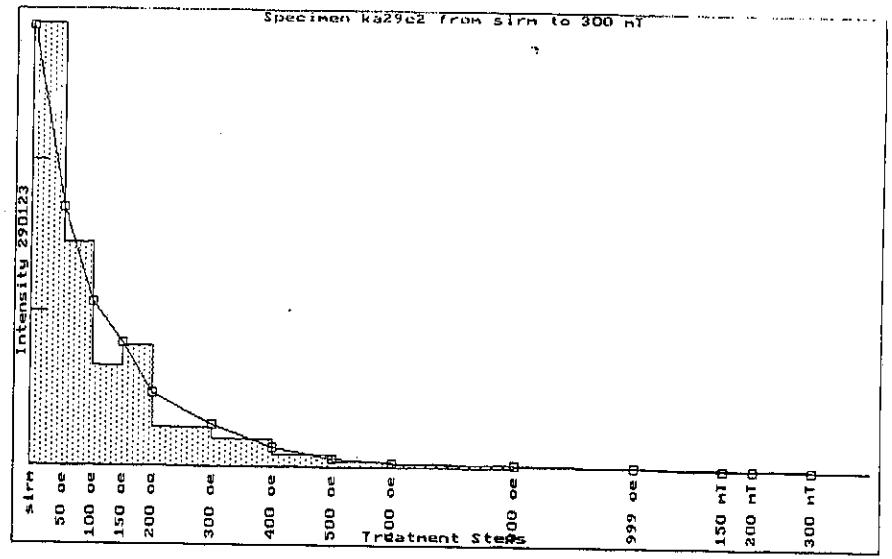
Specimen ka29c2 from sirm to 300 mT
Intensity 290123
sirm
50 oe
100 oe
150 oe
200 oe
300 oe
400 oe
500 oe
600 oe
800 oe
999 oe
150 mT
200 mT
300 mT
Treatment Steps

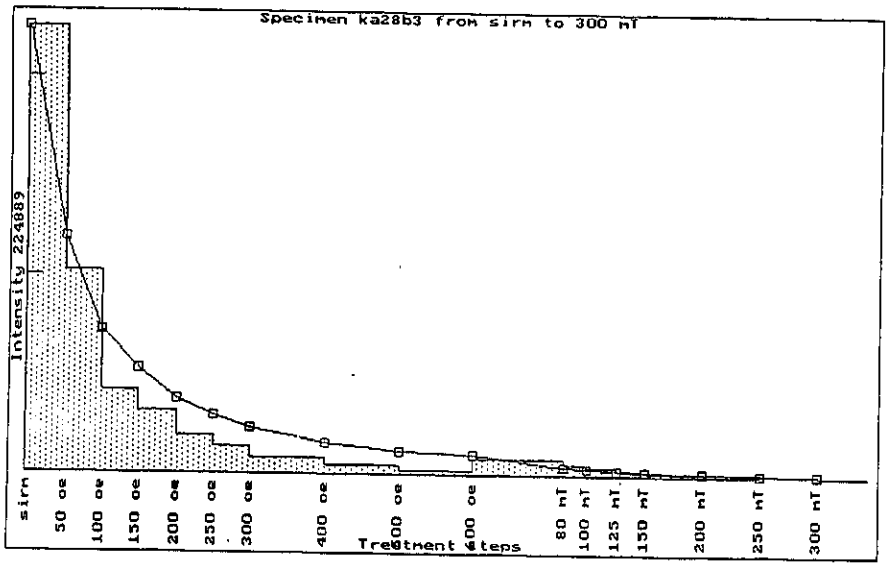
Specimen ka28b3 from sirm to 300 mT
Intensity 224889
sirm
50 oe
100 oe
150 oe
200 oe
250 oe
300 oe
400 oe
600 oe
800 oe
80 mT
100 mT
125 mT
150 mT
200 mT
250 mT
300 mT
Treatment Steps

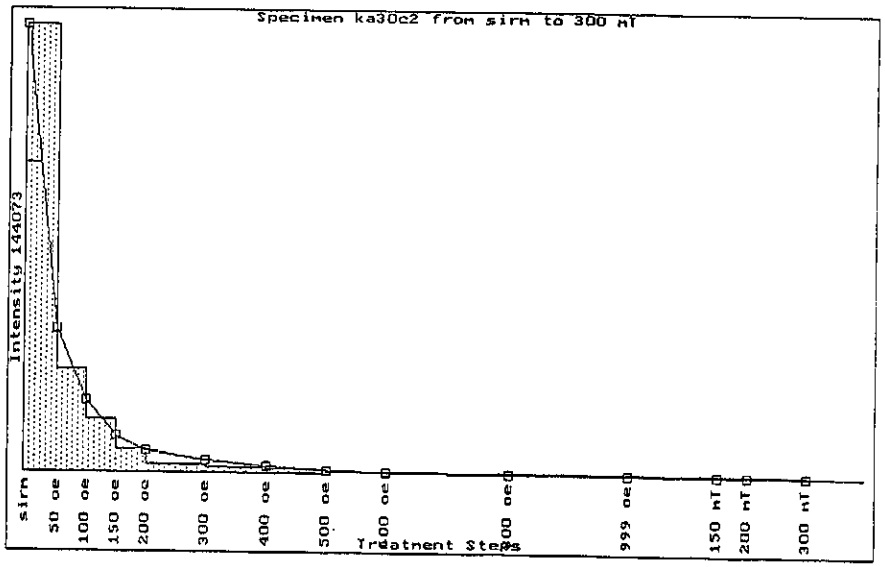
Specimen ka30c2 from sirm to 300 mT
Intensity 144073
sirm
50 oe
100 oe
150 oe
200 oe
300 oe
400 oe
500 oe
600 oe
800 oe
999 oe
150 mT
200 mT
300 mT
Treatment Steps

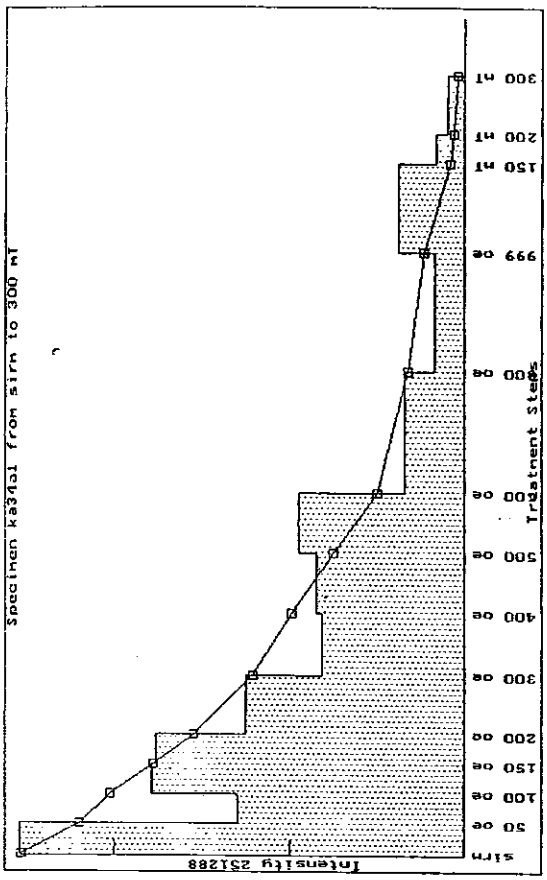
Specimen ka34a1 from sirm to 300 mT
Intensity 251288
Treatment Steps
sirm
50 oe
100 oe
150 oe
200 oe
300 oe
400 oe
500 oe
600 oe
800 oe
999 oe
150 mT
200 mT
300 mT

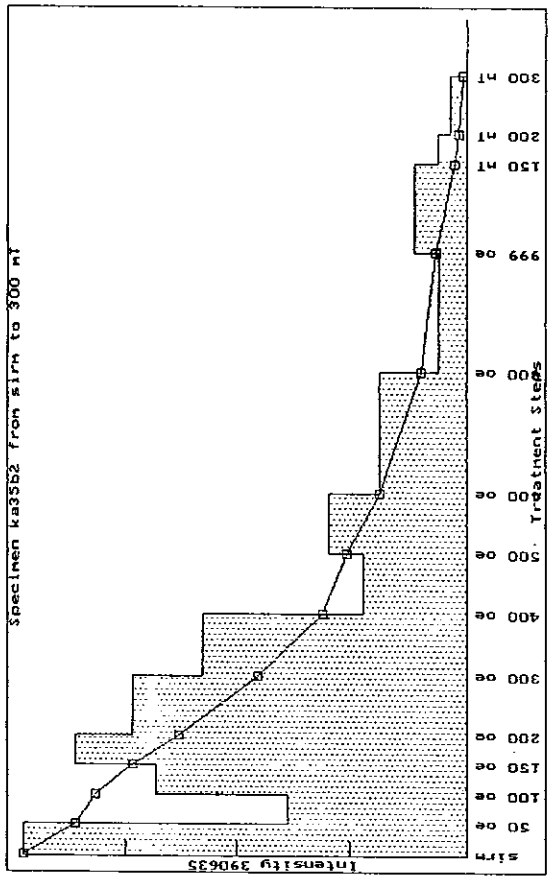
Specimen ka35b2 from sirm to 300 mT
Intensity 390635
Treatment Steps
sirm
50 oe
100 oe
150 oe
200 oe
300 oe
400 oe
500 oe
600 oe
800 oe
999 oe
150 mT
200 mT
300 mT

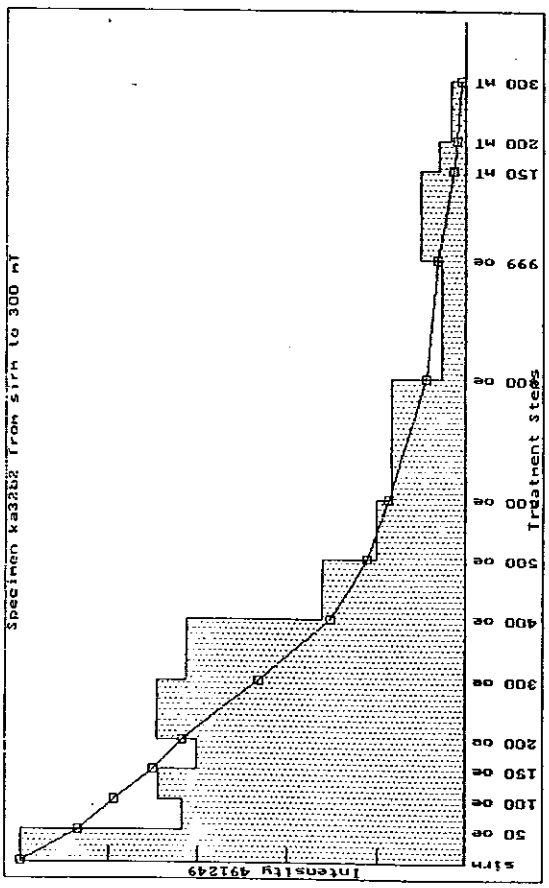
Specimen ka32b2 from sirm to 300 mT
Intensity 491249
Treatment Steps
sirm
50 oe
100 oe
150 oe
200 oe
300 oe
400 oe
500 oe
600 oe
800 oe
999 oe
150 mT
200 mT
300 mT

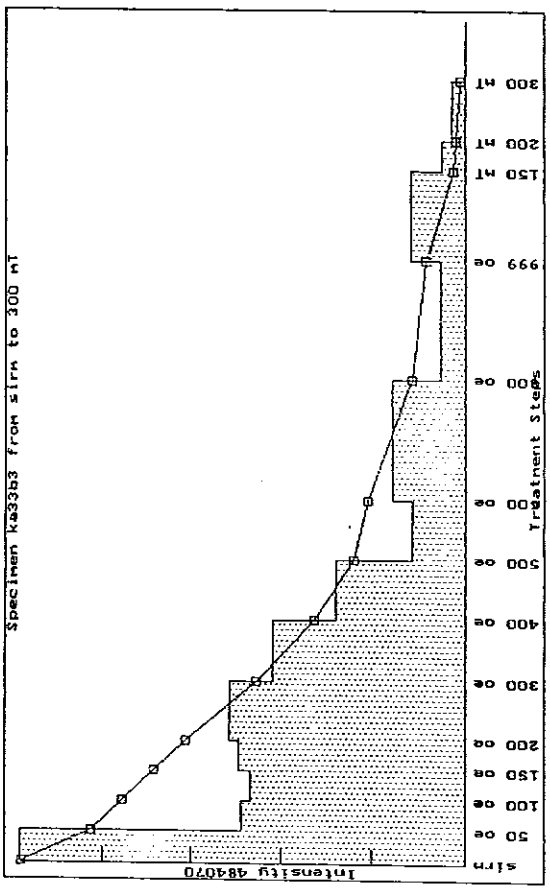
Specimen ka33b3 from sirm to 300 mT
Intensity 484070
Treatment Steps
sirm
50 oe
100 oe
150 oe
200 oe
300 oe
400 oe
500 oe
600 oe
800 oe
999 oe
150 mT
200 mT
300 mT

Specimen ka38a2 from sirm to 300 mT
Intensity 976.231
Treatment Steps
sirm
50 oe
100 oe
150 oe
200 oe
300 oe
400 oe
500 oe
600 oe
999 oe
150 mT
200 mT
300 mT

Specimen ka39b2 from sirm to 300 mT
Intensity 47.592
Treatment Steps
sirm
50 oe
100 oe
150 oe
200 oe
300 oe
400 oe
500 oe
600 oe
999 oe
150 mT
200 mT
300 mT

Specimen ka36b2 from sirm to 300 mT
Intensity 844.438
Treatment Steps
sirm
50 oe
100 oe
150 oe
200 oe
300 oe
400 oe
500 oe
600 oe
999 oe
150 mT
200 mT
300 mT

Specimen ka37b3 from sirm to 300 mT
Intensity 582.167
Treatment Steps
sirm
50 oe
100 oe
150 oe
200 oe
300 oe
400 oe
500 oe
600 oe
999 oe
150 mT
200 mT
300 mT

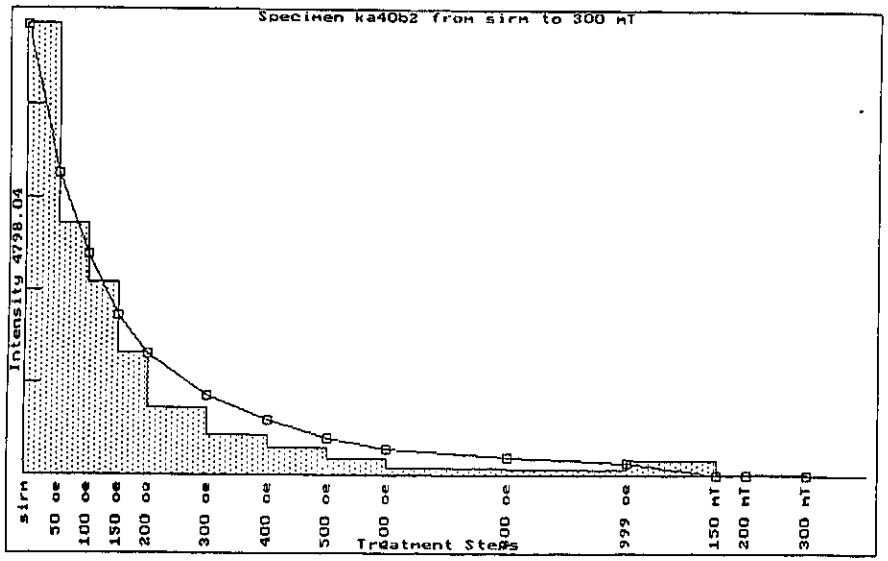
Specimen ka40b2 from sirm to 300 mT
Intensity 4798.04
sirm
50 oe
100 oe
150 oe
200 oe
300 oe
400 oe
500 oe
600 oe
800 oe
999 oe
150 mT
200 mT
300 mT
Treatment Steps

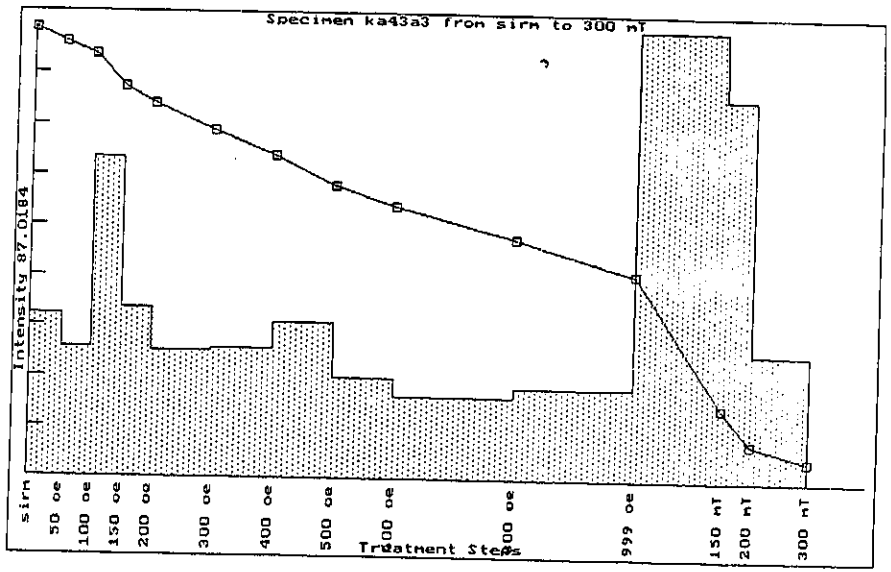
Specimen ka43a3 from sirm to 300 mT
Intensity 87.0184
sirm
50 oe
100 oe
150 oe
200 oe
300 oe
400 oe
500 oe
600 oe
800 oe
999 oe
150 mT
200 mT
300 mT
Treatment Steps

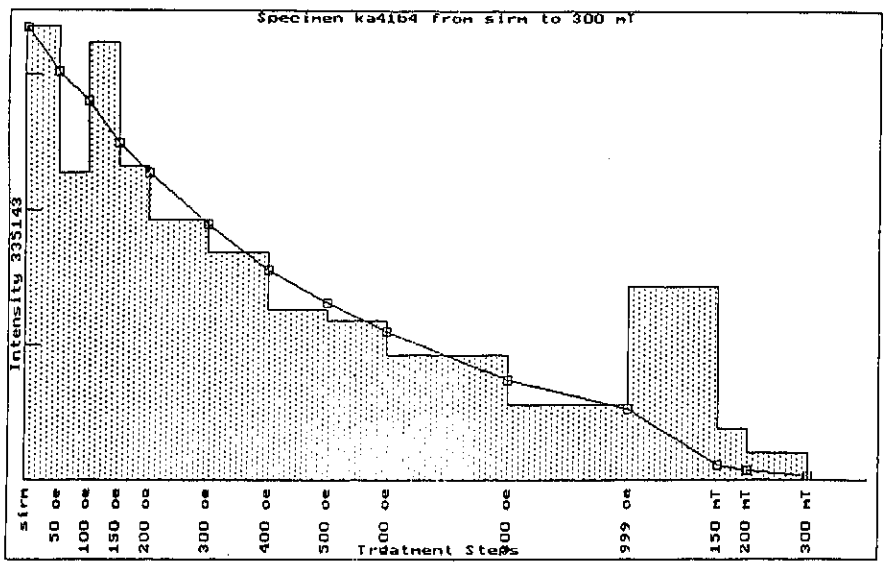
Specimen ka41b4 from sirm to 300 mT
Intensity 335143
sirm
50 oe
100 oe
150 oe
200 oe
300 oe
400 oe
500 oe
600 oe
800 oe
999 oe
150 mT
200 mT
300 mT
Treatment Steps

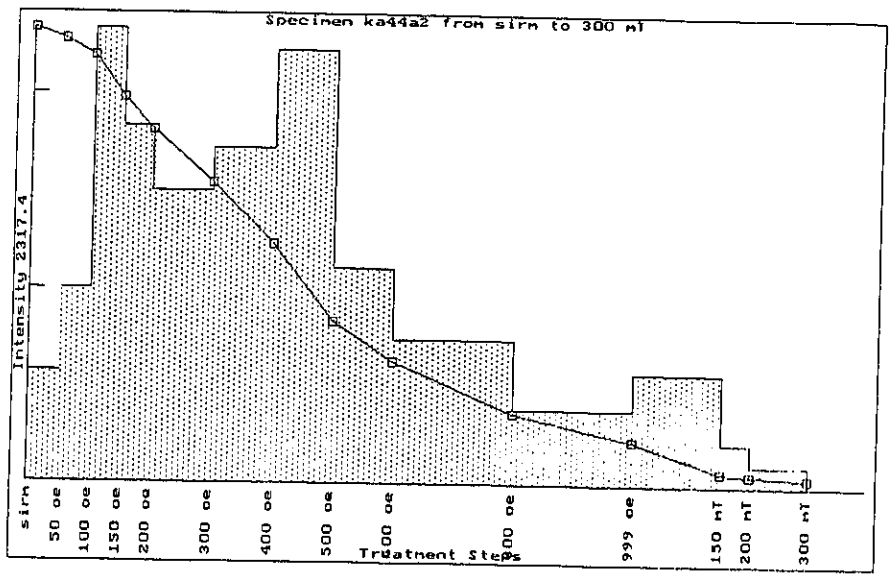
Specimen ka44a2 from sirm to 300 mT
Intensity 2317.4
sirm
50 oe
100 oe
150 oe
200 oe
300 oe
400 oe
500 oe
600 oe
800 oe
999 oe
150 mT
200 mT
300 mT
Treatment Steps

Specimen ka47b2 from sirm to 300 mT
Intensity 896.98
Treatment Steps
sirm
50 oe
100 oe
150 oe
200 oe
250 oe
300 oe
400 oe
500 oe
600 oe
999 oe
80 mT
100 mT
125 mT
150 mT
200 mT
250 mT
300 mT

Specimen ka48a2 from sirm to 300 mT
Intensity 593.114
Treatment Steps
sirm
50 oe
100 oe
150 oe
200 oe
300 oe
400 oe
500 oe
600 oe
999 oe
150 mT
200 mT
300 mT

Specimen ka45a2 from sirm to 300 mT
Intensity 788.14
Treatment Steps
sirm
50 oe
100 oe
150 oe
200 oe
300 oe
400 oe
500 oe
600 oe
999 oe
150 mT
200 mT
300 mT

Specimen ka46a2 from sirm to 300 mT
Intensity 657.359
Treatment Steps
sirm
50 oe
100 oe
150 oe
200 oe
250 oe
300 oe
400 oe
600 oe
80 mT
100 mT
125 mT
150 mT
200 mT
250 mT
300 mT

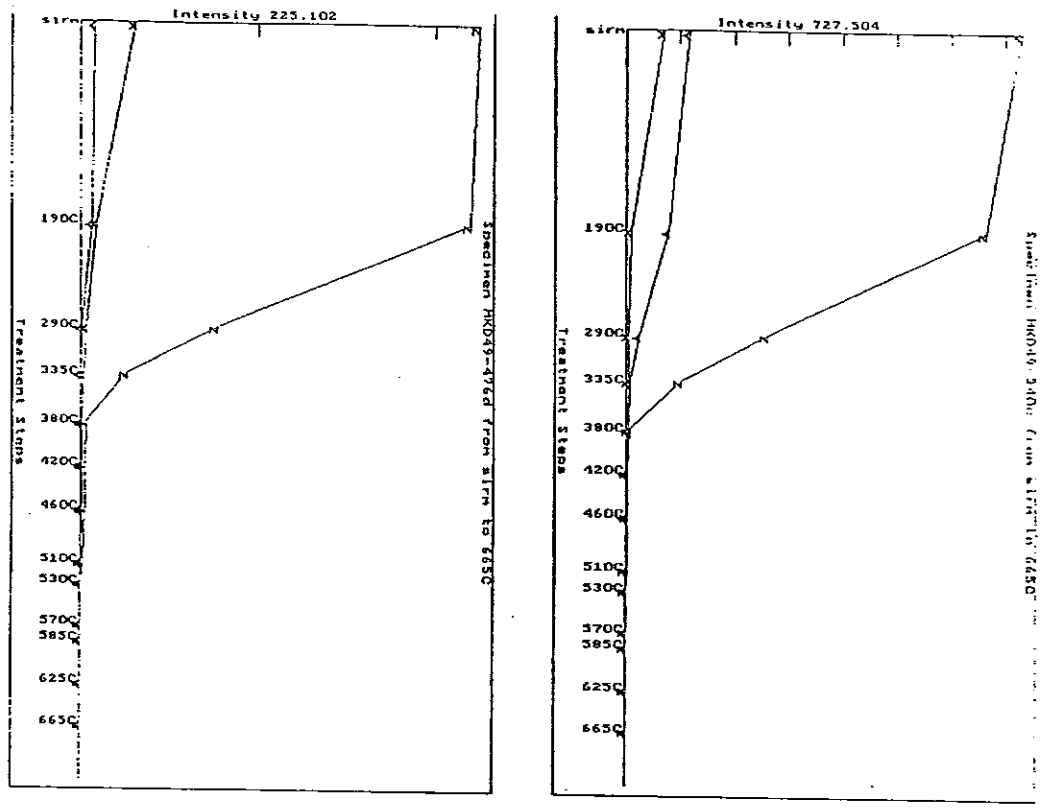

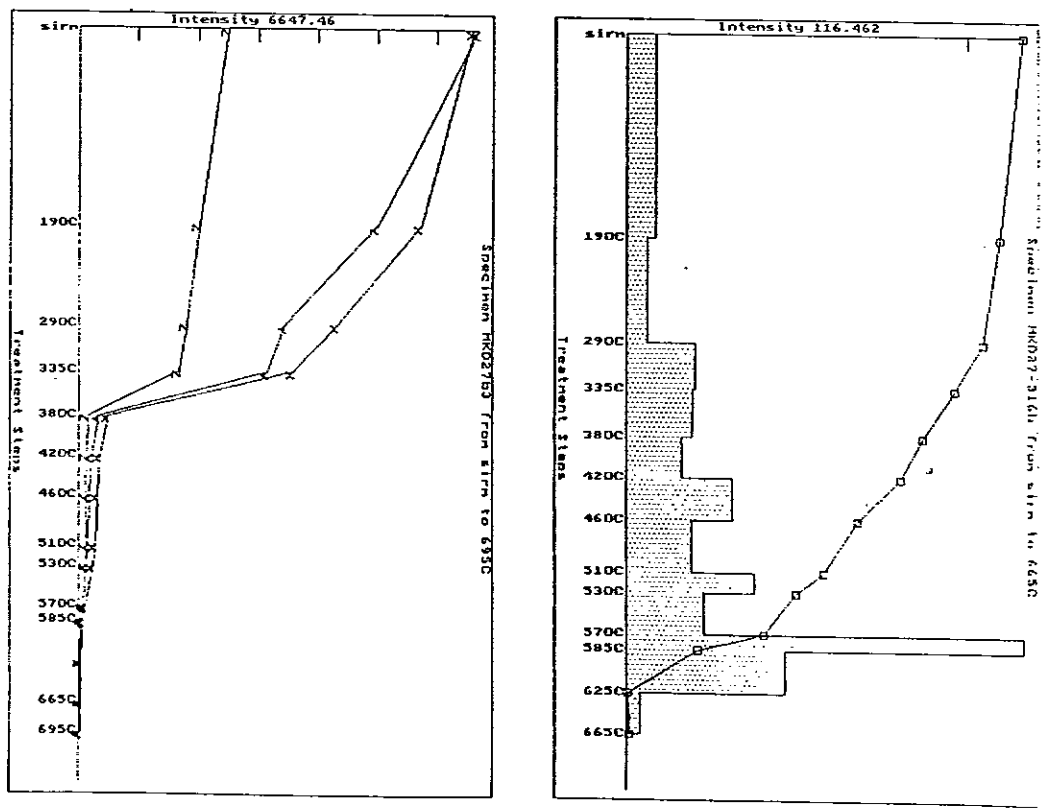

Fig.17 Thermal demagnetisation of 3-component IRM of DDH samples: z-axis = hard component (> 1000 Oe); x-axis = intermediate coercivity component (200-1000 Oe); y-axis = soft component (< 200 Oe)

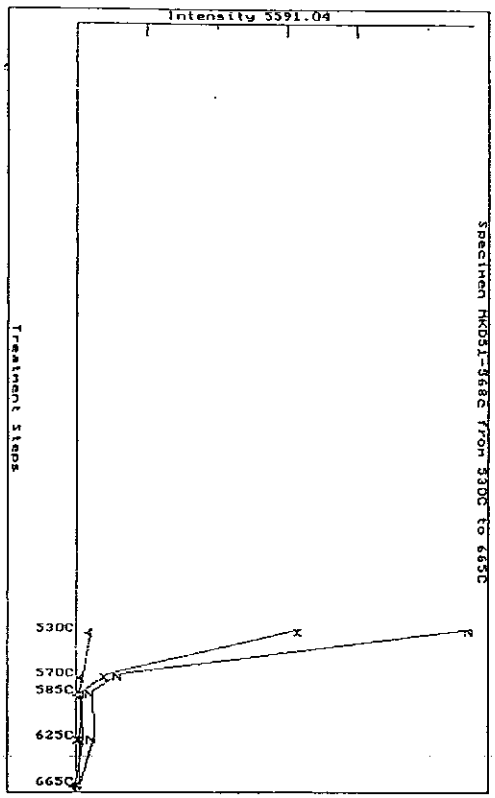
Intensity 5391.04
Treatment steps
Specimen MKDS1-868C from 330C to 665C
530C
570C
585C
625C
665C

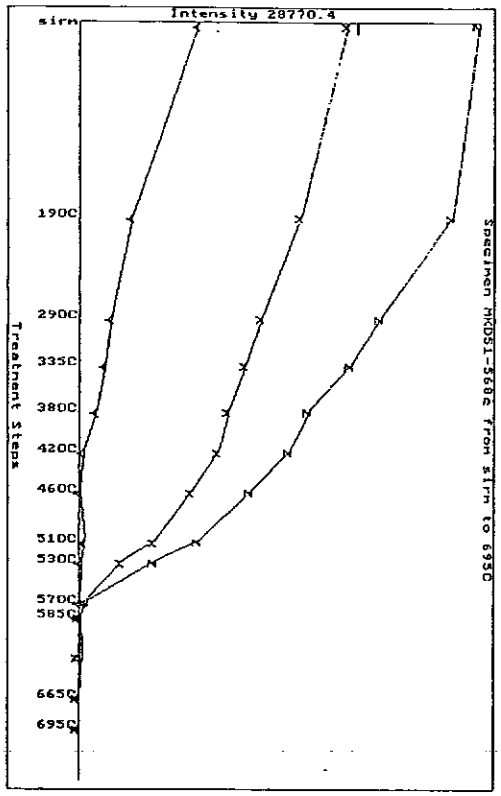
Intensity 28770.4
sirm
Treatment steps
Specimen MKDS1-568C from sirm to 695C
190C
290C
335C
380C
420C
460C
510C
530C
570C
585C
665C
695C

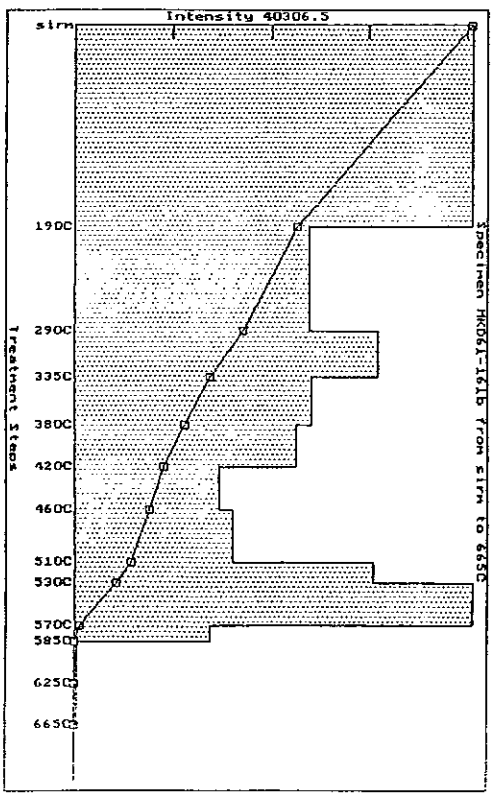
Intensity 40306.5
sirm
Treatment Steps
Specimen MKD6J-161b from sirm to 665C
190C
290C
335C
380C
420C
460C
510C
530C
570C
585C
625C
665C

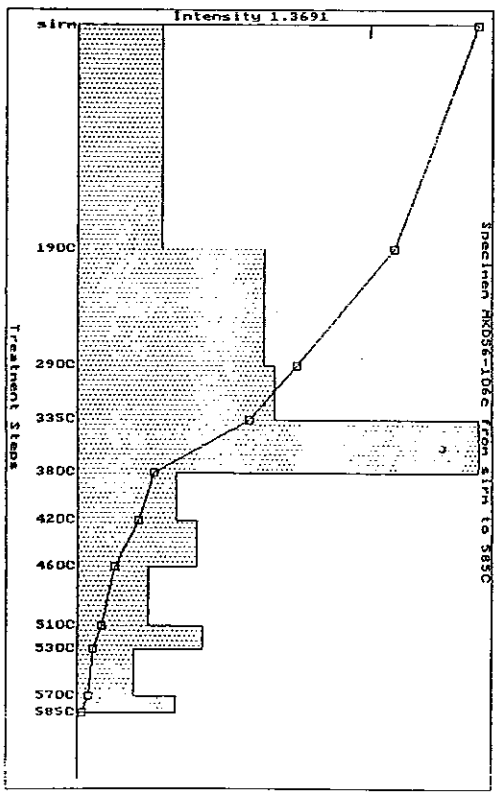
Intensity 1.3691
sirm
Treatment Steps
Specimen MKDS6-106C from sirm to 585C
190C
290C
335C
380C
420C
460C
510C
530C
570C
585C

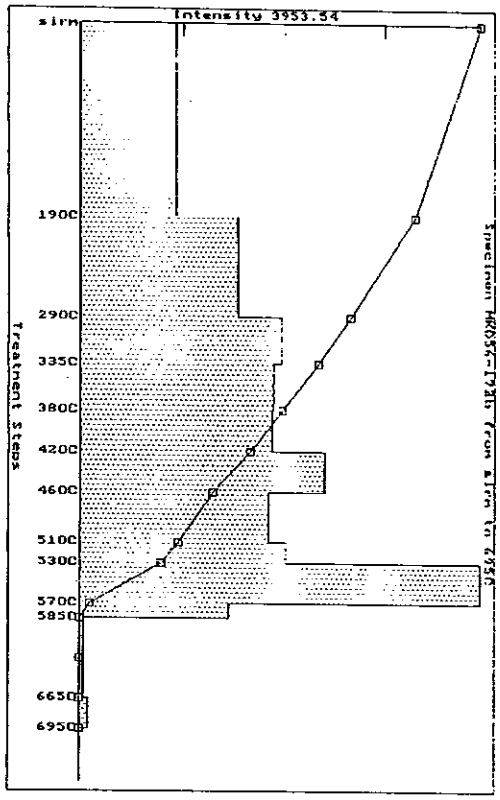
Intensity 3953.54
sirn
190C
290C
335C
380C
420C
460C
510C
530C
570C
585C
665C
695C
Treatment Steps

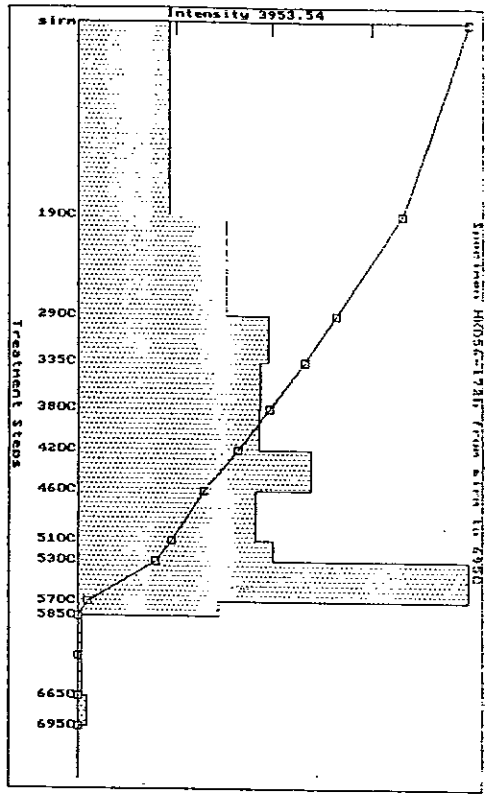
Intensity 3953.54
sirn
190C
290C
335C
380C
420C
460C
510C
530C
570C
585C
665C
695C
Treatment Steps

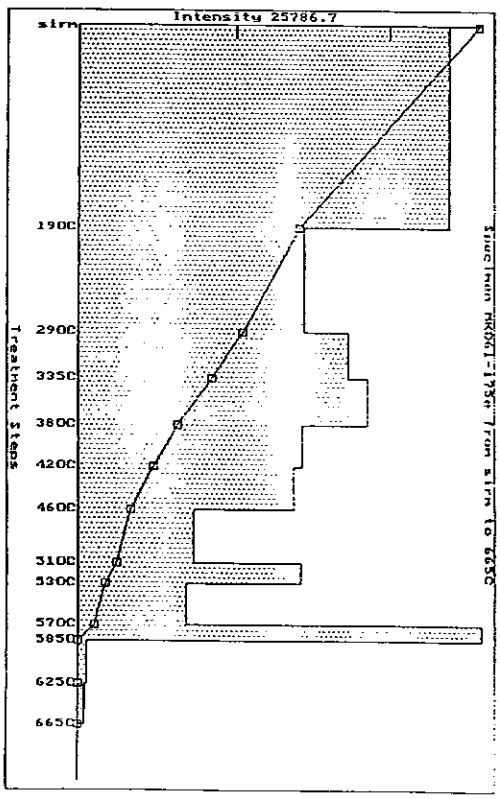
Intensity 25786.7
sirn
190C
290C
335C
380C
420C
460C
510C
530C
570C
585C
625C
665C
Treatment Steps

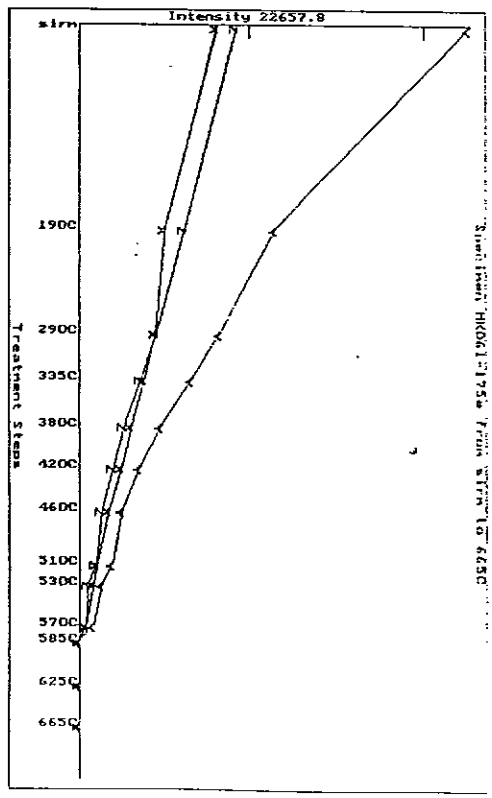
Intensity 22657.8
sirn
190C
290C
335C
380C
420C
460C
510C
530C
570C
585C
625C
665C
Treatment Steps

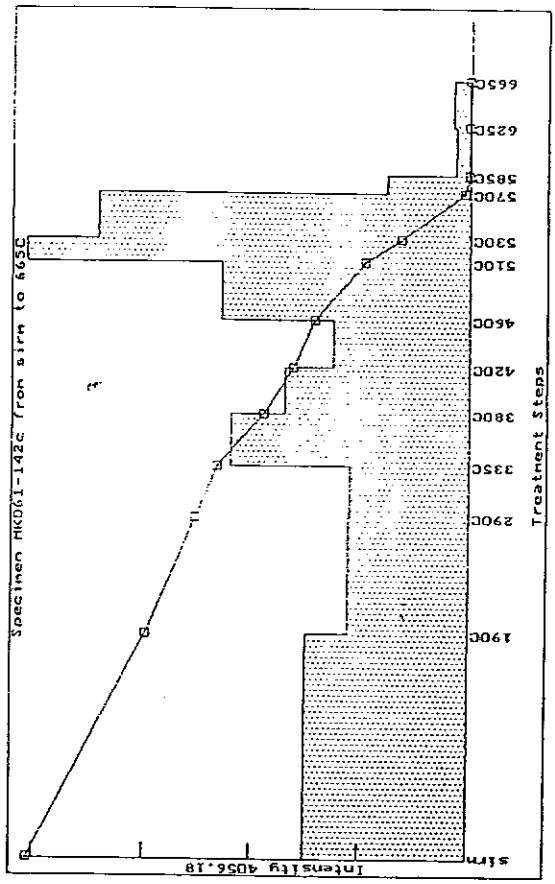
Specimen MKD61-142c from sirm to 665C
Intensity 4056.18
Treatment Steps
sirm
190C
290C
335C
380C
420C
460C
510C
530C
570C
585C
625C
665C

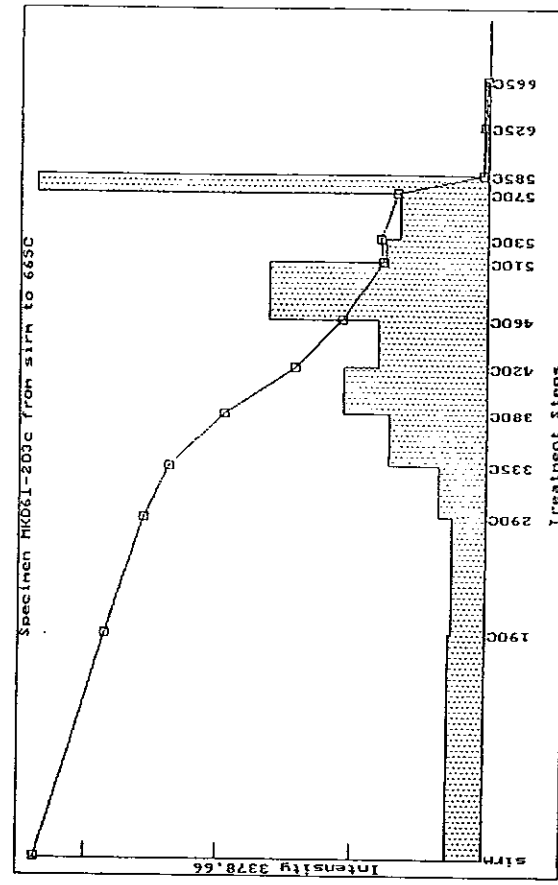
Specimen MKD61-203c from sirm to 665C
Intensity 3378.66
Treatment Steps
sirm
190C
290C
335C
380C
420C
460C
510C
530C
570C
585C
625C
665C

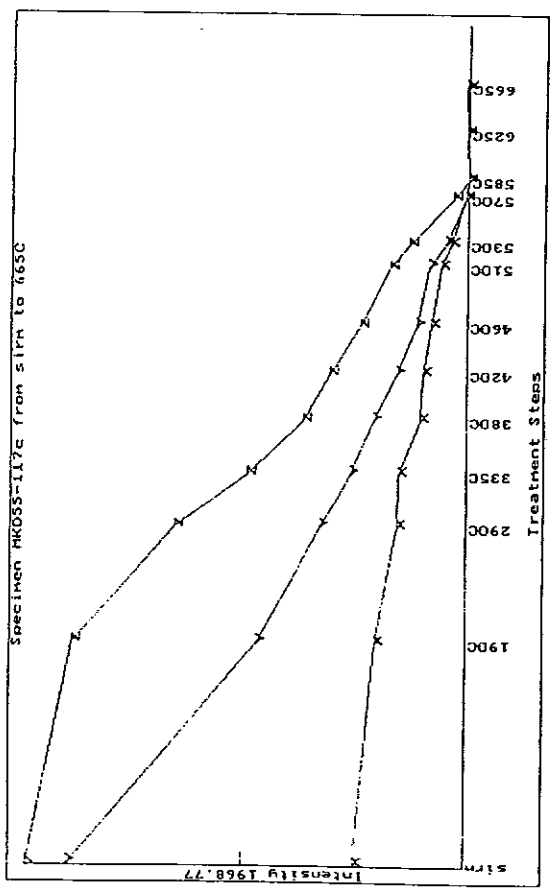
Specimen MKD55-117c from sirm to 665C
Intensity 1968.77
Treatment Steps
sirm
190C
290C
335C
380C
420C
460C
510C
530C
570C
585C
625C
665C

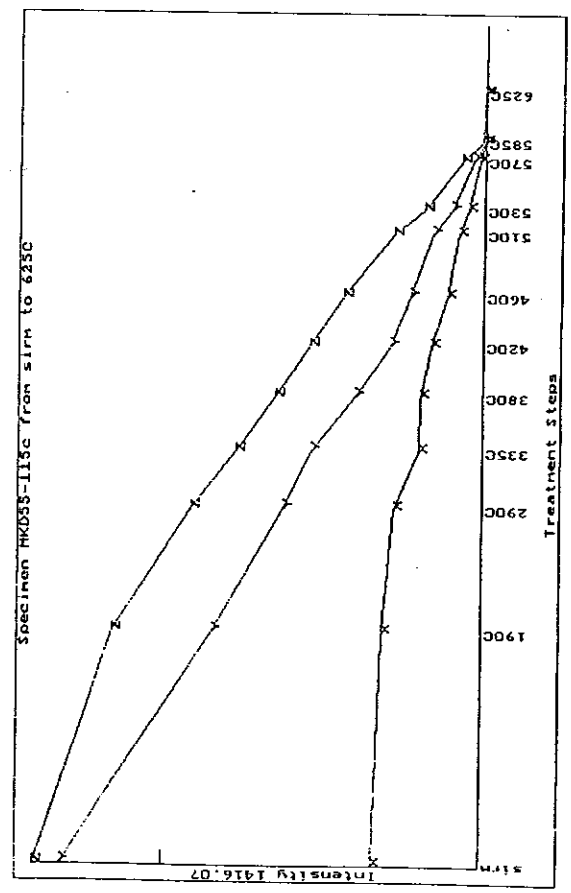
Specimen MKD55-115c from sirm to 625C
Intensity 1416.07
Treatment Steps
sirm
190C
290C
335C
380C
420C
460C
510C
530C
570C
585C
625C

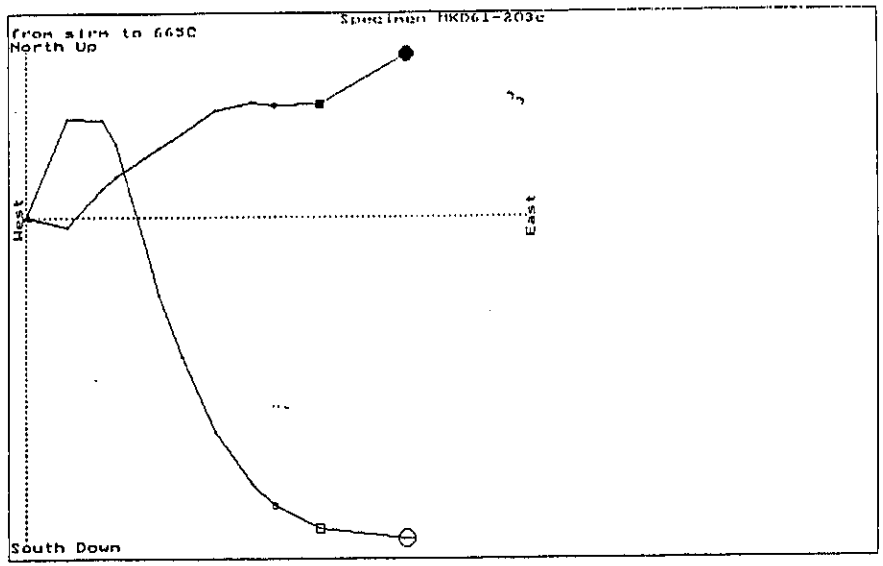
Specimen MKD61-203c
from sirm to 665C
North Up
West
East
South Down

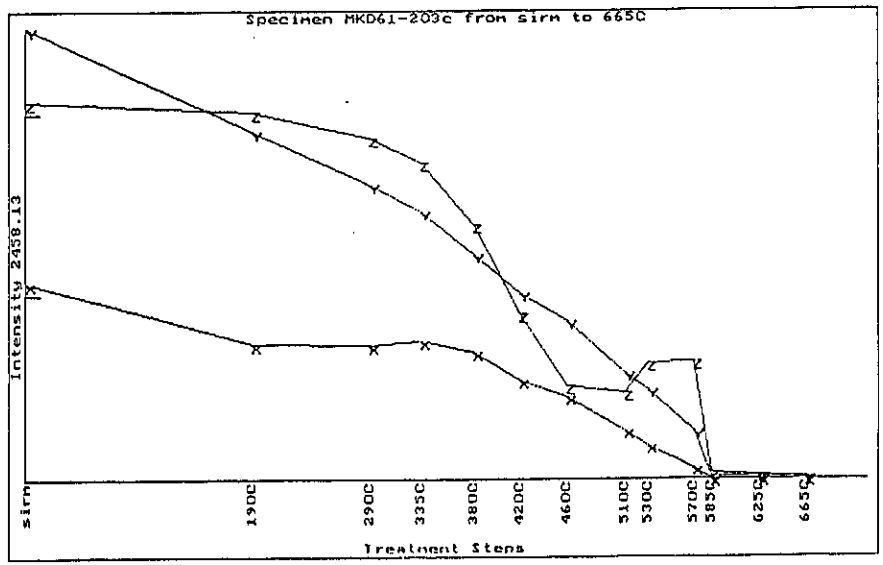
Specimen MKD61-203c from sirm to 665C
Intensity 2458.13
sirm
190C
290C
335C
380C
420C
460C
510C
530C
570C
585C
625C
665C
Treatment Steps

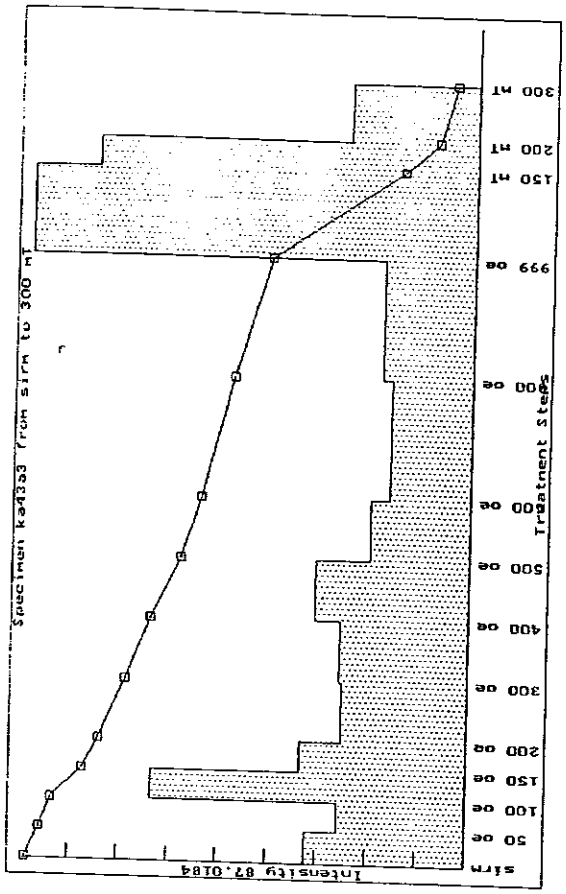
Specimen ka4333 from sirm to 300 mT
Intensity 87.0184
Treatment Steps
sirm
50 oe
100 oe
150 oe
200 oe
300 oe
400 oe
500 oe
600 oe
800 oe
999 oe
150 mT
200 mT
300 mT

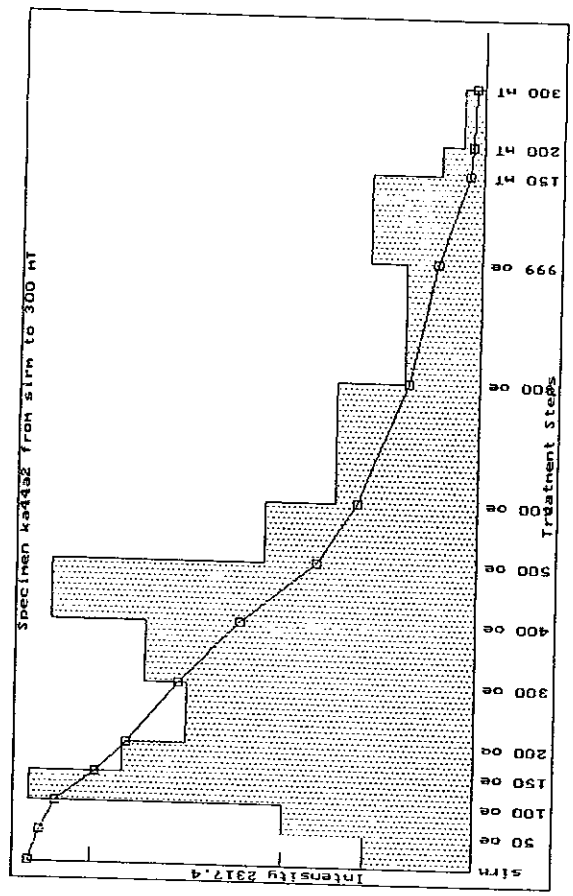
Specimen ka44a2 from sirm to 300 mT
Intensity 2317.4
Treatment Steps
sirm
50 oe
100 oe
150 oe
200 oe
300 oe
400 oe
500 oe
600 oe
800 oe
999 oe
150 mT
200 mT
300 mT

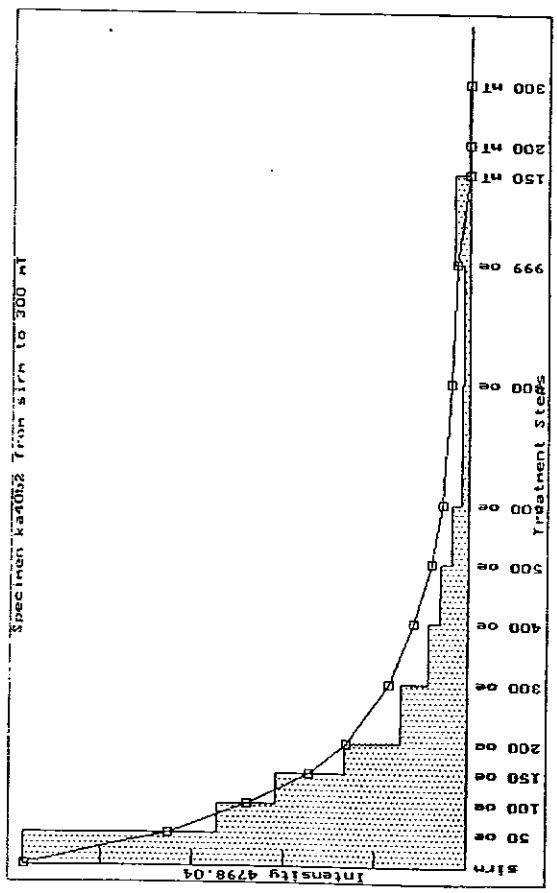
Specimen ka40b2 from sirm to 300 mT
Intensity 4798.04
Treatment Steps
sirm
50 oe
100 oe
150 oe
200 oe
300 oe
400 oe
500 oe
600 oe
800 oe
999 oe
150 mT
200 mT
300 mT

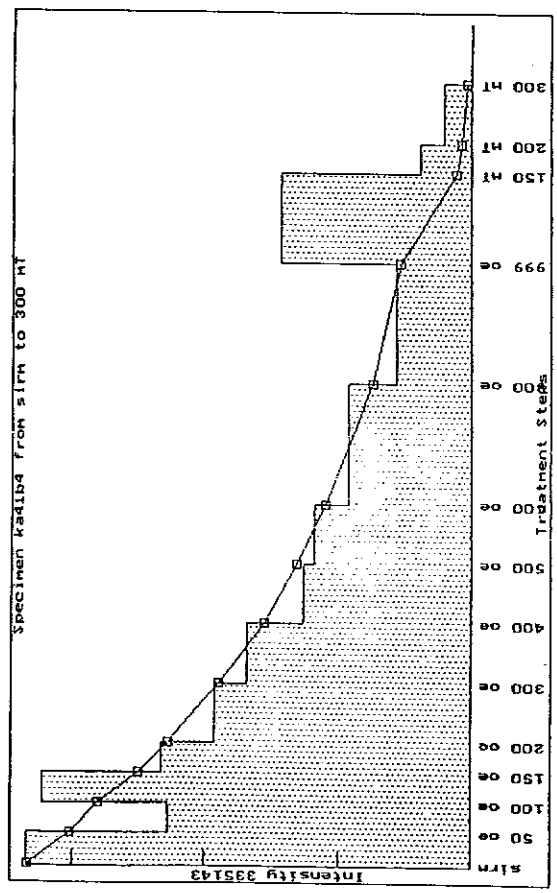
Specimen ka41b4 from sirm to 300 mT
Intensity 335143
Treatment Steps
sirm
50 oe
100 oe
150 oe
200 oe
300 oe
400 oe
500 oe
600 oe
800 oe
999 oe
150 mT
200 mT
300 mT

Specimen ka47b2 from sirm to 300 mT
Intensity 896.98
Treatment steps
sirm
50 oe
100 oe
150 oe
200 oe
250 oe
300 oe
400 oe
500 oe
600 oe
80 mT
100 mT
125 mT
150 mT
200 mT
250 mT
300 mT

Specimen ka48a2 from sirm to 300 mT
Intensity 593.114
Treatment steps
sirm
50 oe
100 oe
150 oe
200 oe
300 oe
400 oe
500 oe
600 oe
999 oe
150 mT
200 mT
300 mT

Specimen ka45a2 from sirm to 300 mT
Intensity 788.14
Treatment steps
sirm
50 oe
100 oe
150 oe
200 oe
300 oe
400 oe
500 oe
600 oe
999 oe
150 mT
200 mT
300 mT

Specimen ka46a2 from sirm to 300 mT
Intensity 637.359
Treatment steps
sirm
50 oe
100 oe
150 oe
200 oe
250 oe
300 oe
400 oe
600 oe
80 mT
100 mT
125 mT
150 mT
200 mT
250 mT
300 mT

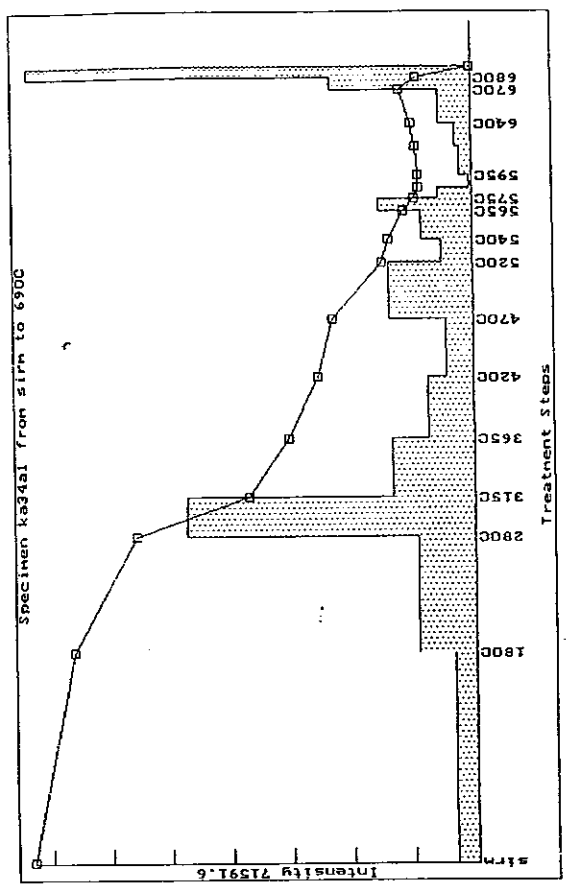

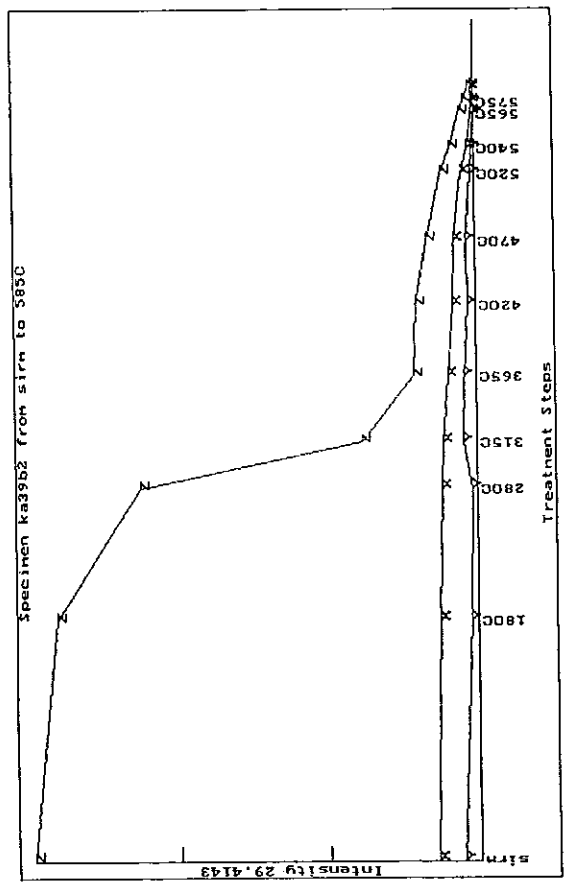

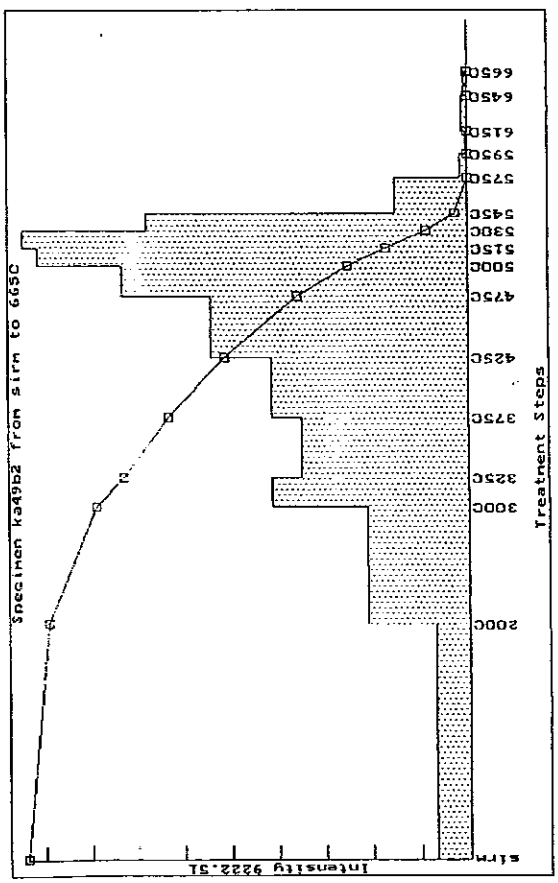

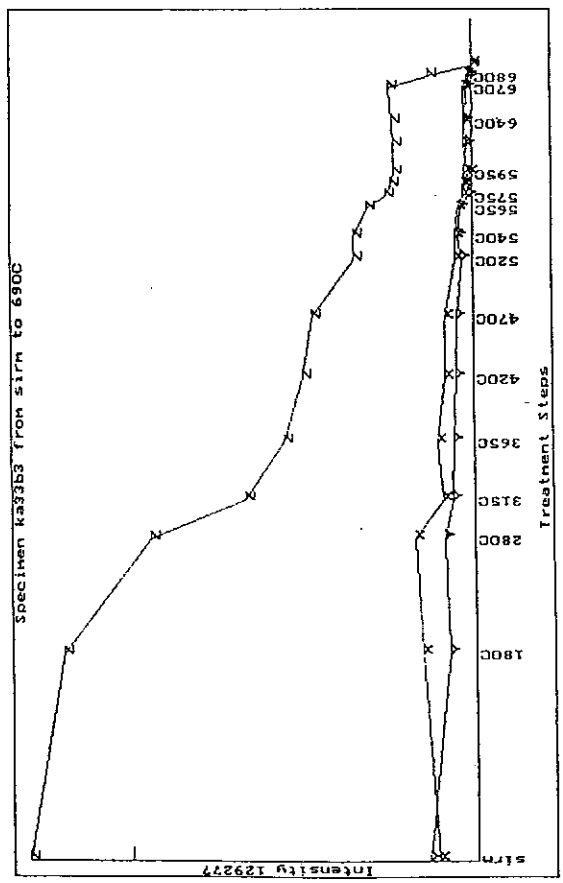

Fig.18 Thermal demagnetisation of 3-component IRM of surface samples: z-axis = hard component (> 1000 Oe); x-axis = intermediate coercivity component (200-1000 Oe);

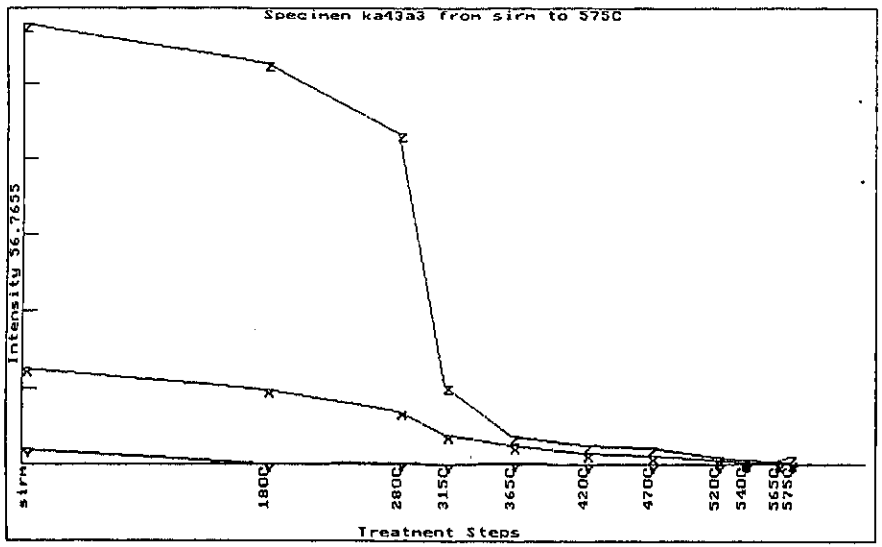
Specimen ka43a3 from sirm to 575C
Intensity 36.7655
sirm
180C
280C
315C
365C
420C
470C
520C
540C
565C
575C
Treatment Steps

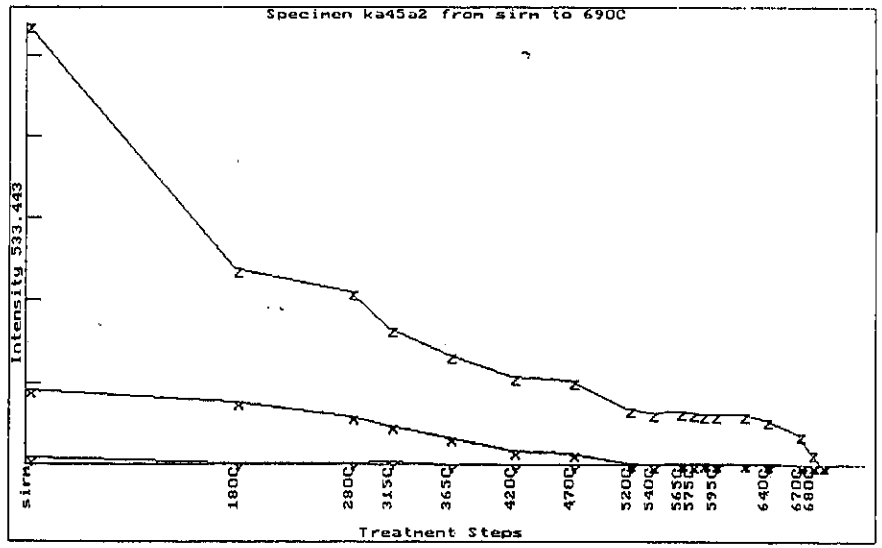
Specimen ka45a2 from sirm to 690C
Intensity 533.443
sirm
180C
280C
315C
365C
420C
470C
520C
540C
565C
575C
595C
640C
670C
690C
Treatment Steps

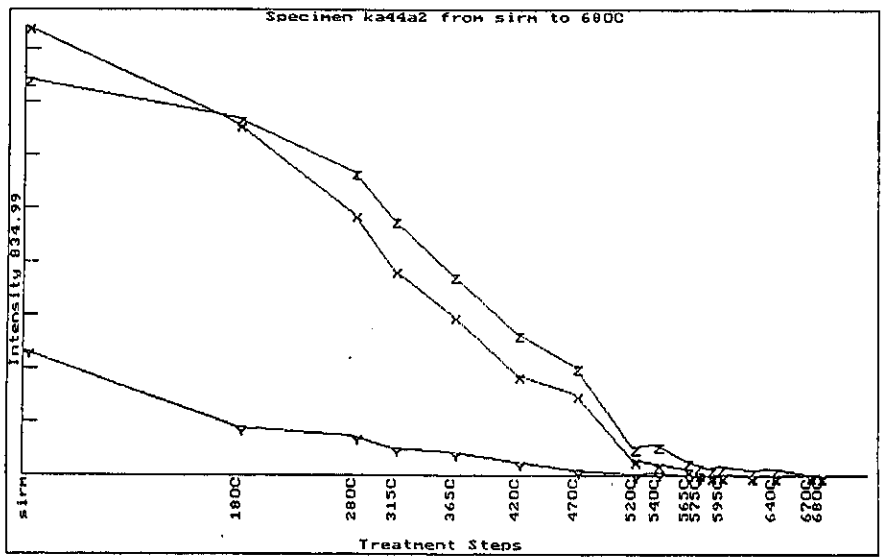
Specimen ka44a2 from sirm to 600C
Intensity 834.99
sirm
180C
280C
315C
365C
420C
470C
520C
540C
565C
575C
595C
640C
670C
680C
Treatment Steps

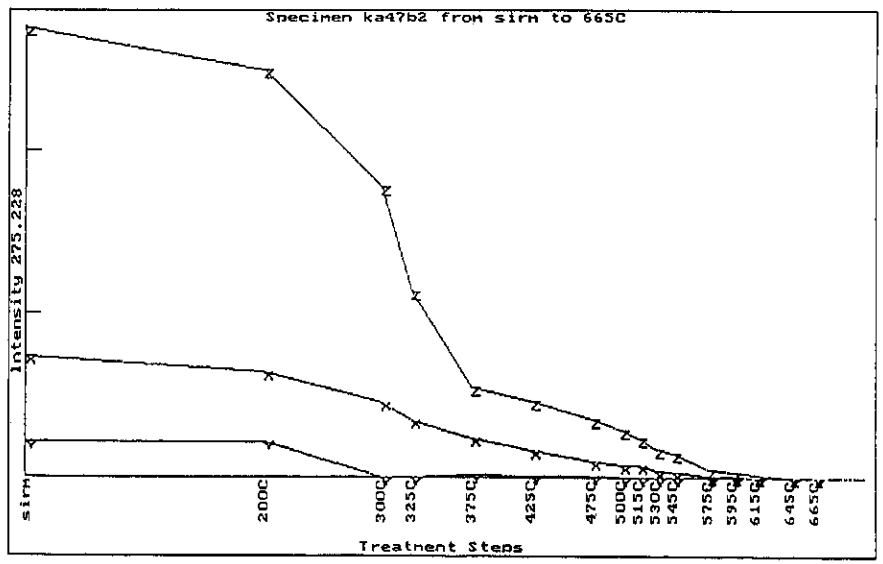
Specimen ka47b2 from sirm to 665C
Intensity 275.228
sirm
200C
300C
325C
375C
425C
475C
500C
515C
530C
545C
575C
595C
615C
645C
665C
Treatment Steps

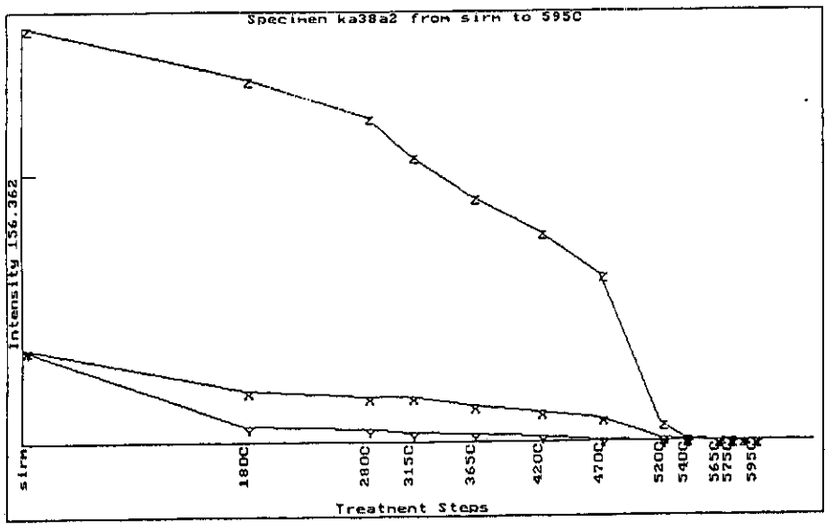
Specimen ka38a2 from sirm to 595C
Intensity 156.362
sirm
180C
280C
315C
365C
420C
470C
520C
540C
565C
575C
595C
Treatment Steps

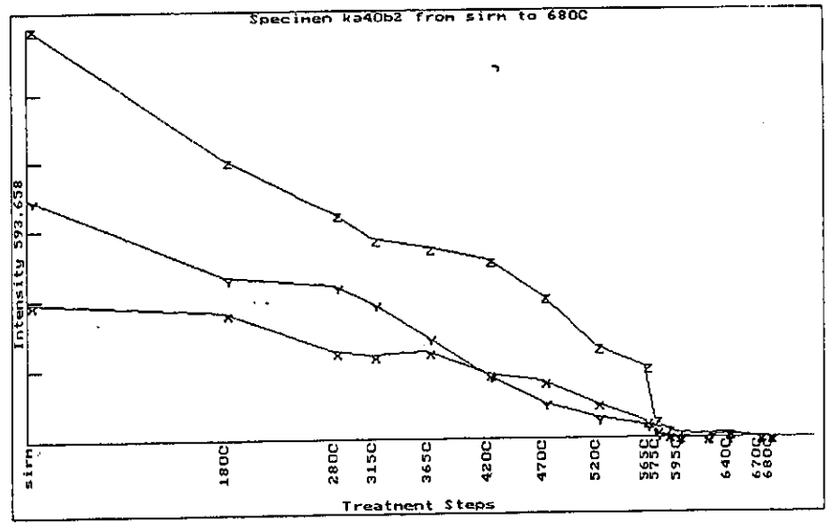
Specimen ka40b2 from sirm to 680C
Intensity 593.658
sirm
180C
280C
315C
365C
420C
470C
520C
565C
575C
595C
640C
670C
680C
Treatment Steps

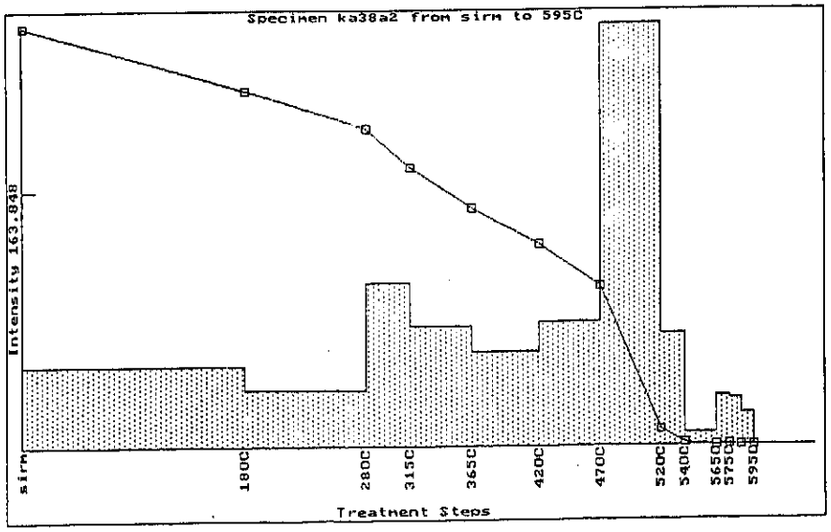
Specimen ka38a2 from sirm to 595C
Intensity 163.948
sirm
180C
280C
315C
365C
420C
470C
520C
540C
565C
575C
595C
Treatment Steps

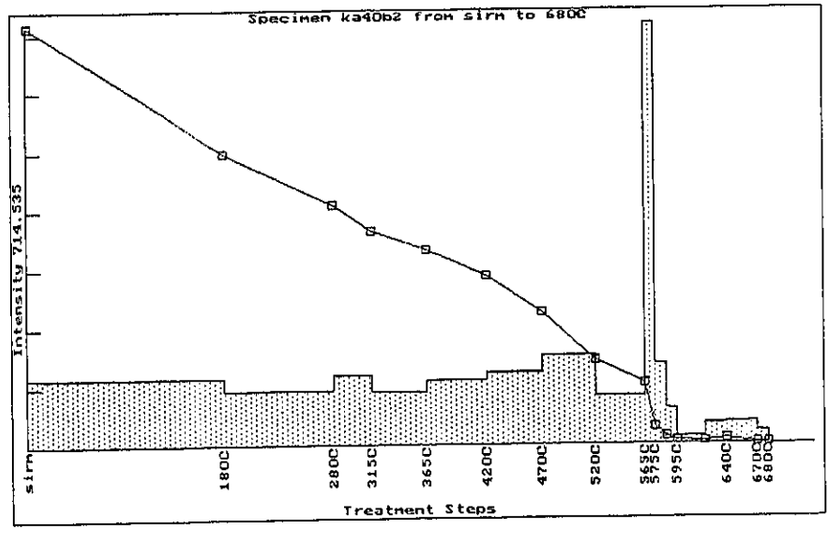
Specimen ka40b2 from sirm to 680C
Intensity 714.535
sirm
180C
280C
315C
365C
420C
470C
520C
565C
575C
595C
640C
670C
680C
Treatment Steps

Mt Keith DDH Samples

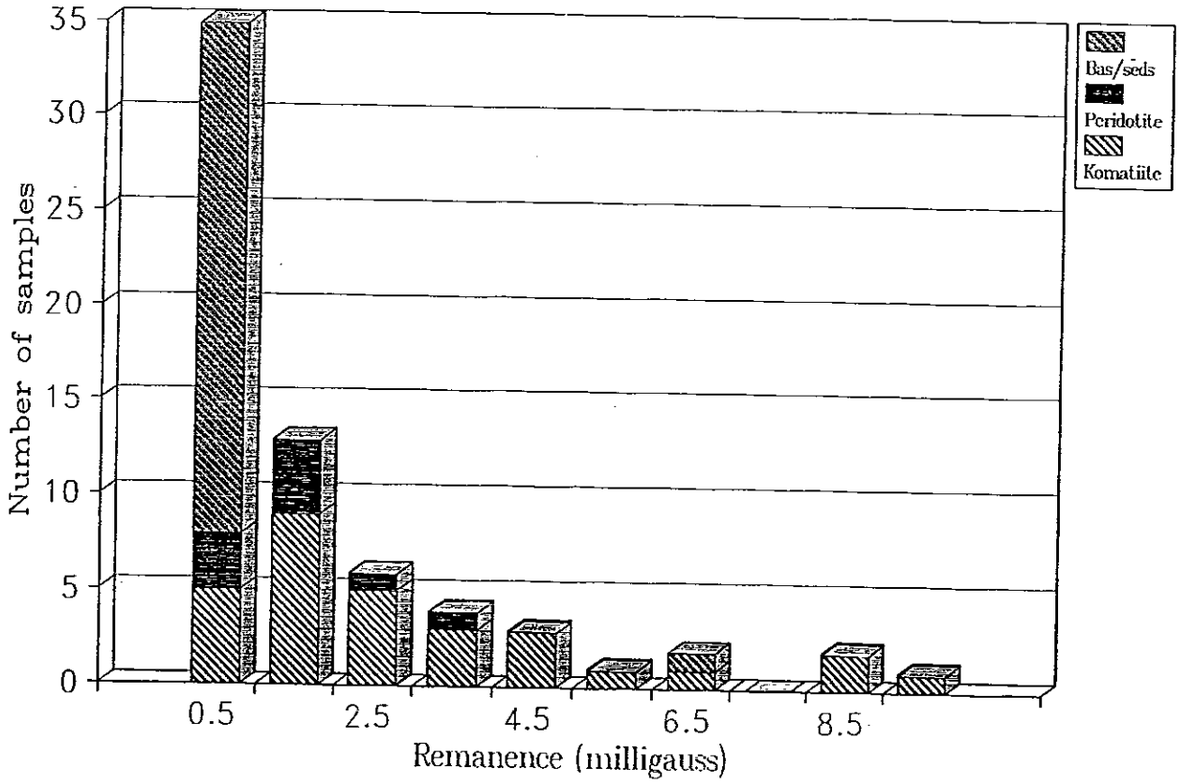

Mt Keith DDH Samples

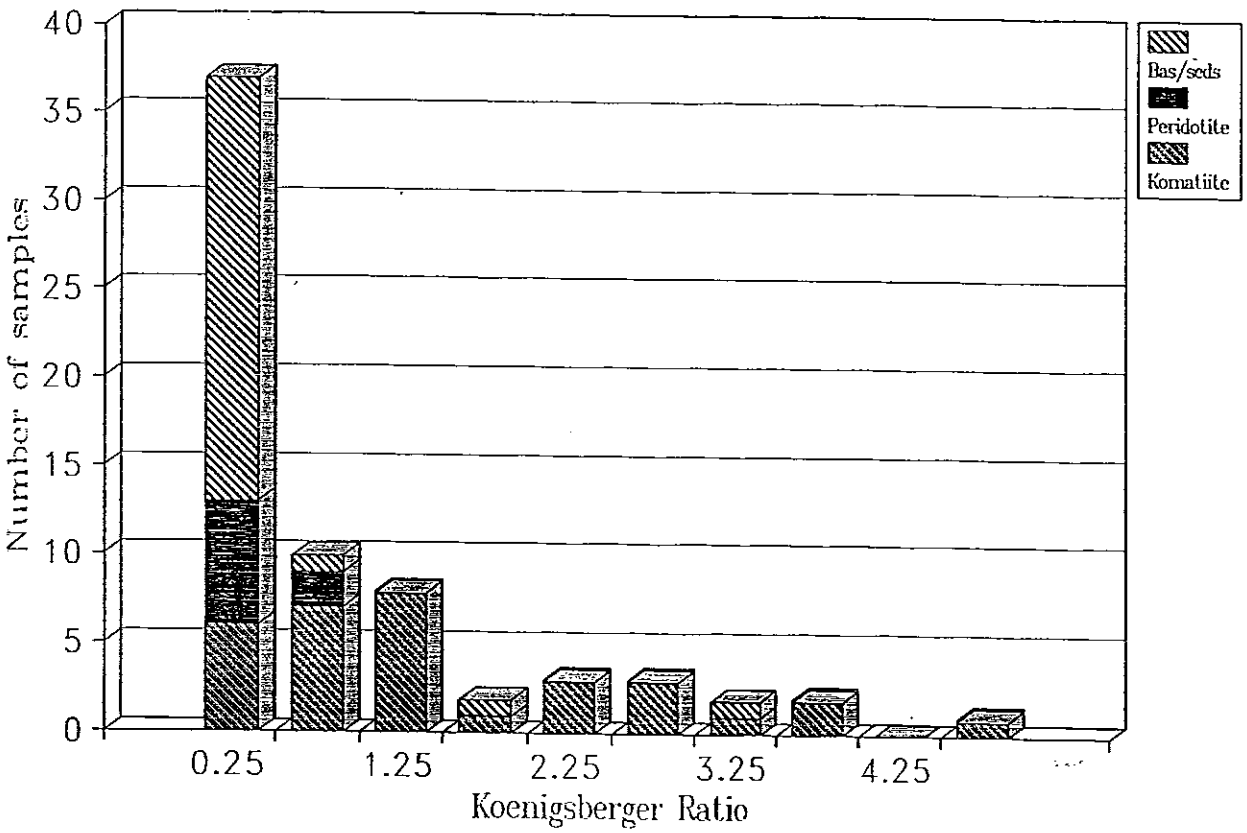

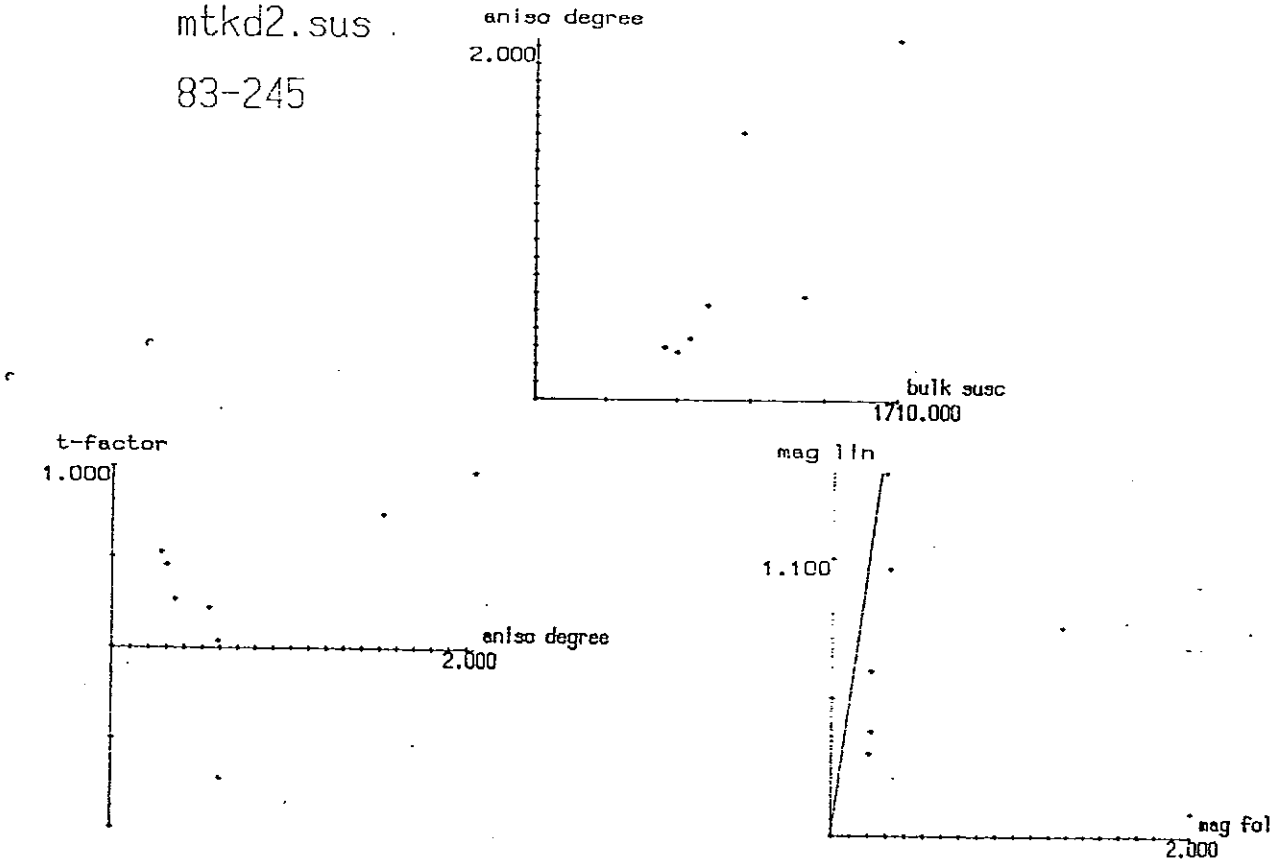

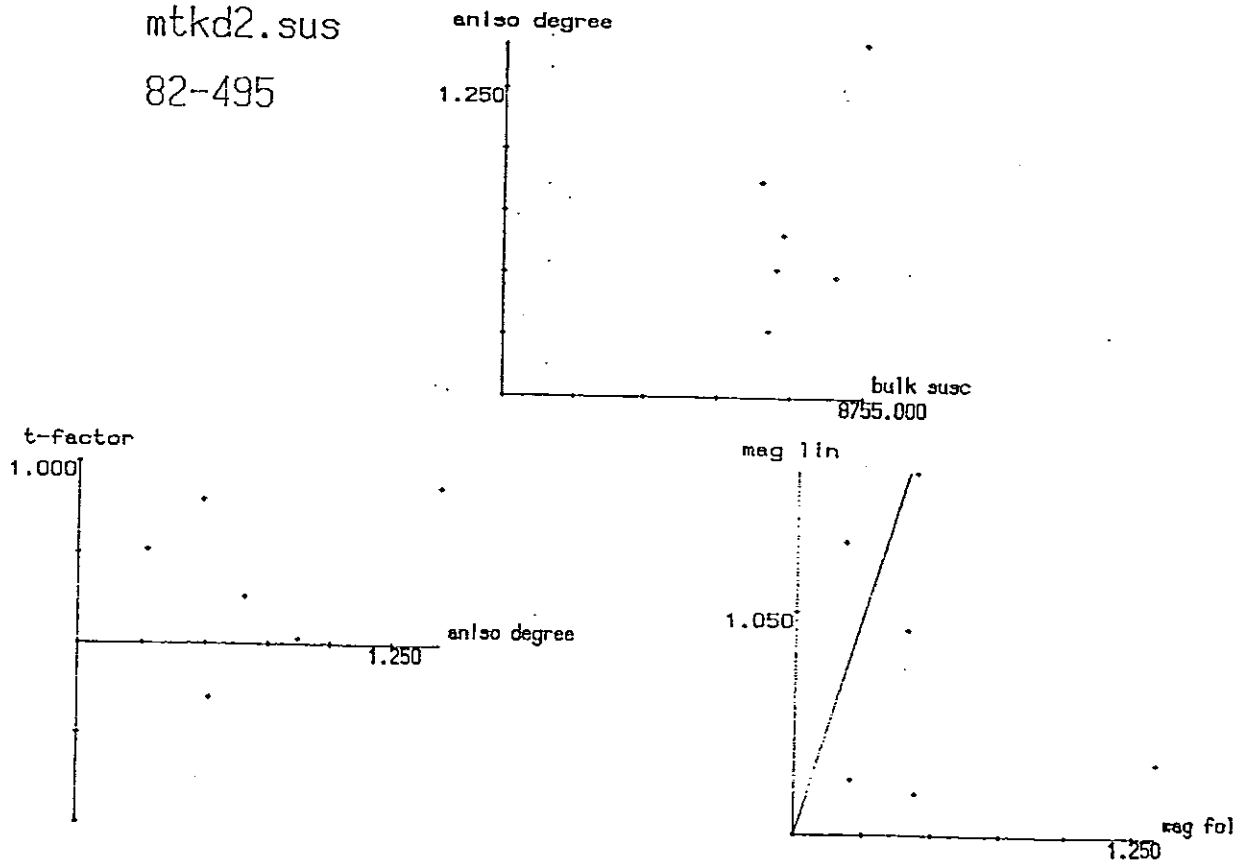

Fig.20 Magnetic fabric

mtkd2.sus
83-245

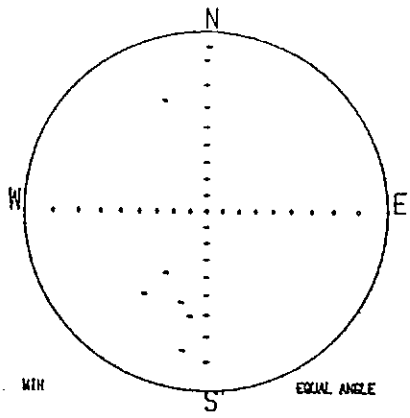

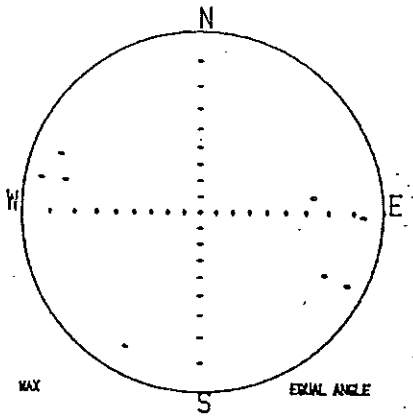

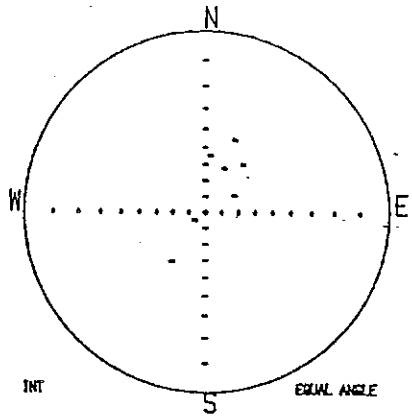

mtkd2.sus
82-495

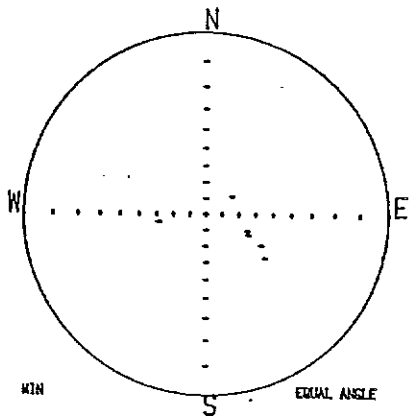

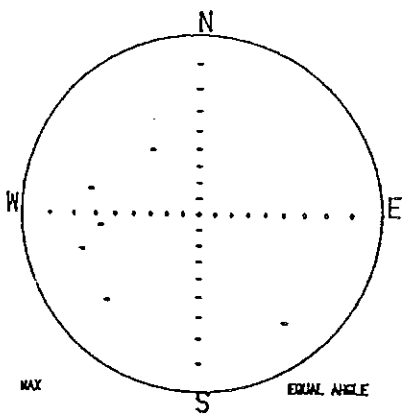

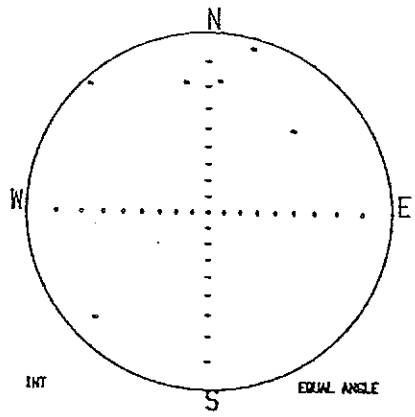

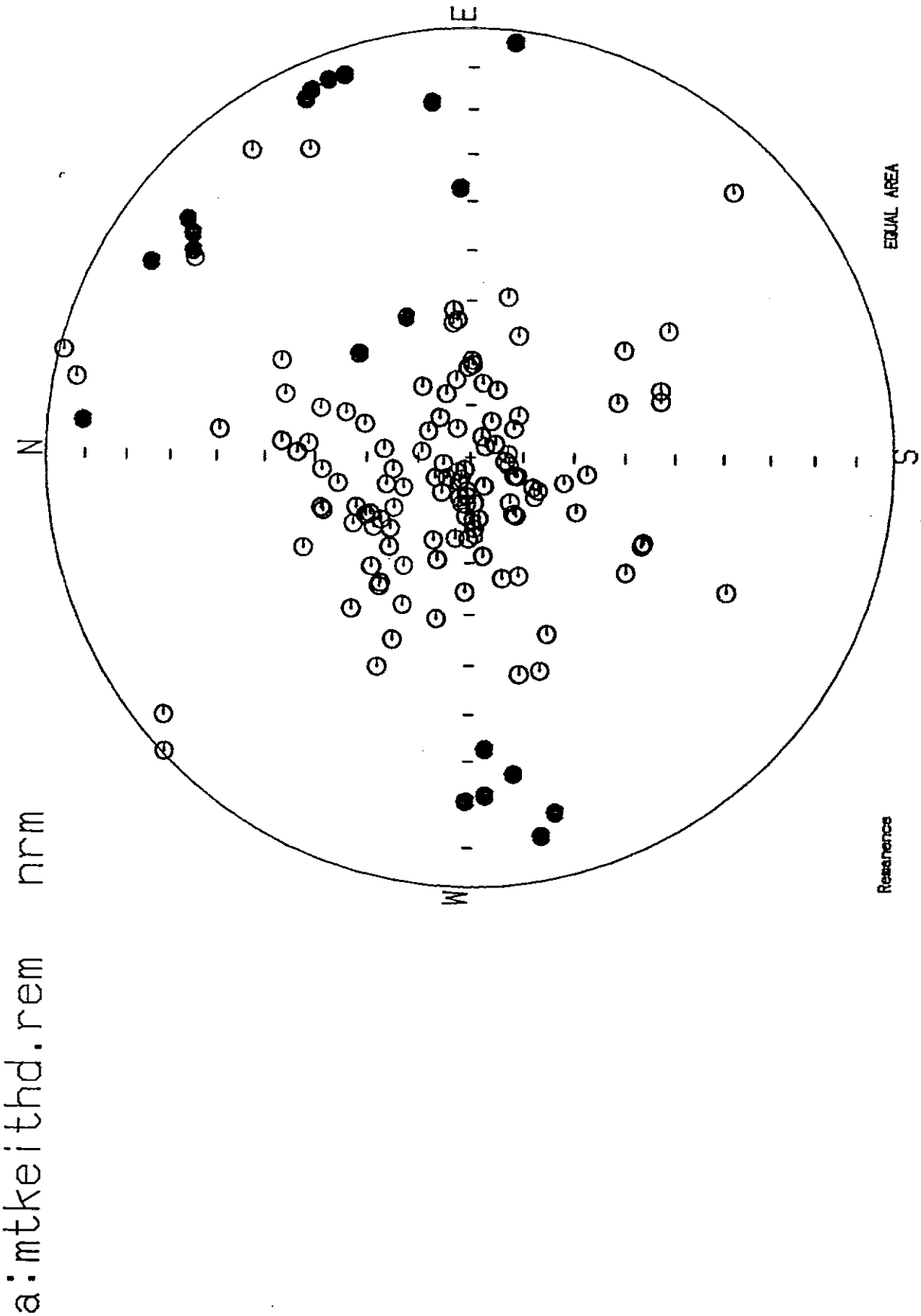

Fig.21 NRM directions with respect to drilling axes

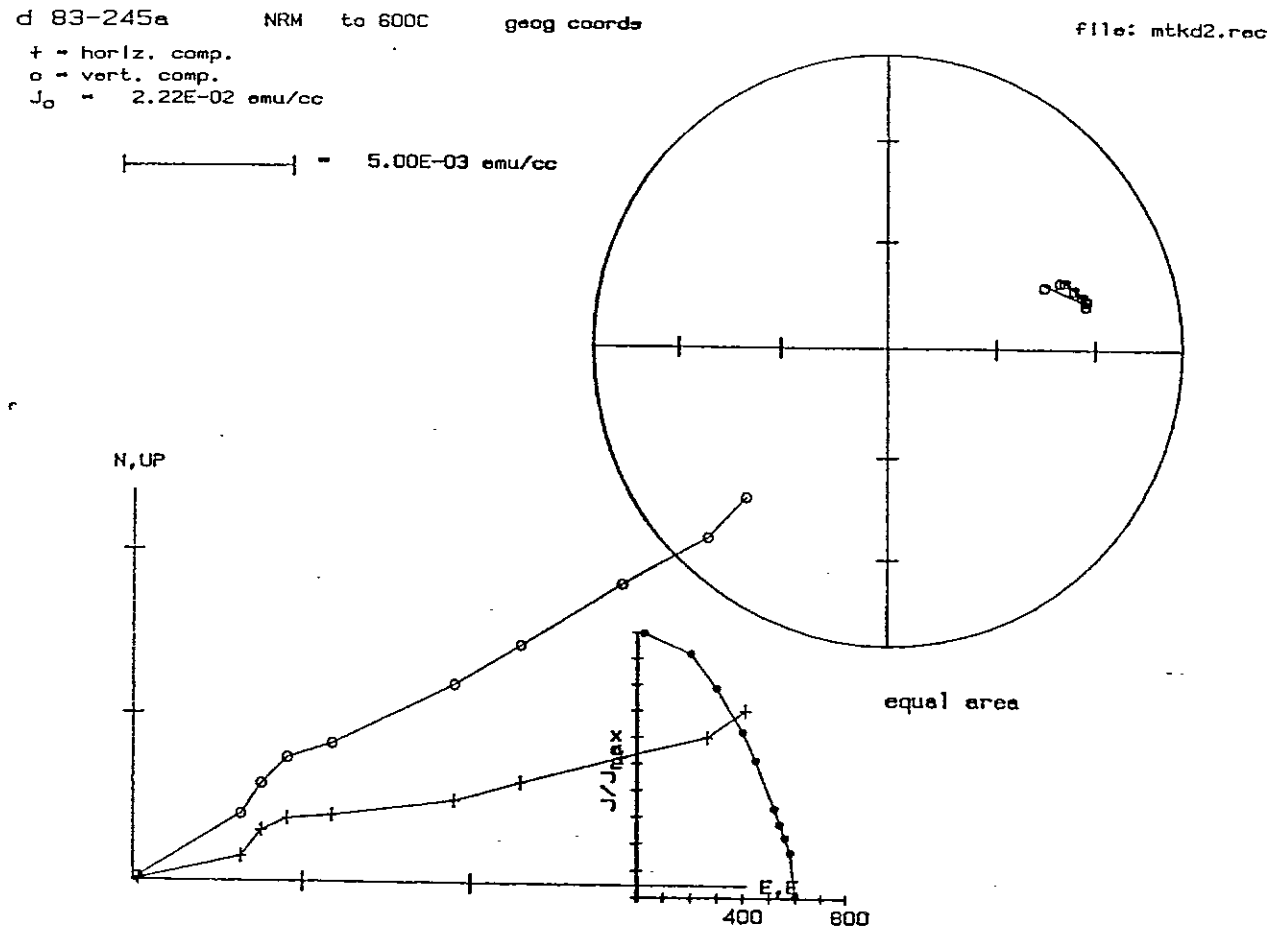

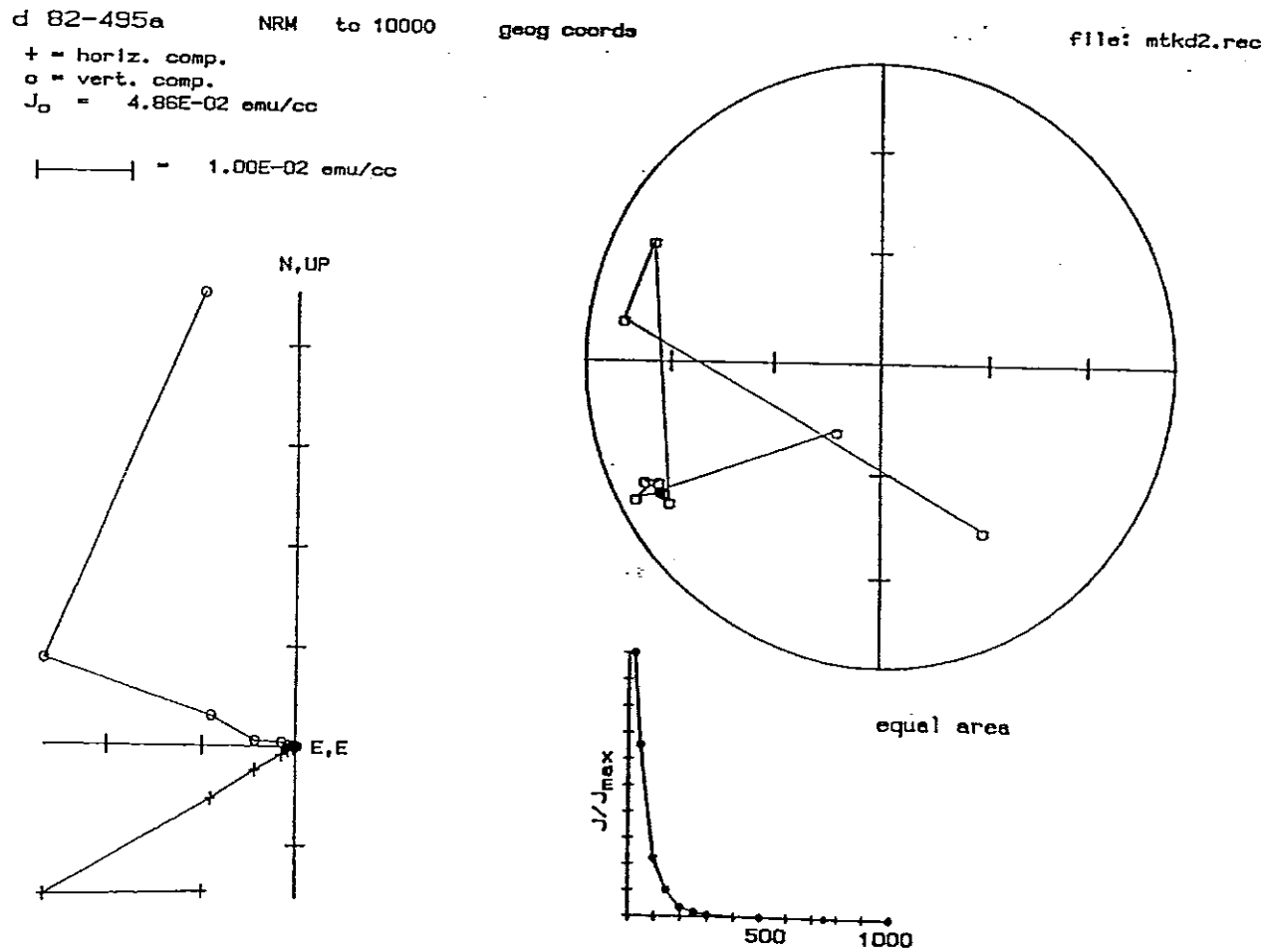

Fig. 22 Directions of DDH samples in geographical coordinates showing AF and thermal cleaning

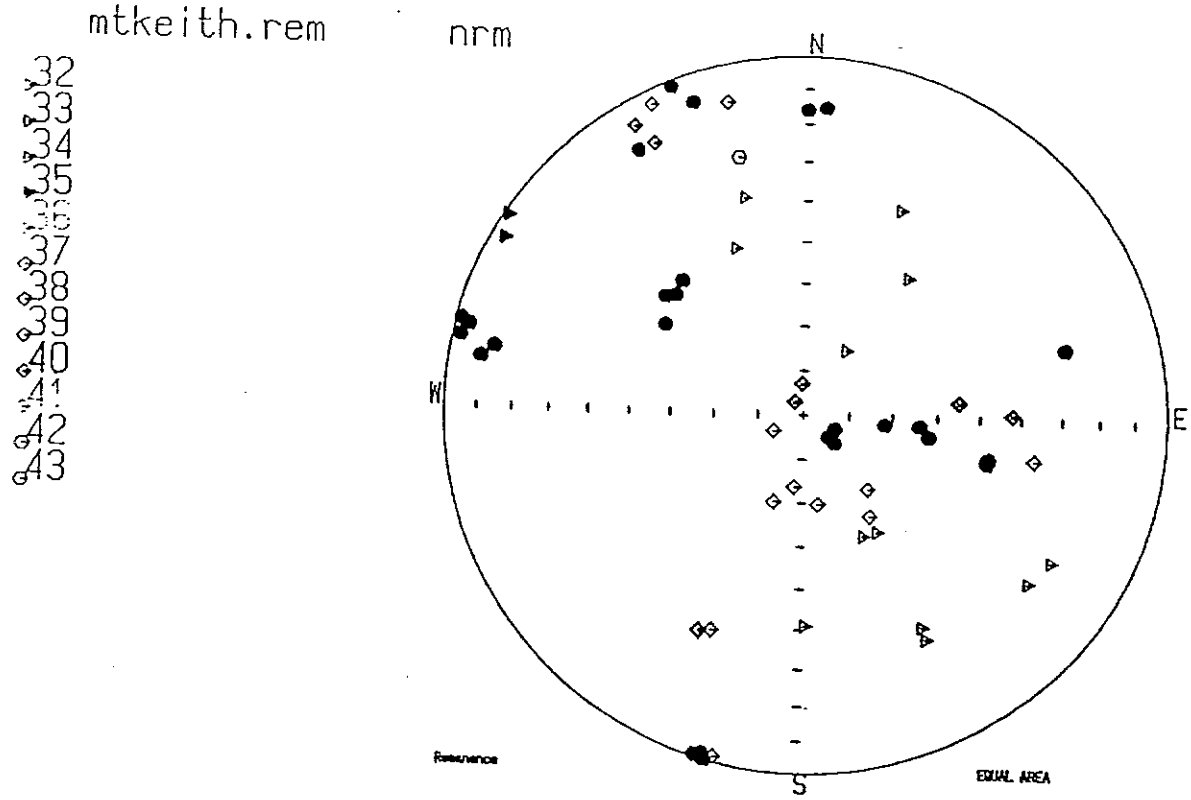

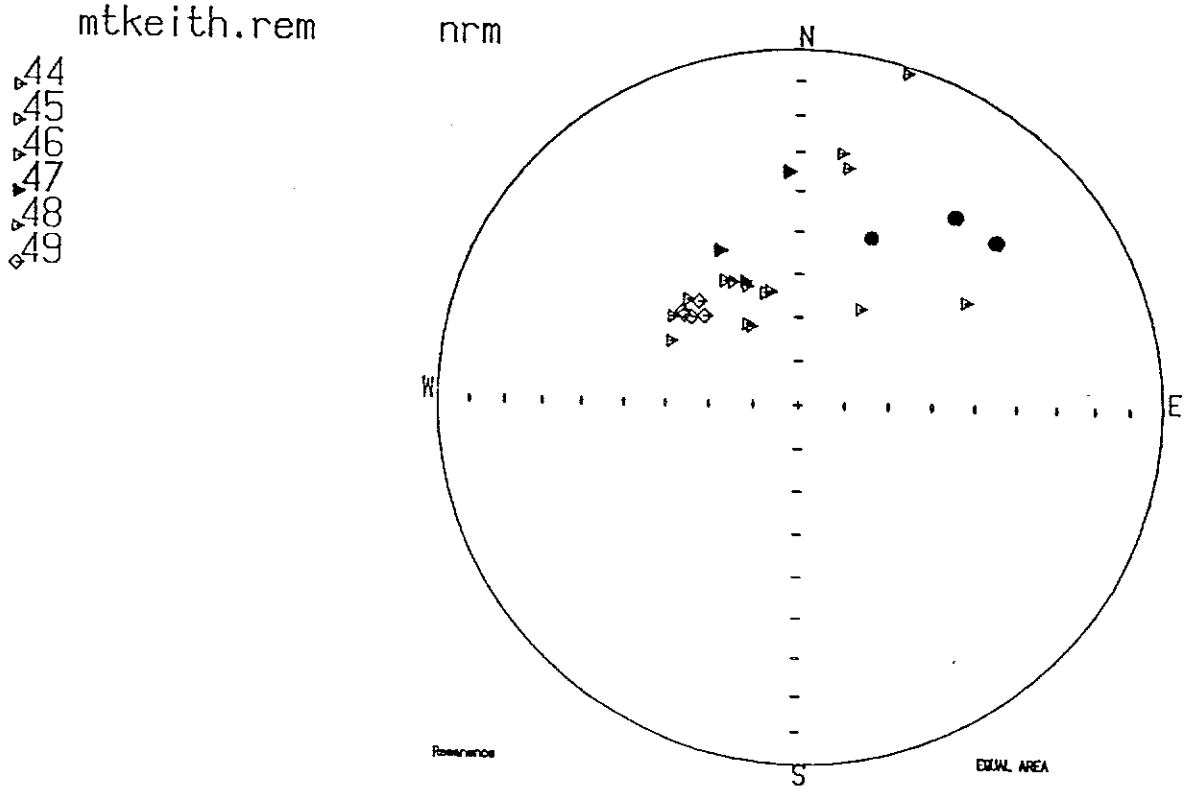

Fig.23 NRM directions of surface samples

ka 25a NRM to 580C geog coords file: mtkeith1.rec

+ = horiz. comp.
o = vert. comp.
J_o = 1.65E-06 emu/cc

⊢——⊣ = 5.00E-07 emu/cc

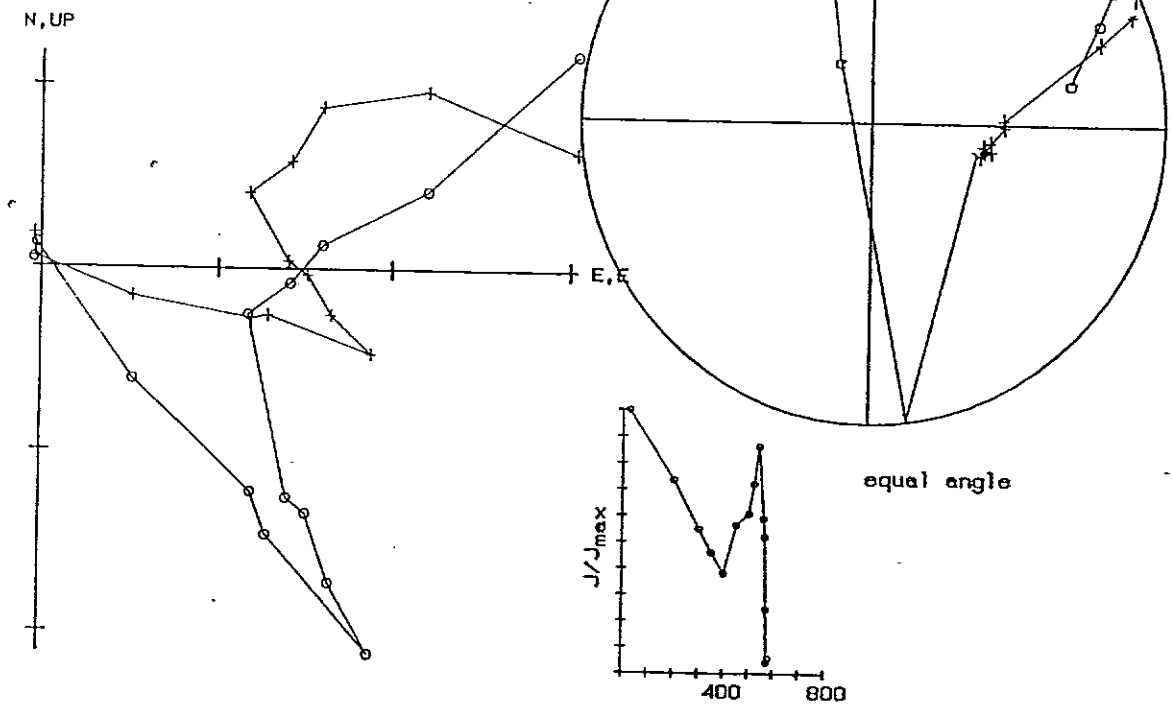

equal angle

ka 49a NRM to 575C geog coords file: mtkeith3.rec

+ = horiz. comp.
o = vert. comp.
J_o = 5.07E-04 emu/cc

⊢—⊣ = 5.00E-05 emu/cc

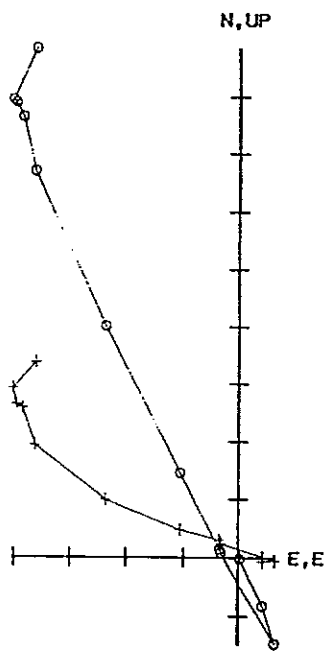

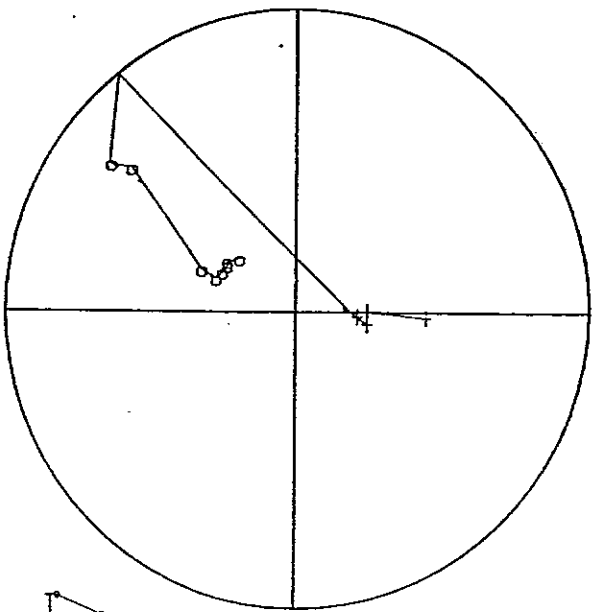

equal angle

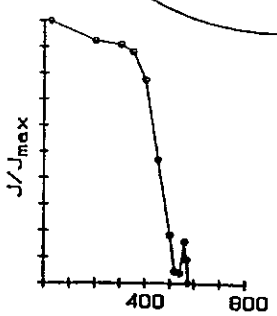

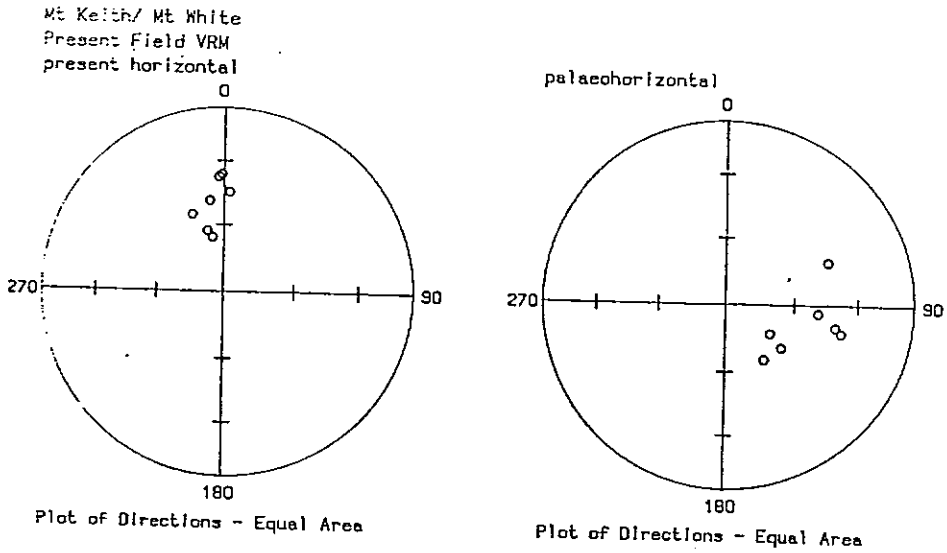

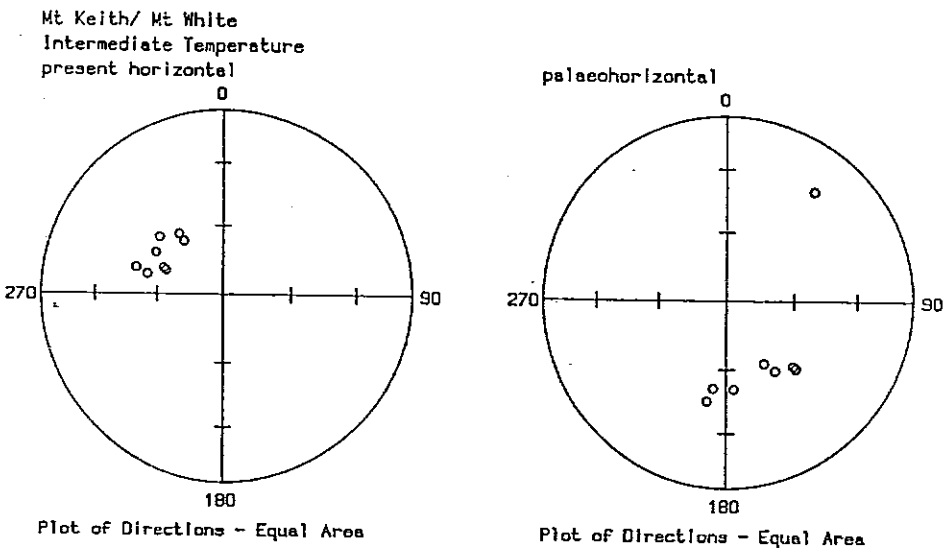

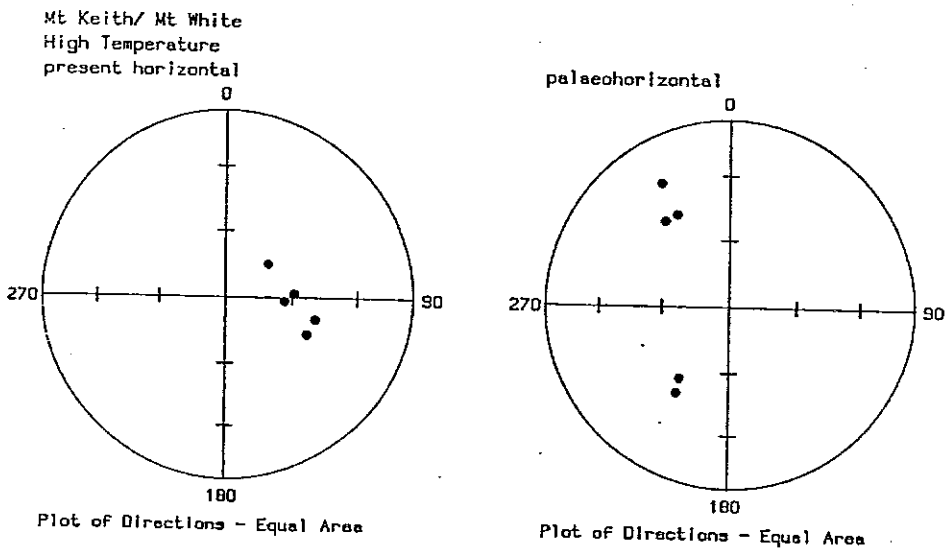

Fig.24 Remanence components resolved by thermal demagnetisation

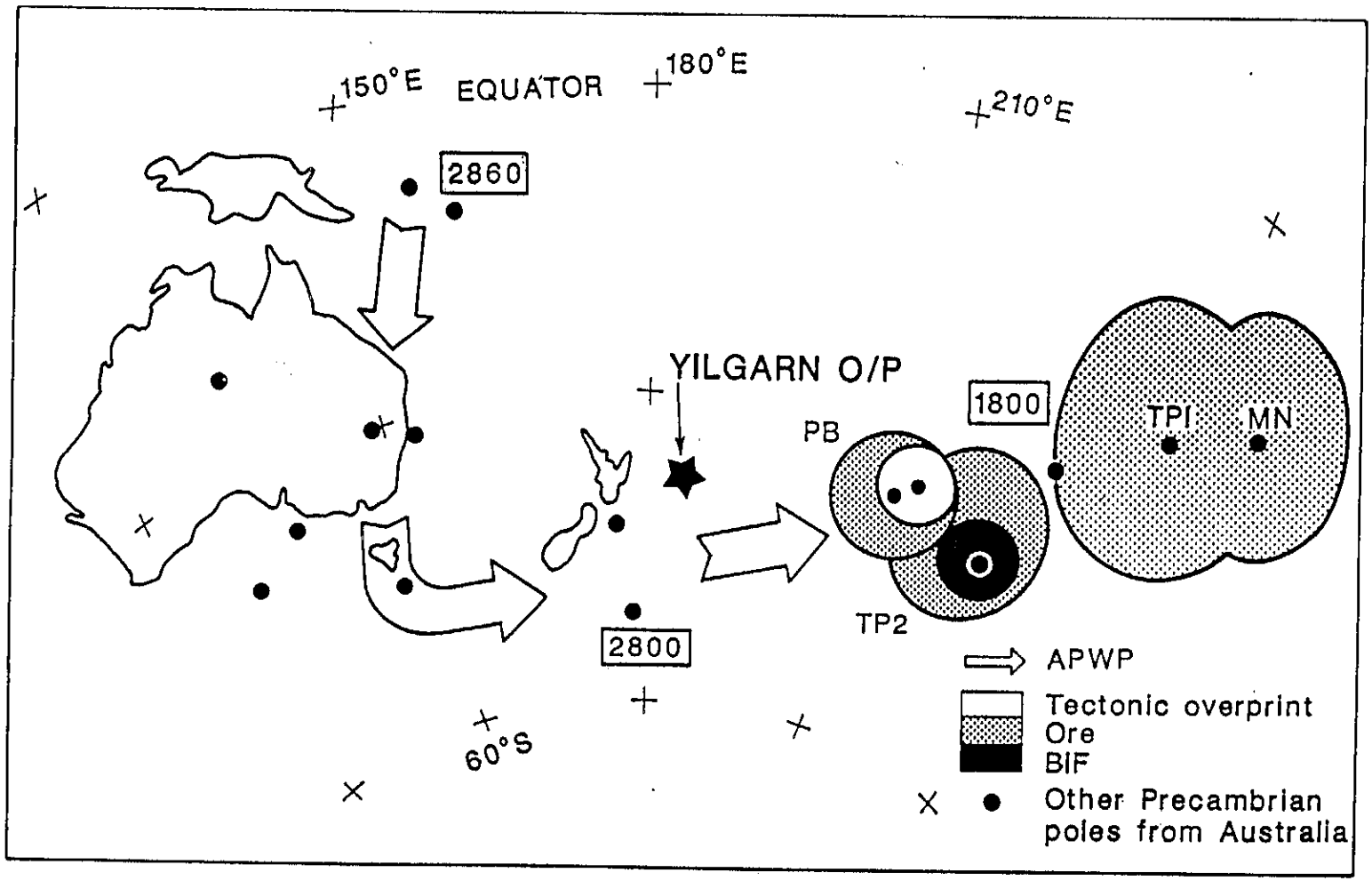

Fig.25 Portion of Precambrian apparent polar wander path for Australia, showing pole corresponding to the high temperature component

Fig.26 Aeromagnetic contours for the Mount Keith-Six Mile area, showing location of sampled drill holes

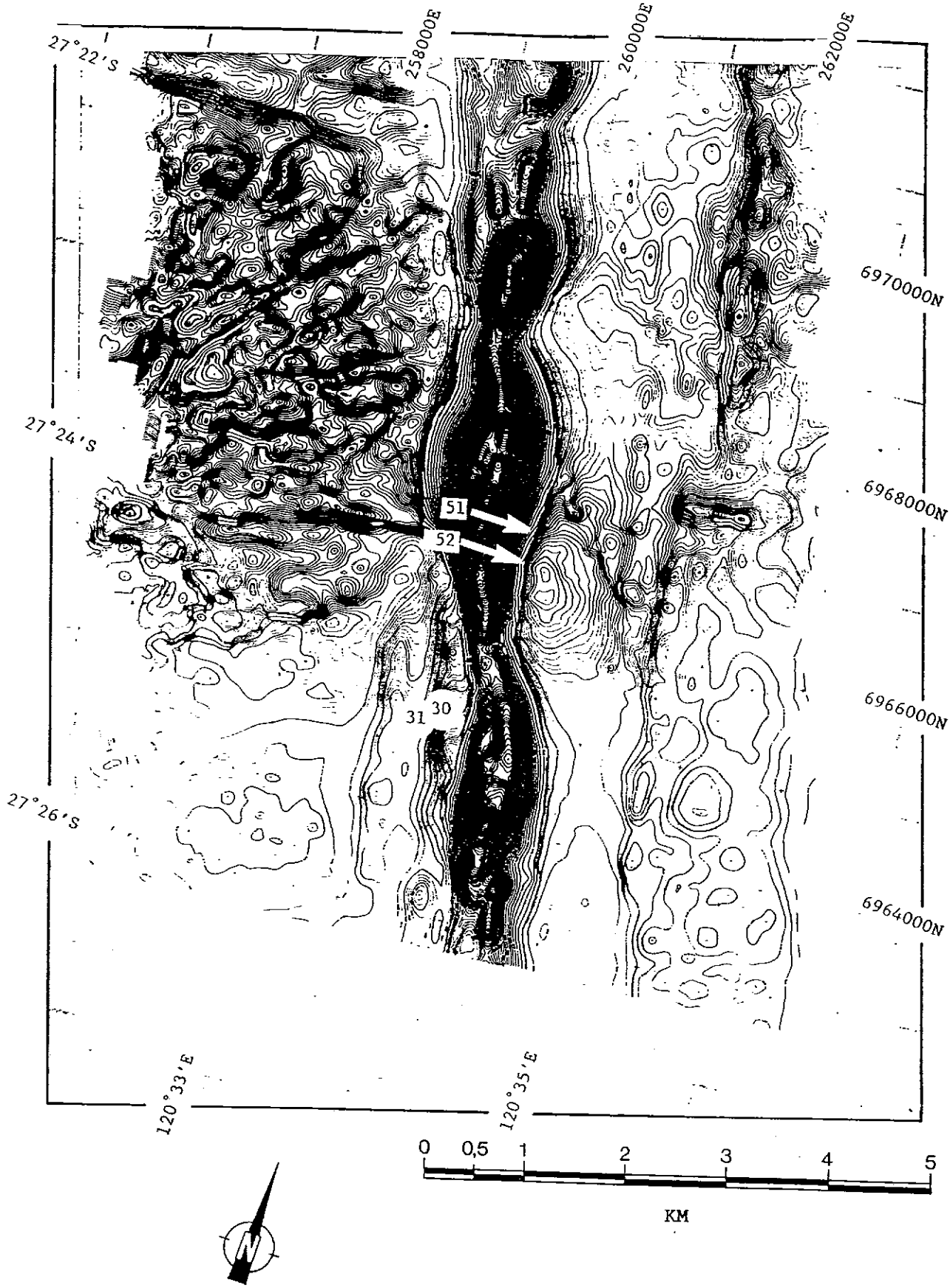
27°22'S
27°24'S
27°26'S
258000E
260000E
262000E
6970000N
6968000N
6966000N
6964000N
51
52
31
30
120°33'E
120°35'E
0
0,5
1
2
3
4
5
KM
N

SHEET 1

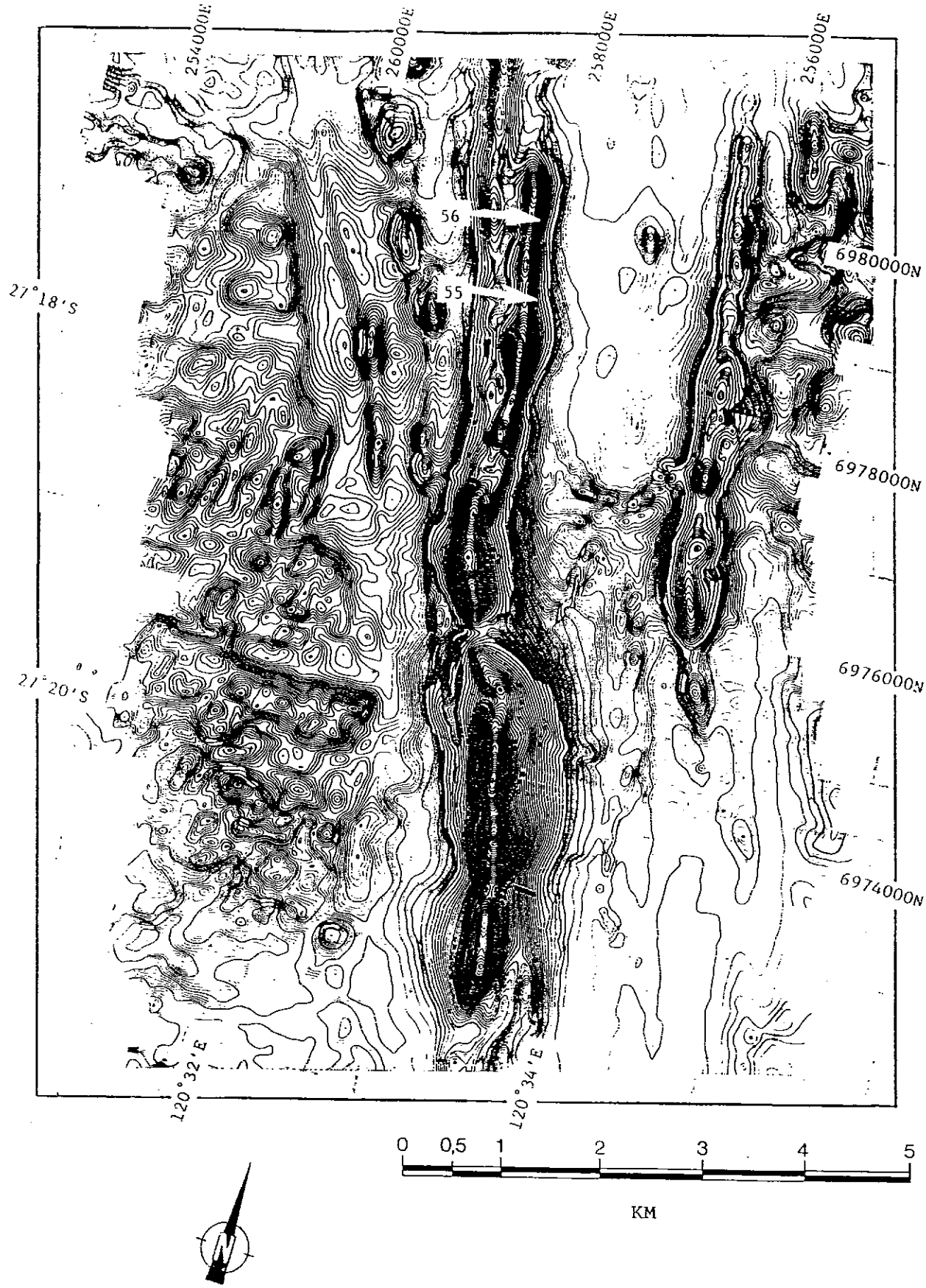
254000E
260000E
258000E
256000E
56
55
6980000N
6978000N
6976000N
6974000N
27°18'S
27°20'S
120°32'E
120°34'E
0 0,5 1 2 3 4 5
KM
N

SHEET 2

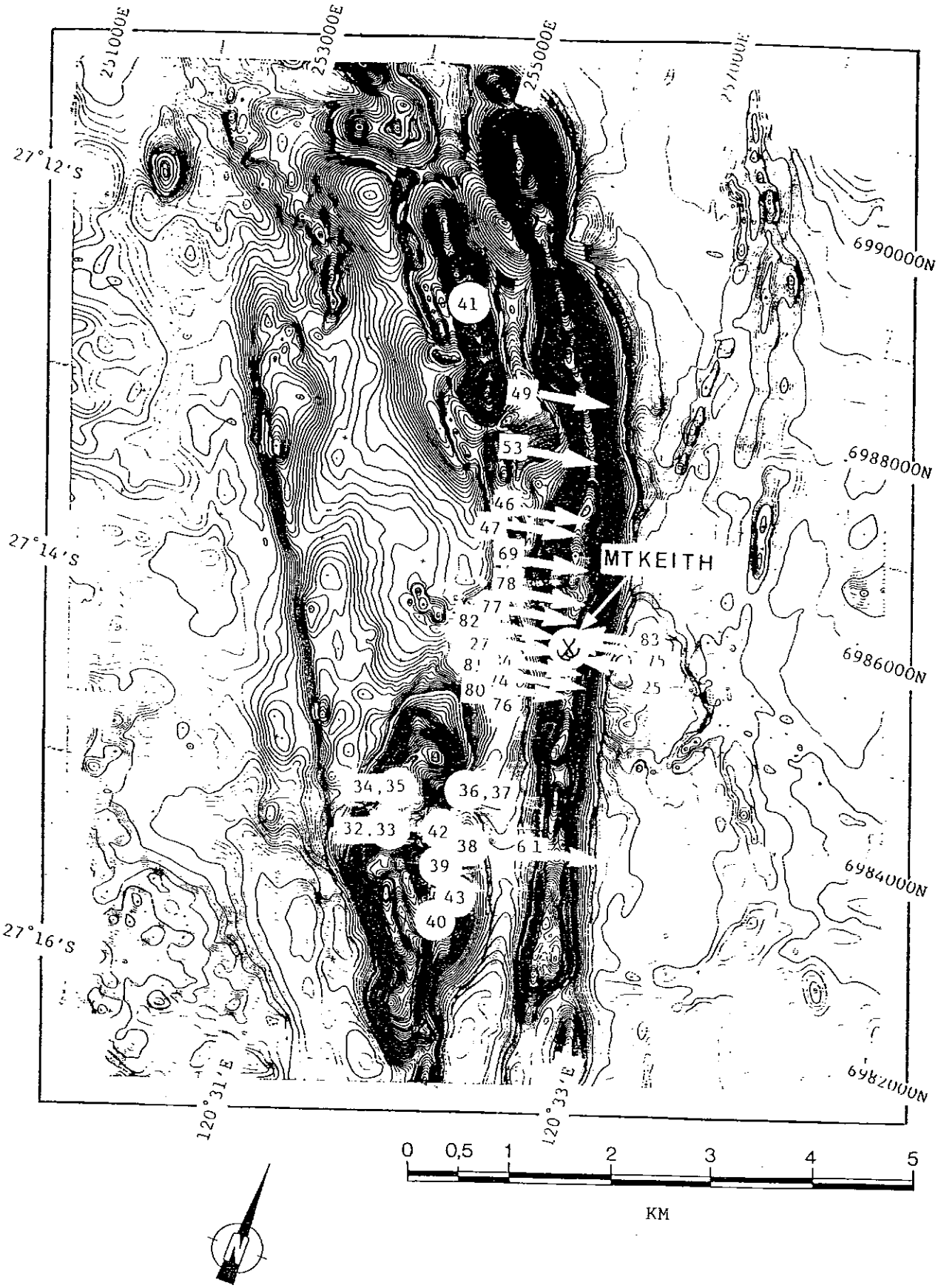
251000E
253000E
255000E
257000E
27°12'S
27°14'S
27°16'S
120°31'E
120°33'E
6990000N
6988000N
6986000N
6984000N
6982000N
MTKEITH
41
49
53
46
47
69
78
77
82
83
80
76
34,35
36,37
32,33
42
38
61
39
43
40
0 0,5 1 2 3 4 5
KM

SHEET3